

DRAWING: Fabrication of Scaffolds for Neural Tissue Engineering

Disertační práce

Studijní program:

P3106 Textilní inženýrství

Studijní obor:

Textilní technika a materiálové inženýrství

Autor práce:

Mgr. Kateřina Strnadová

Školitel práce:

Ing. Věra Jenčová, Ph.D.

Katedra chemie



Prohlášení

Prohlašuji, že svou disertační práci jsem vypracovala samostatně jako původní dílo s použitím uvedené literatury a na základě konzultací s vedoucím mé disertační práce a konzultantem.

Jsem si vědoma toho, že na mou disertační práci se plně vztahuje zákon č. 121/2000 Sb., o právu autorském, zejména § 60 – školní dílo.

Beru na vědomí, že Technická univerzita v Liberci nezasahuje do mých autorských práv užitím mé disertační práce pro vnitřní potřebu Technické univerzity v Liberci.

Užiji-li disertační práci nebo poskytnu-li licenci k jejímu využití, jsem si vědoma povinnosti informovat o této skutečnosti Technickou univerzitu v Liberci; v tomto případě má Technická univerzita v Liberci právo ode mne požadovat úhradu nákladů, které vynaložila na vytvoření díla, až do jejich skutečné výše.

Současně čestně prohlašuji, že text elektronické podoby práce vložený do IS/STAG se shoduje s textem tištěné podoby práce.

Beru na vědomí, že má disertační práce bude zveřejněna Technickou univerzitou v Liberci v souladu s § 47b zákona č. 111/1998 Sb., o vysokých školách a o změně a doplnění dalších zákonů (zákon o vysokých školách), ve znění pozdějších předpisů.

Jsem si vědoma následků, které podle zákona o vysokých školách mohou vyplývat z porušení tohoto prohlášení.

6. dubna 2021

Mgr. Kateřina Strnadová

Abstract

Materials based on orientated fibers have great potential for use in tissue engineering for tissues, where the arrangement of extracellular matrix is fundamental for tissue functionality. The drawing method is extremely suitable method for such applications. It is based on mechanical pulling of a polymer solution out of its base droplet, resulting in a single solidified fiber of determined geometrical characteristics. A new machine designed for lab scale drawing was invented enabling a repeatable quality of drawing conditions. The results demonstrate that by changing the speed of drawing and polymer solution concentration it is possible to influence and define the fiber diameter and its distribution. From the *in vitro* experiments, it is evident that the aligned fibers guide the cell growth in the direction of the fibers. Moreover, the prepared fibers were functionalized with polypyrrole as an example of their versatility. The results from *in vitro* experiments show, that polypyrrole enhanced the biocompatibility of the fibers. These fibers were further used for the preparation of the novel composite spinal cord bridges, which were tested *in vitro* and *in vivo*. The results from *in vitro* experiments show that the oriented fibers support the guidance of neurite outgrowth and narrow the axonal spread which is more focused around the fibers. This phenomenon is even more pronounced, if the fibers are coated with polypyrrole. The new spinal cord bridges were successfully implanted into mice' spinal cord for *in vivo* experiments. The results suggest the non-immunogenicity of the fibrous bridge samples. Moreover, the results show the activation of the pro-healing immune response in the both fibrous bridges. Also, the bridges with PCL fibers show higher axon infiltration compared to control. About 20 % of these axons are myelinated, 75 % of this myelin is derived from the Schwann cells. On the other hand, the axonal infiltration into the bridges with PPy-coated fibers is lower compared to bridges with PCL fibers or compared to control. Nevertheless, the obtained results show, that the oriented fibers enhance the axon infiltration into the spinal cord bridges and that the combination of the currently available approaches with new functionalization methods will be the method of choice for neural tissue engineering.

Keywords:

drawing, fibers, neural tissue engineering, spinal cord, *in vitro*, *in vivo*

Abstrakt

Materiály založené na orientovaných vláknech mají velký potenciál pro využití v tkáňovém inženýrství a to zejména u tkání, kde je organizace mezibuněčné hmoty zcela zásadní pro funkčnost tkáně. Velmi vhodnou metodou pro tyto aplikace je drawing. Ten je založen na mechanickém tažení polymerního roztoku z kapky polymeru umístěné na podložce, což vede k vytvoření vlákna o definovaných geometrických charakteristikách. Pro tyto účely byl navržen a vyvinut laboratorní přístroj, který umožňuje tažení vláken za stálých podmínek. Výsledky ukazují, že změnou rychlostí tažení vláken a změnou koncentrací polymerních roztoků lze ovlivnit a regulovat průměr vláken a zároveň i distribuci jejich průměrů. Z *in vitro* experimentů je patrné, že orientovaná vlákna ovlivňují směr růstu buněk ve směru orientace vláken. Na základě těchto experimentů byly tyto scaffoldy dále funkcionalizovány polypyrrolem, čímž se prokázala jejich univerzálnost pro použití v tkáňovém inženýrství. Výsledky z *in vitro* experimentů s popyrrolovanými vlákny ukazují, že polypyrrole zvyšuje biokompatibilitu vláken. Popyrrolovaná vlákna byla dále použita pro přípravu nových kompozitních míšních můstků, které byly testovány *in vitro* a *in vivo*. Výsledky z *in vitro* experimentů ukazují, že orientovaná vlákna podporují růst a orientaci axonů okolo vláken. Tento jev je ještě více patrný, pokud jsou vlákna potažená polypyrrolem. *In vivo* experimenty byly provedeny na myších, jimž byly můstky implantovány do mích. Hodnocení pro-zánětlivých a apoptotických markerů naznačuje, že vlákenné míšní můstky jsou neimunogenní. Tyto výsledky ukazují aktivaci imunitní reakce, zodpovědné za procesy hojení v těle, a to u obou vlákenných míšních můstků. Míšní můstky obsahující PCL orientovaná vlákna dokonce vykazují vyšší infiltraci axonů do můstků oproti kontrole bez vláken. Okolo 20 % těchto axonů je myelinizovaných, 75 % z tohoto myelinu je odvozeno od Schwannových buněk. Na druhou stranu, u míšních můstků s popyrrolovanými vlákny je infiltrace axonů do můstků oproti kontrole nižší. Nicméně výsledky ukazují, že orientovaná vlákna zvyšují infiltraci axonů do míšních můstků a že kombinace dostupných přístupů a metod funkcionalizace materiálů budou volbou do budoucna pro tkáňové inženýrství nervové tkáně.

Klíčová slova:

drawing, vlákna, tkáňové inženýrství nervové tkáně, mícha, *in vitro*, *in vivo*

Acknowledgements

In the first place I would like to acknowledge my supervisor, dr. Věra Jenčová, for her professional leadership, extensive scientific knowledge, but also for her mental support especially in the last phase of writing the thesis. My acknowledgement also belongs to my consultant, prof. David Lukáš, for his professional approach and kind support.

My great thanks definitely belongs to my family, especially my parents and my husband, who always believed in me and supported me mentally, but also babysat my little daughters, so I could finish writing the thesis. This work would never be written without them.

I must not forget to acknowledge to my colleagues who professionally contributed to this thesis. Namely, dr. Lukáš Stanislav, who constructed the first and second generation of Manipulator and who was at the foundation of drawing research at our department. Dr. Michal Řezanka and dr. Jan Lukášek, who were responsible for the functionalization of the drawn fibers by polypyrrole and part of the conductivity measurements. Michal also largely contributed to our paper and helped finished the draft. I would also like to thank Michal as a friend, who was always supportive. My acknowledgement also goes to dr. Lukáš Voleský and Mgr. Zdeněk Rafaj, who helped with the conductivity measurement. I also need to acknowledge my students, who worked on drawing during their thesis and contributed to this thesis with their scientific work and results, namely Ing. Ilona Krabicová, Ing. Šárka Hauzerová, Bc. Filip Sabol.

The acknowledgements also go to all the grant projects, which supported this thesis financially. And last but not least, I would like to thank to the Fulbright committee for granting me with the Fulbright project, which gave me great opportunity to meet very inspiring people and to learn many new interesting methods. The results achieved during the scholarship gave this work another dimension and helped me to finish this thesis.

Contents

Abstract	i
Abstrakt	ii
Acknowledgements	iii
1 Introduction	1
2 Summary	4
2.1 Tissue engineering	4
2.1.1 Neural tissue engineering with emphasis on spinal cord injuries	5
2.2 Scaffolds	9
2.2.1 Scaffold fabrication techniques	9
2.2.2 Nonwovens in tissue engineering	14
2.2.3 Drawing	18
2.3 Materials	22
2.3.1 Materials used in tissue engineering	22
2.3.2 Polycaprolactone	24
2.4 Functionalization of scaffolds	26
2.4.1 Functionalization in tissue engineering	26
2.4.2 Conductive polymers	28
2.4.3 Polypyrrole	30
2.4.4 Advantages of conductive polymers for tissue engineering .	31
3 Materials and methods	35
3.1 Materials and equipment	35
3.1.1 List of chemicals	35
3.1.2 Primary antibodies	37
3.1.3 Secondary antibodies	37
3.1.4 Primers	37
3.1.5 Commercial kits	38

3.1.6	Cell cultures and animals	38
3.1.7	Polymer solutions	38
3.1.8	Cultivation media and solutions	39
3.1.9	Solutions for biological experiments	40
3.1.10	List of equipment	42
3.1.11	Software	43
3.2	Methods	43
3.2.1	Drawing fibers and their characterization	43
3.2.1.1	Preparation of polymer solutions	43
3.2.1.2	Solution characterization	43
3.2.1.3	Drawing samples	44
3.2.1.4	Fiber characterization and image analysis	45
3.2.1.5	Mechanical testing of drawn fibers	45
3.2.1.6	Functionalization of the fibers by polypyrrole	46
3.2.1.7	Water contact angle (WCA) measurement	46
3.2.1.8	Conductivity measurements	47
3.2.2	Biological testing	48
3.2.2.1	Drawing fibers for the <i>in vitro</i> and <i>in vivo</i> experiments	48
3.2.2.2	<i>In vitro</i> experiments - oriented fibers	49
3.2.2.3	Fabrication of <i>in vivo</i> scaffolds for <i>in vitro</i> testing	51
3.2.2.4	<i>In vitro</i> testing of the <i>in vivo</i> implants	51
3.2.2.5	Surgeries and sample collection	53
3.2.2.6	RNA isolation	55
3.2.2.7	cDNA Synthesis	55
3.2.2.8	qRT-PCR	55
3.2.2.9	Immunohistochemistry	56
3.2.3	Statistics	59
4	Results and discussion	60
4.1	Drawing technology	60
4.2	Influence of the polymer concentration and drawing speed on the fiber diameter	63
4.3	Viscosity and surface tension	69
4.4	Mechanical testing	70
4.5	Functionalization of drawn scaffolds by polypyrrole	73
4.6	Conductivity measurement	75

4.7	Water contact angle	76
4.8	<i>In vitro</i> assessment of sample biocompatibility	78
4.8.1	Fibrous samples drawn in two different directions	78
4.8.2	Fibrous samples coated with polypyrrole	81
4.9	<i>In vivo</i> study - development, construction and characterization of the scaffold	83
4.10	Using drawing for the biocompatibility assessment of fibrous ma- terials	93
4.11	Using drawing for the fabrication of hernia meshes	94
5	Conclusion	96
	Bibliography	99

List of Figures

2.1	Published articles about tissue engineering	5
2.2	Architecture of the spinal cord	6
2.3	Comparison of the microscopic structures of extracellular matrixes and nonwoven textiles	15
2.4	Drawing a polymer fiber from a droplet of polymer solution.	19
2.5	Aligned microfibers and yarns	19
2.6	Structures made from PCL	26
2.7	Drug loading and release from polymeric micro/nanofibers	28
2.8	Chemical structure of representatives of CPs	29
2.9	Schematic illustration of conductivity distribution	29
3.1	Measuring the WCA on the drawn samples	47
3.2	Drawn PPy-PCL fibers fixed within a Teflon frame in between an aluminum foil	48
3.3	Macroscopic picture of <i>in vitro</i> samples fixed within a supporting ring	49
3.4	SEM images of the <i>in vivo</i> and <i>in vitro</i> scaffolds	52
4.1	The manipulator representing the drawing movement	61
4.2	Image of the manipulator	62
4.3	Fibers' morphology depending on the speed of drawing and the polymer concentration	64
4.4	Histograms showing the fiber diameter distribution	65
4.5	SEM image of the fibers drawn from the 8% PCL solution	66
4.6	SEM images showing the morphology of the fibers	66
4.7	Images from SEM showing the drawn fibers of PCL and PVA at different concentrations.	67
4.8	Comparison of viscosities and surface tensions of the polymer so- lutions	69
4.9	Diagram of the tensile curves of the individual measurements	71
4.10	Diagram of the tensile curves with the emphasis on the beginning of the measurement	72

4.11	Macroscopic image of the <i>in vitro</i> samples	73
4.12	SEM images showing the PPy modified PCL fibers	74
4.13	SEM images of PPy coated PCL fibres	74
4.14	The SEM image of the micro fractures of the PPy layer on PCL fibers	76
4.15	The diagram of water contact angles for PCL and PCL-PPy samples.	77
4.16	Comparison of the surface structure of the plain PCL fibers and the PPy coated fibers	78
4.17	Macroscopic image and SEM images of the <i>in vitro</i> samples	79
4.18	Results from the MTT assay of the <i>in vitro</i> experiments	80
4.19	Images from the fluorescent microscope from the <i>in vitro</i> experiments	80
4.20	SEM images of the samples from the <i>in vitro</i> experiments	81
4.21	Images from fluorescent microscope from the <i>in vitro</i> experiments with PPy	82
4.22	Diagram of the viability measured by MTT assay from the <i>in vitro</i> experiments with PPy	83
4.23	The SEM images of the fibers aligned along the channels	84
4.24	Axonal spread and axon elongation <i>in vitro</i>	86
4.25	Lateral hemisection at T9 spinal cord region and the bridge implantation	87
4.26	Immune response to the bridges with PCL / PPy fibers	89
4.27	Quantification of immune response using qPCR	90
4.28	Axon infiltration and myelination 8 weeks after injury	91
4.29	Using the polymer grid made by drawing for the biocompatibility assessment.	93
4.30	Hernia meshes prepared by drawing implanted into rabbits <i>in vivo</i>	95

List of Tables

2.1	Polymer based scaffolds' fabrication techniques in TE	10
2.2	Functions of ECM in native tissues and of scaffolds in engineered scaffolds	16
2.3	General properties of certain natural polymers	23
2.4	Degradable polymers and representative applications	24
2.5	Conductivity of common CPs	30
2.6	Doping levels and conductivities of a variety of CPs	30
2.7	Conducting polymers in biological applications	32
3.12	Sudan Black and β -3-tubulin staining	53
3.13	Gene primers' sequences used for qRT-PCR	56
3.14	Arginase 1, F4/80 staining	57
3.16	NFM 200, MBP, P0, staining	58
4.1	Comparison of the fibers' tension made by different spinning techniques.	71

List of Abbreviations

18S rRNA	18S ribosomal RNA
ATB	Antibiotics
cDNA	Complementary DNA
DAPI	4',6-diamidin-2-fenylindol
DRG	Dorsal root ganglia
FBS	Fetal bovine serum
FITC	Fluorescein isothiocyanate
HBSS	Hanks' balanced salt solution
IgG	Immunoglobulin G
IgY	Immunoglobulin Y
IPA	Isopropyl alcohol
mRNA	Messenger RNA
MTT	3-(4,5-dimethylthiazol-2-yl)-2,5-diphenyltetrazolium bromide
NGF	Neuronal growth factor
NoF	Bridge with no fibers
O/N	Over night
PA-6	Polyamide-6
PBS	Phosphate buffered saline
PCL	Polycaprolactone
PFA	Paraformaldehyde
PLGA	Poly lactide-co-glycolide acid
PMMA	Polymethylmethacrylate
PPy	Polypyrrole
PVA	Polyvinylalcohol
qPCR	Quantitative polymerase chain reaction
RNA	Ribonucleic acid
RT	Room temperature
SEM	Scanning electron microscope / standard error of the mean
TRIS	Trizma hydrochloride solution
TUL	Technical University of Liberec
WCA	Water contact angle

List of Units

kPa	Kilopascal
M	Mole
GΩ	Giga-ohm
G	Gauge
°C	Degree of Celsius
m·s ⁻¹	Meter per second
μl	Microliter
nm	Nanometer
MPa	Megapascal

List of Symbols

Symbol	Name	Unit
a	distance	m
P	power	W ($\text{J}\cdot\text{s}^{-1}$)
ω	angular frequency	rad
σ	tension	MPa
ϵ	relative elongation	%
l	length	mm
t	fiber fineness	tex
s	area	m^2
E	Young's modules	MPa

Chapter 1

Introduction

The first successful organ transplanted to human was kidney in 1954 by Joseph Murray and his team (Murray, Merrill, and Harrison, 1955). This breakthrough gave rise to new fields of reconstructive medicine, the transplantation biology and immunology. Over the next 25 years, transplantations of kidneys together with transplantations of bone marrow evolved rapidly. Transplantations of other organs remained experimental until the late 1970s. Short after the boom of organ transplantations at the late 1970s it started to be evident that even though the organ transplantations were promising and successful way to replace the non-functional organs, the supply of donor organs highly exceeded the demand (Vacanti et al., 1988). It was clear that the inoculation of the cells only will not be sufficient to repair or replace the whole tissue. Even then, scientists knew that there is a need to immobilize the cells within a scaffold. The scaffold should serve as and should resemble a native extracellular matrix, provide the cells suitable environment for proliferation, harbor the cells from the hostile environment and help the cells to survive after implantation. Probably the first experiment carried out with scaffolds seeded with cells and implanted into an animal model was carried out by Vacanti and co-workers in 1988 (Vacanti et al., 1988). They prepared different types of scaffolds (from different polymers and by different techniques), which were seeded with cells isolated either from liver, pancreas or intestine. Seeded scaffolds were implanted into mice 3 to 4 days after cell seeding. These experiments can be definitely considered to be the first evidence of modern tissue engineering. Nevertheless, it took several years to establish this new discipline as an independent scientific field.

Even though tissue engineering is young developing discipline interconnecting a huge variety of sometimes very unrelated scientific disciplines, their goal is the same - to develop and replace nonfunctional tissue.

In the case of healing the spinal cord, tissue engineering might be one of the key approaches. Each year 250,000 to 500,000 people in the world suffer from spinal cord injuries (World Health Organization, 2013), with the annual incidence of 17 thousand people in the USA. In the Czech Republic, the annual incidence of acute spinal cord injury ranges between 250 and 300 cases (Kriz et al., 2017). These pathologies represent a great health risk for patients. It affects their quality of life, the incorporation of the patients back into society and increases the costs of living. And yet, there is no effective treatment for spinal cord injuries. Current treatment options are the use of high dose methylprednisolone to suppress the immune system and decrease inflammation, surgical intervention to stabilize and decompress the spinal cord and rehabilitative care (Mothe and Tator, 2013). However, none of these approaches does support active regeneration of neural tissue. Therefore, enormous efforts are being made to enable neural regeneration by various approaches. Neural tissue engineering offers a promising approach to treating nervous system injuries. But scaffolds alone are not sufficient for the regeneration of neural tissue. Neural cells proliferate through the injury with difficulties and do not extend their neurites enough, the cells forming glial scars instead (Li and Lepski, 2013). In the literature, there are studies into the implementation of stem cell therapy and the combination of stem cells with various types of scaffolds (Liu et al., 2012). Although, hydrogels (from synthetic or natural polymers) are very favored materials because they are able to mimic the mechanical properties of natural tissues due to their high water content (Grijalvo et al., 2019), fabrication of fibrous scaffolds for neural tissue engineering is also highly pronounced. Nowadays, electrospinning is mainly used to prepare fibrous scaffolds for neural tissue engineering due to its versatility to use different polymers (Yang et al., 2004; Novikova et al., 2008; Lee et al., 2009). Scaffolds are made from synthetic (poly- β -hydroxybutyrate - PHB, poly(lactic-co-glycolic acid) - PLGA) (Yang et al., 2004; Novikova et al., 2008; Lee et al., 2009) as well as bio-polymers (collagen) (Liu et al., 2012), but the results of these studies of neural regeneration are often inconsistent and neither of which has been successfully introduced into practice so far. The latest studies show that the future for neural scaffolds is in the combination of methods for scaffold fabrication with surface functionalization and drug release (Chudickova et al., 2015; Dumont et al., 2018; Smith et al., 2019).

It has been shown that the neural cells prefer aligned scaffolds that guide their neurite outgrowth (Corey et al., 2007). They also prefer microfibers instead of nanofibers; microfibers promote the neurite extension better than nanofibers. The aligned microfibers also promote the migration of Schwann cells (Wang

et al., 2010). And there are also many other factors that can influence neuron proliferation and neurite extension, such as the use of conductive polymers (Guimard, Gomez, and Schmidt, 2007; Lee et al., 2009), and the addition of growth factors and other signal molecules (Chudickova et al., 2015).

The goal of this work is to develop and optimize functional scaffold, which will foster the growth of neural cells and neurite outgrowth enough to bypass the injury and which will promote the recovery of neurotransmission. To achieve this goal, various techniques of scaffold fabrication and surface modification were combined. Drawing was used to prepare oriented microfibers. The surface of these microfibers was further functionalized with polypyrrole and such scaffolds were incorporated into the complex composite spinal cord implant to enhance the infiltration of neural cells into the inner structure.

Chapter 2

Summary

This thesis is focused on the fabrication of scaffolds with oriented structure made by drawing, which are used for neural tissue engineering, specifically spinal cord. There are many approaches dealing with the healing of the spinal cord, including various nonwoven technologies or specific functionalization techniques. Drawing is very specific method of fiber fabrication, which produces highly oriented structures and would thus be very promising method of choice for such application.

2.1 Tissue engineering

Tissue engineering is a multidisciplinary field combining diverse scientific disciplines ranging from engineering, material sciences to cell biology, immunology, medicine and many others. And even though the idea of tissue replacement accompanies the humankind from time immemorial, the term “tissue engineering” was first, but loosely used since the mid 1980'. However, by that time it was mostly used for the manipulation with tissues, organs or when using prosthetics. The beginning of the independent scientific discipline called tissue engineering, as we know it today, is dated to 1988 and attributed to J. Vacanti (Vacanti, 2006; Meyer, 2009). Since that time the number of publications related to tissue engineering grows exponentially every year reaching over 85 thousand titles in 2020 (total) (*Web of Science [v.5.34] - Web of Science Core Collection Result Analysis 2020*), out of which, over 3,000 publications are related to neural tissue engineering.

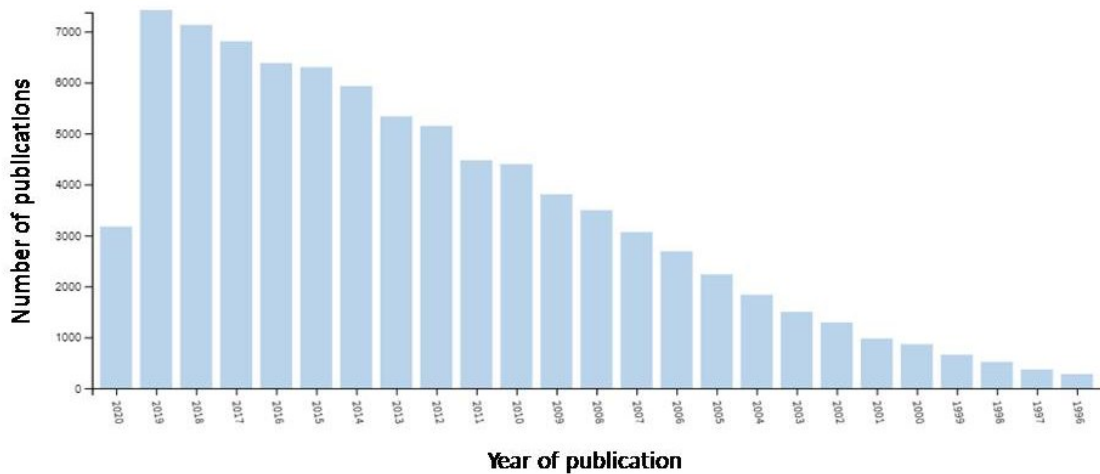


FIGURE 2.1: Diagram of the numbers of published articles about tissue engineering. (*Web of Science [v.5.34] - Web of Science Core Collection Result Analysis 2020*)

Tissue engineering is using scaffolds to replace the impaired tissue. Scaffolds should mimic the extracellular matrix (ECM) of the native tissue. They support the cells and guide the cells' growth to form the desired tissue, and they provide mechanical stability of the nascent tissue (Theocharis et al., 2016). The requirements for the scaffold vary according to the targeted tissue. Biocompatibility is the key factor of each scaffold. Other requirements as mechanical properties and scaffold architecture consistent with the targeted tissue are no less important. Additionally, bioactivity or in some cases even biodegradability of the scaffold can be beneficial. Depending on the tissue being replaced, its architecture and properties, the appropriate combination of method of scaffold fabrication and material is chosen to address the structural, mechanical, biochemical, physical and other properties of the tissue (O'Brien, 2011).

2.1.1 Neural tissue engineering with emphasis on spinal cord injuries

Neural tissue is highly organized structure. It is divided in to the central and peripheral nervous system (CNS and PNS, respectively). It is built from many types of neural and supporting cells, which form various structures as nerves, spinal cord to the brain tissue (Fig. 2.2). The neural cells, which are responsible for the transmission of the action potential (neural signal), have many cytoplasmic projections called dendrites (conduct impulses towards the cell body) and axons (conduct impulses away from cell body) which can be up to tens of centimeters

long. Depending on the architecture of dendrites and axons we distinguish between the anaxonic, bipolar, unipolar and multipolar neurons. They are usually site specific for different neural structures and function. The supporting cells called neuroglia are also specific for the CNS (microglia, astrocytes, oligodendrocytes, ependymal cells) and for the PNS (Schwann cells, satellite cells). They preserve the physical and biochemical structure of neural tissue.

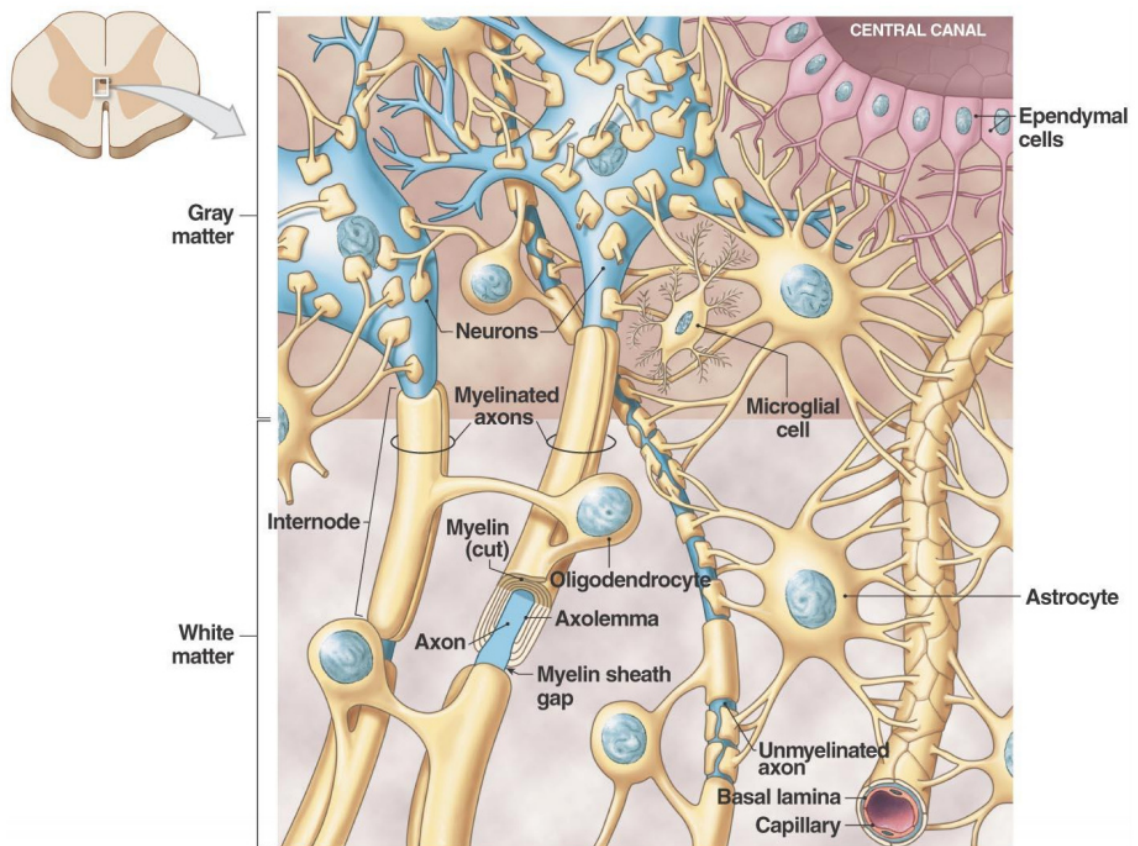


FIGURE 2.2: Diagram of the neural cells' architecture in the white and gray matter of the spinal cord (downloaded from (LaPres, 2009))

There are studies using the cell therapy for spinal cord injuries by implanting stem cells into the injury site *in vivo* (Vawda et al., 2019). Some researchers use the stem cells in the combination of carrier scaffold for the cells (Liu et al., 2012; Dumont et al., 2018). There are also ongoing clinical trials implanting stem cells (clinicaltrials.gov). Yet, none of such research was translated into the practice. One of the main reasons is the poor regeneration capability of the neural tissue. The neural cells have slow proliferation rate, the axons do not extend enough to reconnect and the injury site is filled with fibroblasts instead, forming

a glial scar (Li and Lepski, 2013). Once the glial scar is formed it acts as physical and chemical barrier which prevents repair and regeneration of the damaged neural tissue.

Because the neural tissue suffers from poor regeneration potential, it is desirable in neural tissue engineering to design complex scaffolds, which will support the cell attachment, proliferation, axon elongation and myelination. This will be achieved by a combination of various scaffold fabrication techniques and functionalization.

The spinal cord is a highly organized structure with predominantly rostral-caudal alignment of axons and myelin. Thus, the aligned spinal cord implants represent ideal microenvironment for directed axonal growth (Pawar et al., 2015). Moreover, those polymer spinal cord bridges are characterized by high degree of porosity, allowing for infiltration of progenitors that differentiate into myelinating oligodendrocytes resulting in axon re-growth and also myelination of these axons (Thomas et al., 2013). On the other hand, such polymeric spinal cord implants do not meet other biophysical parameters of the spinal cord, as modulus and viscoelastic properties (Thomas et al., 2013). One possibility is to inject the hydrogels directly into the injury site (Macaya and Spector, 2012). The big advantage of such *in situ*-forming scaffold is that there is no need for surgical invasive procedures, the hydrogels can conform specifically to the shape of the defect and can create an integrative implant–tissue interface. On the other hand, these injectable materials do not have a high degree of control over the porosity or alignment and do not provide good axonal guidance (Rose et al., 2018). To overcome the problem with the cell guidance and directional growth, hydrogels can be mixed e.g. with magnetically responsive additives such as superparamagnetic iron oxide nanoparticles (Rose et al., 2018). Alternatively, the hydrogels can be mold in specific shapes prior to implantation. The hydrogel implants can thus provide an orientation to guide axon regeneration following spinal cord injury. For instance, photosensitive hydrogels can utilized by stereolithography to form specific 3D implants (Arcaute, Mann, and Wicker, 2010). Eventually, the primary hydrogel beads are annealed into a tubular structure, which is later assembled into a larger implant filling the injury (Dumont et al., 2019). The advantage of this approach is that the hydrogel microspheres control the porosity of the structure and facilitate regenerative support cells.

Other group of spinal cord implants are non-woven fibrous scaffolds, out of which the aligned fibrous scaffolds had been shown as the most suitable ones

in vitro (Corey et al., 2007). The oriented structure guides the cell growth and orientation of the cytoplasmic projections in the direction of the fiber alignment. This phenomenon is especially important in the axon orientation. The aligned fibrous scaffold could enhance the axon elongation and could improve the axon guidance in the required direction. This would lead to reconnection of the interrupted axons and to the functional recovery.

Oriented structures in tissue engineering are most often prepared by electrospinning using different polymers (Yang et al., 2004; Novikova et al., 2008; Lee et al., 2009). Eventually, forcespinning can be used to prepare oriented fibers as well (Li et al., 2003; Liu et al., 2013). Different studies used synthetic (poly- β -hydroxybutyrate - PHB, poly(lactic-co-glycolic acid) - PLGA) (Yang et al., 2004; Novikova et al., 2008; Lee et al., 2009) as well as natural polymers (collagen) (Liu et al., 2012). These methods produce mainly nanofibers and are reasonably productive. On the other hand, the degree of orderliness of the fibers is often not very high, but can be sufficient depending on the application. Nevertheless, it was shown that the neural cells prefer microfibers to nanofibers (Wang et al., 2010). The axons elongate along the microfibers compared to nanofibers where the cells spread their axons in all directions. Also, the oriented fibers support the migration of Schwann cells (Wang et al., 2010), which are crucial for the tissue regeneration and proper function of the tissue.

Nevertheless, the fibrous scaffolds alone are not sufficient enough to support the full regeneration of the injured tissue and further functionalization or combination of several methods is needed. Some approaches use growth factors or other signaling molecules to functionalize the surface of the scaffolds (Chudickova et al., 2015). Furthermore, it is possible to use advanced molecular techniques such as lentivirus delivery into the implant to deliver specific anti-inflammatory molecules (Park et al., 2018) or molecules supporting the neural cells' regeneration (Tuinstra et al., 2013). It is also possible to modify the surface by conducting polymers such as polypyrrole, polyaniline and others (Guimard, Gomez, and Schmidt, 2007; Lee et al., 2009). It had been shown that the conducting polymers promote the axon elongation and they also promote the propagation of action potential along the neural cell. Transmission of the action potential is a crucial property of the neural cells which leads to functional recovery of the whole system (Zeng et al., 2013; Yang et al., 2015). Due to the enormous complexity and functional specificity of the neural tissue it is necessary to combine various techniques of scaffold fabrication and its functionalization (Chudickova et al., 2015; Dumont et al., 2018; Park et al., 2018).

2.2 Scaffolds

2.2.1 Scaffold fabrication techniques

Depending on the scaffold's application, suitable fabrication method is used (Table 2.1). Below are listed some of the methods that can be used depending on the achieved final structure of the scaffold.

Highly porous structures can be made by solvent casting / particle leaching method for preparing scaffolds for orthopedics (Mikos et al., 1993; Prasad, Sankar, and Katiyar, 2017). Another approach is gas foaming / salt leaching method used for example for fabrication of spinal cord bridges (Mooney et al., 1996; Yang et al., 2009).

Microspheres can be made by various techniques as well, of which solvent evaporation (Woo et al., 2001), freeze drying (Kim and Park, 2004; Quian and Zhang, 2013), cryopreparation (Ando et al., 1999; Yang et al., 2005b), or even electro-spraying (Zhou et al., 2019; Giménez et al., 2020) can be named. These methods are most widely used in the drug / protein / DNA delivery systems and for the gradual release of these substances.

Very popular these days are scaffolds made by inject printing (Yeong et al., 2006) or melt-based rapid prototyping (Mironov et al., 2003; Rampichova et al., 2018). These methods are usually used for fabrication of whole 3D organs, namely e.g. cartilage, bone and others.

Interesting method of scaffold preparation is the decellularization process (Cebotari et al., 2002; Hopkins, 2005). This method is completely different from the other mentioned. It uses native tissue as template, washes out all the cells, but preserves its extracellular matrix, which then serves as scaffold.

Nevertheless, from all of the methods available, probably the most widely used methods nowadays are the nonwoven techniques. They produce fibrous matrix (nano- and microfibers) resembling the extracellular matrix. Worth mentioning is definitely electrospinning (Prabhakaran et al., 2008; Duan et al., 2013; Krchová et al., 2014; Horakova et al., 2018), melt-blown (Erben et al., 2015, Erben et al., 2016) or centrifugal spinning (Li et al., 2019; Lukášová et al., 2019). Electrospun scaffolds are mainly used for wound healing, neural tissue regeneration, vascular grafts fabrication and others. Centrifugal spinning yields fluffy structure and is thus suitable for loading with cells or cell derivatives as platelets and is further used for other tissue engineering applications. Melt-blown also produces mainly fluffy structure and was used for example for bone tissue engineering. But there

are other nonwoven techniques which have a big potential in tissue engineering such as drawing (Tokarev et al., 2015; Yuan, Cambron, and Keynton, 2015; Strnadová et al., 2019) or AC spinning (Pokorny et al., 2014).

TABLE 2.1: Polymer based scaffolds' fabrication techniques in tissue engineering applications (Dhandayuthapani et al., 2011)

Method	Polymers	Unique factors	Application
Biodegradable porous scaffold fabrication			
Solvent casting/salt leaching method	Absorbable polymer (PLLA, PLGA, collagen, etc.)	Biodegradable controlled porous scaffolds	Bone and cartilage tissue engineering
Ice particle leaching method	PLLA & PLGA	Control of pore structure and production of thicker scaffolds	Porous 3D scaffolds for bone tissue engineering
Gas foaming/salt leaching method	PLLA, PLGA & PDLA	Controlled porosity and pore structure sponge	Drug delivery and tissue engineering
Microsphere fabrication			
Solvent evaporation technique	PLGA, PLAGA	High-density cell culture, due to the extended surface area	Bone repair
Particle aggregated scaffold	Chitosan, HAP	High mechanical stability	Bone, cartilage, or osteochondral tissue engineering
Freeze drying method	PLGA, PLLA, PGA, PLGA/PPF Collagen, and Chitosan	3D porous sponge structure durable and flexible	Tissue engineering scaffolds
Thermally induced phase separation	PEG, PLLA	Highly porous scaffold for cellular transplantation	Complicated shapes for tissue engineering applications
Injectable gel scaffold fabrication			
Ceramic-based injectable Scaffolds	CP ceramics, HAp, TCP, BCP and BG	Porosity and biore-sorbability	Cartilage tissue engineering

Hydrogel-based injectable scaffolds	Hydrophilic/ hydrophobic diblock and triblock copolymer combinations of PLA, PGA, PLGA, and PEG. Copolymers of PEO and PPO and polyoxamer, alginates, collagen, chitosan, HA, and fibroin	Biomimetically, exhibit biocompatibility and cause minimal inflammatory responses, thrombosis, and tissue damage	Cartilage, bone tissue engineering, and drug delivery
Hydrogel scaffold fabrication			
Micromolding	Alginate, PMMA, HA, PEG	Microgels, biologically degradable, mechanical and physical Complexity	Microgels, microsensors, cell-based diagnostics
Photolithography	Chitosan, fibronectin, HA, PEG, PNIAAm, PAA, PMMA, PAam, and PDMAEM	Microwells, microarrays, controlled size and shape	Microdevices, biosensors, growth factors, matrix components, forces, and cell-cell interactions
Microfluidics	PGS, PEG, calcium alginate, silicon and PDMS	Microbeads, microrods, valves, and pumps	Sensing, cell separation, cell-based microreactors, and controlled microreactors
Emulsification	Gelatin, HA, and collagen	Microgels, microsensors, cell-based diagnostics	Sustainable and controllable drug delivery therapies
Emulsification	Gelatin, HA, and collagen	Microgels, microsensors, cell-based diagnostics	Sustainable and controllable drug delivery therapies

Acellular scaffold fabrication			
Decellularisation process	Biological tissues	Retain anatomical structure, native ECM, and similar biomechanical properties	Tissue engineering
Keratin scaffold fabrication			
Self-assembled process	Keratin	Biocompatibility	Drug delivery, wound healing, soft tissue augmentation, synthetic skin, coatings for implants, and scaffolds for tissue engineering
Fibrous scaffold fabrication			
Nanofiber electrospinning process	PGA, PLA, PLGA, PCL copolymers, collagen, elastin, and so forth	High surface area, biomechanical, and biocompatibility	Drug delivery, wound healing, soft tissue synthetic skin, and scaffolds for tissue engineering
Microfiber wet-spinning process	PLGA, PLA, chitosan, and PCL	Biocompatible fibres with good mechanical properties	Solar sails, reinforcement, vascular grafts, nonwetting textile surfaces, and scaffolds for tissue
Nonwoven fibre by melt-blown process	Polyesters, PGA, and PDO	Submicron fiber size, highly porous scaffold	Filtration, membrane separation, protective military clothing, biosensors, wound dressings, and scaffolds for tissue engineering

Functional scaffold fabrication			
Growth factor's release process	Growth factor's release process	Membranes, hydrogels, foams, microsphere, and particles	Angiogenesis, bone regeneration, and wound healing
Ceramic scaffold fabrication			
Sponge replication method	PU sponge, PVA, TCP, BCP or calcium sulfate	Interconnected porous ceramic scaffolds	Bone tissue engineering
Simple calcium phosphate coating method	Coating on: metals, glasses, inorganic ceramics and organic polymers (PLGA, PS, PP, silicone, and PTFE), collagens, fibres of silk, and hairs	Improve biocompatibility or enhance the bioreactivity	Orthopedic application
Automation and direct organ fabrication			
Inkjet printing process	Sodium alginate	To build complex tissues composed of multiple cell types (Hydrogel scaffold)	Biosensor development, microdeposition of active proteins on cellulose, biochips and acellular polymeric scaffolds
Melt-based rapid prototyping Process	Biodegradable polymers or Blends	Complex 3D solid object, good mechanical strength	Honey comb structure scaffold, hard-tissue scaffolds
Computer-aided design (CAD) data manipulation techniques		Design and fabrication of patient-specific scaffolds and automated scaffold assembly algorithm	Develop a program algorithm that can be used to design scaffold internal architectures
Organ printing	Tubular collagen gel	Layer by layer deposition of cells or matrix	To print complex 3D organs with computer-controlled

All the above mentioned methods of scaffold fabrication as well as the used materials define the surface structure and properties, which are very important features of the scaffold. They affect the biocompatibility of the material, cell adhesion and proliferation. Nowadays, we can combine various techniques and materials together to achieve specific characteristics of the fabricated scaffold and thus enhance the biocompatibility (Erben et al., 2016; Rampichova et al., 2018; Fuchs et al., 2019; Romanova et al., 2019). Moreover, the surface properties can be modified by functionalization step. There are many ways how to functionalize the scaffold (section: 2.4) from different surface modification techniques (Lerman et al., 2019; Lukasek et al., 2019; Peng et al., 2019), various drug delivery (Mickova et al., 2012; Buzgo et al., 2013; Wang and Windbergs, 2019) / gene delivery systems (Laporte, Yan, and Shea, 2009; Park et al., 2018) to loading the scaffolds with specific cell lines (Dumont et al., 2018; Hausherr et al., 2018).

2.2.2 Nonwovens in tissue engineering

In general, very promising methods currently used in tissue engineering are non-woven technologies. These technologies produce micro- and nanofibers, which resemble the fibrous extracellular matrix of native organs (Fig. 2.3). Depending on the targeted tissue, its architecture and physical and mechanical properties, the method of scaffold fabrication and the polymer are chosen (Table 2.2).

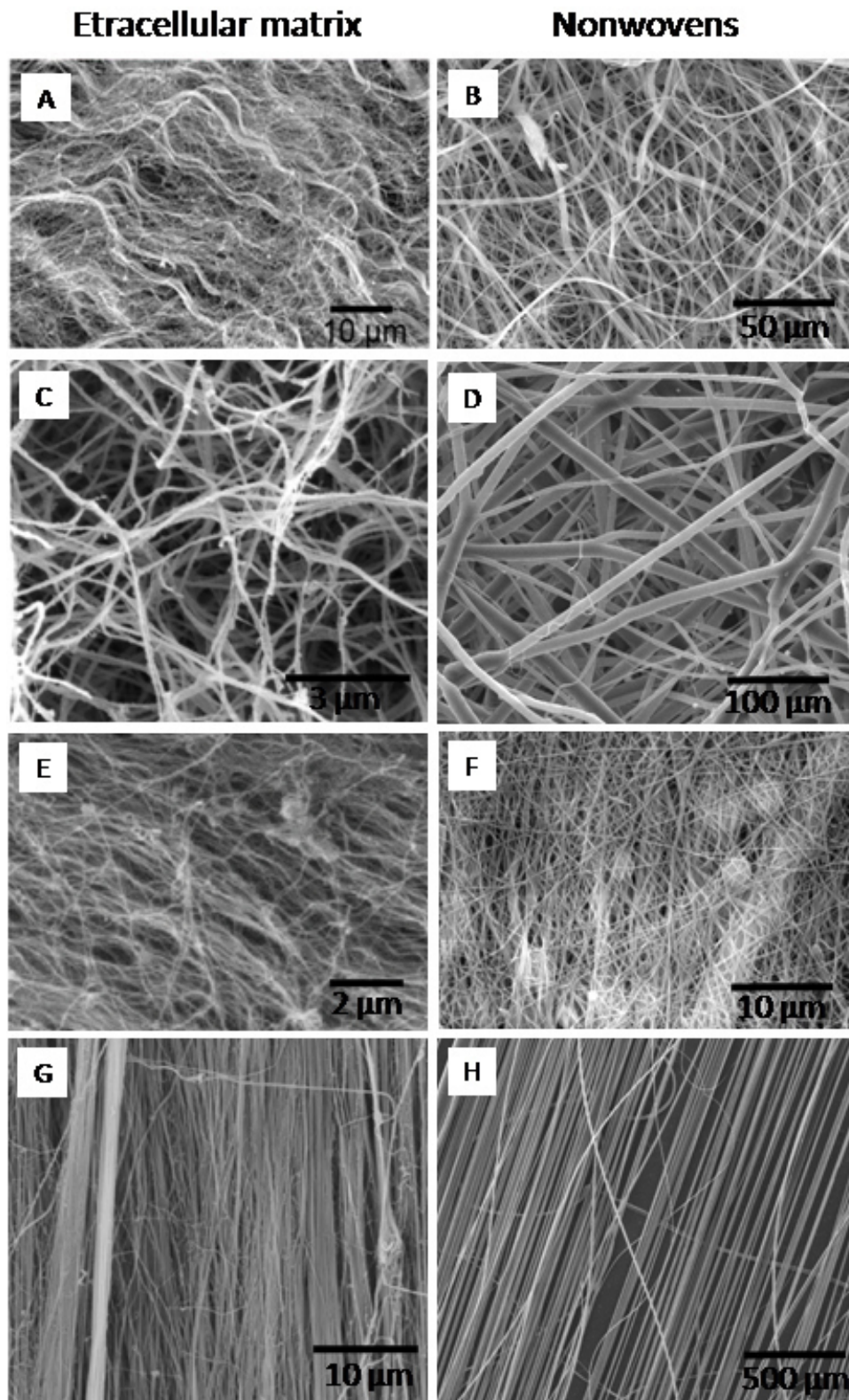


FIGURE 2.3: Comparison of SEM images of the extracellular matrixes and nonwoven textiles. (A) ECM of the decellularized porcine aortic valve (scale bar: 10 μm) (Ye et al., 2013), (B) Force-spun PCL fibers (scale bar: 50 μm), (C) Fibrin clots (scale bar: 3 μm) (Neergaard-Petersen et al., 2013), (D) Melt-blown PCL fibers (scale bar: 100 μm), (E) ECM of the decellularized bovine corneal stroma (scale bar: 2 μm) (Dai et al., 2012), (F) Electrospun PCL fibers (scale bar: 10 μm), (G) ECM of the decellularized tendon (scale bar: 10 μm) (Youngstrom et al., 2013), (H) Drawn PCL fibers (scale bar: 500 μm).

TABLE 2.2: Functions of ECM in native tissues and of scaffolds in engineered scaffolds (Chan and Leong, 2008)

Functions of ECM in native tissues	Analogous functions of scaffolds in engineered tissues	Architectural, biological, and mechanical features of scaffolds
1. Provides structural support for cells to reside	Provides structural support for exogenously supplied cells to attach, grow, migrate and differentiate <i>in vitro</i> and <i>in vivo</i>	Biomaterials with binding sites for cells; porous structure with interconnectivity for cell migration and for nutrients diffusion; temporary resistance to biodegradation upon implantation
2. Contributes to the mechanical properties of tissues	Provides the shape and mechanical stability to the tissue defect and gives the rigidity and stiffness to the engineered tissues	Biomaterials with sufficient mechanical properties filling up the void space of the defect and simulating that of the native tissue
3. Provides bioactive cues for cells to respond to their microenvironment	Interacts with cells actively to facilitate activities such as proliferation and differentiation	Biological cues such as cell-adhesive binding sites; physical cues such as surface topography
4. Acts as the reservoirs of growth factors and potentiates their actions	Serves as delivery vehicle and reservoir for exogenously applied growth-stimulating factors	Microstructures and other matrix factors retaining bioactive agents in scaffold
5. Provides a flexible physical environment to allow remodeling in response to tissue dynamic processes such as wound healing	Provides a void volume for vascularization and new tissue formation during remodeling	Porous microstructures for nutrients and metabolites diffusion; matrix design with controllable degradation mechanism and rates; biomaterials and their degraded products with acceptable tissue compatibility

There is a wide range of synthetic as well as natural polymers, containing both biodegradable and non-biodegradable polymers, which can be utilized by the nonwoven technologies. Typical synthetic degradable polymers are polycaprolactone (PCL) (Ebersole et al., 2012; Erben et al., 2015), poly(lactic-co-glycolic acid) (PLGA)(Wang et al., 2017), poly-L-lactic acid (PLLA) (Yang et al., 2004, Yang et al., 2005a), polyvinylalcohol (PVA) (Porto et al., 2019), or polyethylene glycol (PEG) (Dumont et al., 2019). From the non-biodegradable polymers,

polyamide-6 (PA6) (Valtera et al., 2019), polyvinylbutyral (PVB) (Valtera et al., 2019), polyurethane (PU) (Khil et al., 2003), or poly- β -hydroxybutyrate (PHB) (Novikova et al., 2008) can be named.

The most widely used natural polymers are silk (Wenk, Merkle, and Meinel, 2011), collagen (Fullana and Wnek, 2012; Bacakova et al., 2017), gelatin (Adeli-Sardou et al., 2019), fibrin (Bacakova et al., 2017), hyaluronic acid (Qian et al., 2015), and others. Usually, the biopolymers are combined with synthetic polymers due to the better spinnability and to achieve desired mechanical and functional properties of the scaffold (Schnell et al., 2007; Ghasemi-Mobarakeh et al., 2008; Wenk et al., 2009; Duan et al., 2013). The combination of synthetic polymers with biopolymers enhances the scaffold's cytocompatibility, modifies the cellular response and enhances the cell adhesion, because often these natural polymers are part of the native ECM.

Depending on the used method, the polymers can be combined by various approaches. Polymer blends are mixtures of different polymers, which are then spun together, resulting in the fibers with randomly distributed polymers within the fiber (Schnell et al., 2007; Ghasemi-Mobarakeh et al., 2008). The second approach is to spin two or more polymers separately from separate reservoirs, resulting in the scaffold with two or more types of fibers. The polymers can be either spun together, the fibers are mixed randomly, or individually one by one, the fibers form different layers (Fu et al., 2014). The third approach is the co-axial spinning, which results in the formation of the core-shell fibers (Buzgo et al., 2013; Wang and Windbergs, 2019). Different approach is to use co-polymers, which are then spun with desired method (Rentsch et al., 2014; Horakova et al., 2018).

Considering various nonwoven technologies, morphologically different scaffolds can be prepared. Most of the methods produce meshes with randomly oriented nano- / microfibers (Qu et al., 2013; Erben et al., 2015). The fiber diameter is influenced by the method itself (e.g. melt-blown produces mainly microfibers), but also by the used polymer, solvent system and also by the machine settings (Yang et al., 2005a; Wang et al., 2010). The thickness of the scaffold can be controlled by the spinning settings as well, although, some techniques produce thicker structures than others (e.g. melt-blown) (Erben et al., 2015, Erben et al., 2016), thus producing 3D scaffolds rather than thin layers (e.g. electrospinning) (Wang et al., 2010; Qu et al., 2013). Also, some of the methods can be adjusted to produce oriented structures. It can be achieved either by using the rotating collector in the case of electrospinning (Yang et al., 2004; Novikova et al., 2008; Lee et al., 2009), or by changing the rotation speed of the nozzle in the case

of forcespinning (Li et al., 2003; Liu et al., 2013; Badrossamay et al., 2014). Different case is the method called drawing, where the single fibers are produced by mechanical force only and can be placed in any direction, thus controlling the orientation of single fibers (Yuan, Cambron, and Keynton, 2015; Strnadová et al., 2020).

Regarding the nonwoven technologies, the most widely used method in TE is definitely direct current (DC) electrospinning. Electrospinning produces micro- to nanofibrous mats, which are widely used as wound dressings (Rujitanaroj, Pimpha, and Supaphol, 2008; Krchová et al., 2014; Vázquez-Torres et al., 2019), vascular grafts (Wang et al., 2017; Horakova et al., 2018), hernia meshes (Ebersole et al., 2012), or for tendon (Olvera et al., 2019; Ramos et al., 2019) or bone repair (Carvalho et al., 2019), or even for neural tissue repair (Qu et al., 2013; Zeng et al., 2013; Yang et al., 2015).

Centrifugal spinning or melt-blown uses either centrifugal force or airflow, respectively, to produce fibers. They can be used for production of thin layers as well as thicker fluffy scaffolds (Rampichová et al., 2014; Erben et al., 2015, Erben et al., 2016; Lukášová et al., 2019). Such scaffolds can be used for bone / cartilage replacement.

Another promising nonwoven technique is AC (alternating current) electrospinning (Kessick, Fenn, and Tepper, 2004; Pokorny et al., 2014; Valtera et al., 2019). AC electrospinning has no need for a collector compared to DC electrospinning, producing a smoke-like plume of nanofibers. It is highly productive method, but it was not used in tissue engineering so far.

Very unique nonwoven method is drawing. Drawing uses mechanical power to pull fibers from polymer solution or melt. Its uniqueness lies in the single fiber production enabling to produce very specific structures (Yuan, Cambron, and Keynton, 2015; Strnadová et al., 2019). This could be advantageous in tissues with oriented structure, e.g. tendons, nerves or neural tissue in general.

2.2.3 Drawing

Drawing is one of the many non-woven techniques, which can be used for scaffold preparation. Drawing is a method of pulling a single fiber from a droplet of polymer solution without using an electrical field (Fig. 2.4) (Boys, 1887; Ondarcuhu and Joachim, 1998), and it is possible to do it even by hand. The fibers can be made from various types of polymers, varying in diameter from nano-

to micro-scale. Also, different structures can be obtained; it depends on the direction of the fiber-pulling, the combination of nano- and microfibers, and the combination of polymers. With additional processing we can also obtain yarns (Fig. 2.5).

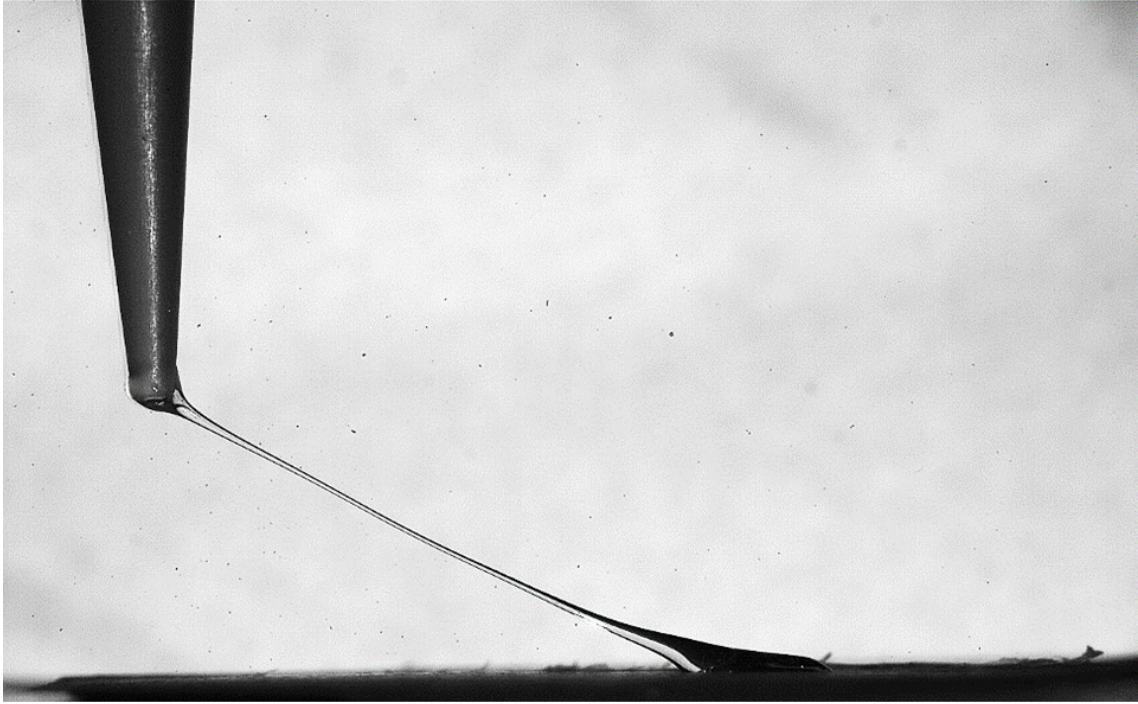


FIGURE 2.4: Drawing a polymer fiber from a droplet of polymer solution.

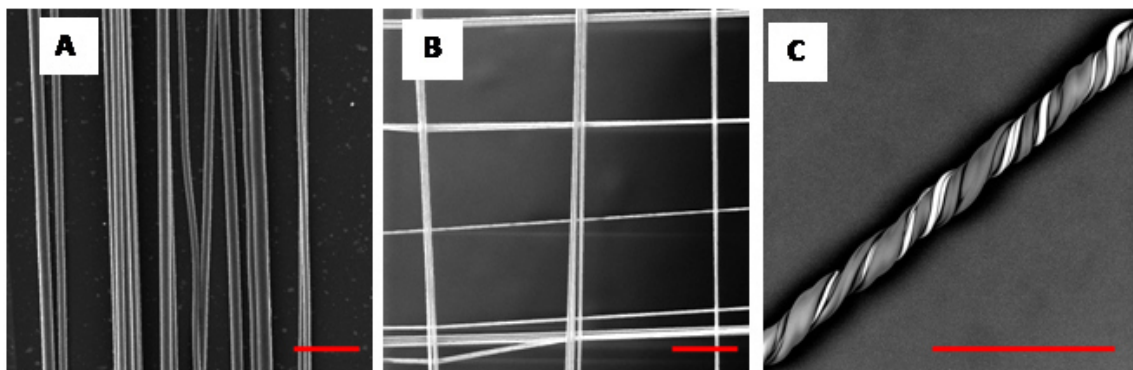


FIGURE 2.5: Aligned microfibers made by drawing from polycaprolactone, oriented either in one (A) or in two (B) directions (scale bar: $100\ \mu\text{m}$). C: Yarn made from different types of polymers (PVB and PVA) (scale bar: $240\ \mu\text{m}$). (Stanislav and Bajáková, 2013)

Mechanical drawing of fibers has been known for centuries. It can be divided into two categories: drawing from a melt (Xing, Wang, and Li, 2008) or a solution (Nain, Amon, and Sitti, 2005, Nain, Amon, and Sitti, 2006; Nain et al., 2006; Yang et al., 2008). The first attempt to draw a fiber was already realized in the 19th

century. The fiber was prepared by shooting an arrow from a droplet of a melted polymer by a crossbow (Boys, 1887). The resulting fiber was several hundreds of meters long. By that time there was no imaging technique available to examine the fiber diameter. Nevertheless, by using the existing instruments they estimated the fiber diameter to be under 2,5 μm (Boys, 1887). In 1988, Vacanti *et al.* (Vacanti et al., 1988) used drawn fibers (drawn from molten polymers, 30 μm in diameter) for one of the first experiments in the tissue engineering field. Since then, nobody showed any interest into this method. In 1998 a modern experiment on a microscopic scale was conducted by Ondarcuhu and coworkers. They were able to draw a single nanofiber from a droplet of a polymer solution using a retracting tip of STM (Scanning Tunneling Microscope). The fiber was tens of nanometers in diameter and was hundreds of micrometers long (Ondarcuhu and Joachim, 1998). Nowadays, drawing is used to produce fibers mainly for optical devices: optical sensing, nanophotonic fibers in the range of tens of nanometers in diameter and up to tens of centimeters in length (Gu et al., 2008; Xing, Wang, and Li, 2008; Yang et al., 2008; Meng et al., 2011).

Drawing is not common method when talking about tissue engineering. One of the reasons can be the low productivity of fibers compared to other nonwoven technologies, e. g. electrospinning, forcespinning, melt-blown and others, which are often used for fabrication of micro- or nanofibers from various types of polymers (Yarin, Pourdeyhimi, and Ramakrishna, 2014). They are reasonably productive, nevertheless, they can produce the oriented structures just in layers, and often the orderliness is not so accurate as well. The other reason, why drawing is not widely used, might be the lack of information about the fiber production as well. It is known that the fiber drawing is influenced by various extrinsic parameters as humidity, temperature, solvent evaporation, trajectory and the speed of drawing (Nain, Amon, and Sitti, 2005, Nain, Amon, and Sitti, 2006; Nain et al., 2006). Also the concentration of the polymer solution as well as the molecular weight of the polymer play very important role in drawing (Mckinley and Sridhar, 2002). Often, these correlations are described just theoretically, occasionally by basic experiments, but the description of the physical principles is missing.

On the other hand, even Vacanti in 1988 used drawn fibers as one of the scaffolds in his experiments (Vacanti et al., 1988). He had drawn the fibers from a polymer melt, the fibers were 30 μm in diameter and formed tufts. He seeded the tufts with cells and implanted them into rats and mice to examine the biocompatibility, angiogenesis and immune response (Vacanti et al., 1988). Recently, drawing was used to fabricate various random and oriented polymers structures by S. Minko

and colleagues (Tokarev et al., 2015), or by R. S. Keynton and co-workers (Yuan, Cambron, and Keynton, 2015).

In contrast to other methods, drawing has lower fiber productivity, but is able to produce highly oriented structures and patterns. This is enabled due to the manipulation of a single fiber. Every single emerging fiber can be manipulated while drawing. This way we can prepare more complicated structures and patterns. Even though electrospinning with a rotational collector provides aligned fibers as well (Li et al., 2003), the fibers can be oriented just in one direction in one layer without the possibility to manipulate the fibers, thus unable to provide more sophisticated fibrous structures. These features make drawing a suitable method for the fabrication of scaffolds for specific tissues with oriented extracellular matrix and cells. Muscles and tendons are a good example of such tissue. Another use of these scaffolds could be in neural tissue engineering. The neural tissue as nerves have highly oriented structure. Even the neural cells alone, specifically their axons need to be extended and oriented in specific direction. It had been shown previously that oriented scaffolds enhance the axon elongation and orientation along the fibers (Novikova et al., 2008; (Lee et al., 2009); Wang et al., 2010; Yang et al., 2015). So this makes drawing the method of choice for such application.

Due to the possibility of manipulation with single fiber during drawing we can prepare various fibrous patterns. This feature opens up new possibilities of application. One of them is definitely the hernia, or rather the hernia meshes (see chapter 4.11).

Other promising field of study is the life cell imaging of the cell behavior on the polymer grids made by drawing. This method enables us to study the biocompatibility of the used material by following the cell behavior in contact with the polymer fiber. By drawing we can define the spacing between the fiber and thus define the size of the pores. The big advantage of this approach is that we track the cells life with no need of any fluorescent staining. This is completely impossible to do with other nonwoven textiles (see chapter 4.10).

2.3 Materials

2.3.1 Materials used in tissue engineering

Materials used in tissue engineering can be divided to several groups, i. e. metals, ceramics (including carbons, glass-ceramics, and glasses), polymers and natural materials (including those from both plants and animals). It is essential to recognize that no one material is suitable for all biomaterial applications. Thus, very often, the combination of different materials is favorable. Such materials are called composites (Ratner et al., 2013; Rampichova et al., 2018).

Metals mechanically and chemically stable and immunologically inert and are mostly used for replacement or reinforcement of hard tissue, i.e. orthopedic implants, prostheses, bone replacement, oral, maxillofacial implants, periodontal treatment, alveolar ridge augmentation and others. The implants are mostly prepared by investment casting (the “lostwax” process), conventional and computer-based machining (CAD/CAM), forging, powder metallurgical processes (e.g., hot isostatic pressing, or HIP), and a range of grinding and polishing steps. There is a variety of methods because different alloys often require different fabrication process. Another step in the fabrication process is the surface treatment, which involves various coatings or introduction of surface roughness. The surface coating or roughening can take various forms and require different fabrication technologies, but it improves the fixation of implants in bone (Ratner et al., 2013).

Ceramics, glasses, and glass-ceramics include a broad range of inorganic/non-metallic compositions. These materials are generally used to repair or replace skeletal hard connective tissues. In the medical industry, these materials are used for eyeglasses, diagnostic instruments, chemical ware, thermometers, tissue culture flasks, etc.. Ceramics are also widely used in dentistry as restorative materials such as in gold–porcelain crowns, glass-filled ionomer cements, and dentures. There is variety of fabrication methods, which correlates with the amount of materials used (Ratner et al., 2013).

Polymers represent the largest class of biomaterials used in tissue engineering. Polymers may be derived from natural sources, or from synthetic organic processes. The natural polymers include plant materials such as cellulose, sodium alginate, and natural rubber, animal materials include tissue-based heart valves and sutures, collagen, glycosaminoglycans (GAGs), and hyaluronic acid, and other natural materials (Table 2.3) (O’Brien, 2011). Their big advantage is that they are often very similar to other macromolecules in the body, thus functioning

biologically at the molecular level. They are easier processed metabolically, but on the other hand, natural polymers are often immunogenic. Moreover, they are structurally more complex than synthetic polymers, their technological manipulation is more complicated. Also, natural polymers have structural variability not only between species but also between one tissue to another, which makes the processing difficult (Ratner et al., 2013).

TABLE 2.3: General properties of certain natural polymers (Ratner et al., 2013)

	Polymer	Incidence	Physiological function
A. Proteins	Silk	Synthesized by arthropods	Protective cocoon
	Keratin	Hair	Thermal insulation
	Collagen	Connective tissues (tendon, skin,...)	Mechanical support
	Gelatin	Partly amorphous collagen	(Industrial product)
	Fibrinogen	Blood	Blood clotting
	Elastin	Neck ligament	Mechanical support
	Actin	Muscle	Contraction, motility
	Myosin	Muscle	Contraction, motility
	Cellulose (cotton)	Plants	Mechanical support
	Amylose	Plants	Energy reservoir
B. Polysaccharides	Dextran	Synthesized by bacteria	Matrix for growth of organism
	Chitin	Insects, crustaceans	Provides shape and form
	Glycosaminoglycans	Connective tissues	Contributes to mechanical support
C. Polynucleotides	Deoxyribonucleic acids (DNA)	Cell nucleus	Direct protein biosynthesis
	Ribonucleic acids (RNA)	Cell nucleus	Direct protein biosynthesis

On the other hand, there is a huge variety of synthetic polymers available. Synthetic polymeric biomaterials range from hydrophobic, non-water-absorbing materials such as polyesters (polycaprolactone (PCL), polylactic acid (PLA), polyvinylalcohol (PVA), polyglycolic acid (PGA) and their co-polymers such as poly(lactic-co-glycolic acid) (PLGA)), silicone rubber (SR), polyethylene (PE), polypropylene (PP), poly(ethylene terephthalate) (PET), polytetrafluoroethylene (PTFE), and poly(methyl methacrylate) (PMMA) to more polar materials such as poly(vinyl chloride) (PVC) or nylons, to water-swelling materials such as poly(hydroxyethyl methacrylate) (PHEMA) and beyond, to water-soluble materials such as poly(ethylene glycol) (PEG) (Gunatillake, Adhikari, and Gadegaard, 2003; (Ratner et al., 2013)).

Some polymers are hydrolytically unstable and degrade in the body while others may remain essentially unchanged for the lifetime of the patient. The advantage of biodegradable scaffolds is, that after some time after implantation the scaffold degrades, the degradation products are metabolized, and at the same time the scaffold is replaced by new tissue. However, this is associated with the fulfillment of stringent requirements in terms of their biocompatibility compared to non-degradable materials. In addition to the potential problem of toxic contaminants leaching from the implant (residual monomers, stabilizers, polymerization initiators, emulsifiers, sterilization by-products, crosslinking agents), one

must also consider the potential toxicity of the degradation products and subsequent metabolites (Ratner et al., 2013). Polymers can be used both for the hard tissue replacement as well as for soft tissue replacement. Depending on the fabrication method, various structures can be prepared, e.g. 2D / 3D materials made of random / oriented fibers, highly porous, fluffy materials or hydrogels (physically / chemically crosslinked), etc. (Table 2.4)

TABLE 2.4: Degradable polymers and representative applications under investigation (Ratner et al., 2013).

Degradable polymer	Current major research applications
Synthetic degradable polyesters	
Poly(glycolic acid), poly(lactic acid), and copolymers	Barrier membranes, drug delivery, guided tissues regeneration (in dental applications), orthopedic applications, stents, staples, sutures, tissue engineering
Polyhydroxybutyrate (PHB), Polyhydroxyvalerate (PHV), and copolymers thereof	Long-term drug delivery, orthopedic applications, atents, sutures
Polycaprolactone	Long-term drug delivery, orthopedic applications, staples, stents
Polydioxanone	Fracture fixation in non-load-bearing bones, sutures, wound clip
Other synthetic degradable polymers	
Polyanhydrides	Drug delivery
Polycyanoacrylates	Adhesives, drug delivery
Poly(amino acids) and "pseudo"-Poly(amino acids)	Drug delivery, tissues engineering, orthopedic applications
Poly(ortho ester)	Drug delivery, stents
Polyphosphazenes	Blood contracting devices, drug delivery, skeletal reconstruction
Poly (propylene fumarate)	Orthopedic applications
Some natural resorbable polymers	
Collagen	Artificial skin, coatings to improve cellular adhesion, drug delivery, guided tissue regeneration in dental applications, orthopedic applications, soft tissue augmentation, tissue engineering, scaffold for reconstruction of blood vessels, wound closure
Fibrinogen and fibrin	Tissue sealant
Gelatin	Capsule coating for aoral drug delivery, hemorrhage arrester
Cellulose	Adhesion barrier, hemostat
Various polyxacharides such as chitosan, alginate	Drug delivery, encapsulation of cells, sutures, wound dressings
Starch and amylose	Drug delivery

2.3.2 Polycaprolactone

Among the most widely used polymers in tissue engineering belong aliphatic polyesters such as poly- ϵ -caprolactone (PCL), polylactide (PLA), and poly(lactide-co-glycolide) (PLGA) and their co-polymers (e.g. poly(L-lactide-co- ϵ -caprolactone)). These polymers were approved by the Food and Drug Administration of the United States of America (FDA) for many medical applications. They are biodegradable, bioresorbable and biocompatible. They have reactive groups which are the target for functionalization, to alter their hydrophobicity, degradation rate, cell adhesion and other properties (Nair and Laurencin, 2007; Tian et al., 2012).

Poly- ϵ -caprolactone (PCL) has been used most frequently from the mentioned polymers. It is synthesized by the ring-opening reaction. It is a semi-crystalline polymer, and has a good solubility in a variety of organic solvents, therefore it can be blended with wide range of polymers. PCL has low melting point (55 - 60 °C) and glass transition temperature (-60 °C). The physical, thermal and mechanical

properties of the polymer mainly depend on the molecular weight and the degree of crystallinity. PCL is highly hydrophobic, which leads to lower cell adhesion rates, therefore PCL is often spun with other polymers or bioactive molecules (Nair and Laurencin, 2007; Bacakova et al., 2019).

The polymer undergoes hydrolytic degradation due to the presence of hydrolytically labile aliphatic ester linkages and products of its degradation are non-toxic in the nature (Wang et al., 2005). The acid by-products of polyester degradation can result in inflammatory reaction *in vivo* (Bergsma et al., 1995; Ceonzo et al., 2006). Important factor which is influencing the inflammation responses is the site of implantation, e.g. the poor vascularization or low metabolic activity, may lead to local accumulation of the degradation by-products, which causes the inflammation (Bostman et al., 1990). However, due to the slow degradation of PCL, this risk is significantly lower (2 - 3 years) compared to PLA and PLGA, which degrade significantly faster (Woodruff and Hutmacher, 2010). The slow degradation can be beneficial for some specific applications, such as drug delivery (Freiberg and Zhu, 2004).

PCL is used in many different forms and for various applications (Fig. 2.6). Because PCL is more hydrophobic than PLA and particularly PLGA, and thus it is less supportive for cell adhesion (Bacakova et al., 2019), it is often used as a blend with other polymers or bioactive molecules (Schnell et al., 2007; Ghasemi-Mobarakeh et al., 2008; Merrell et al., 2009).

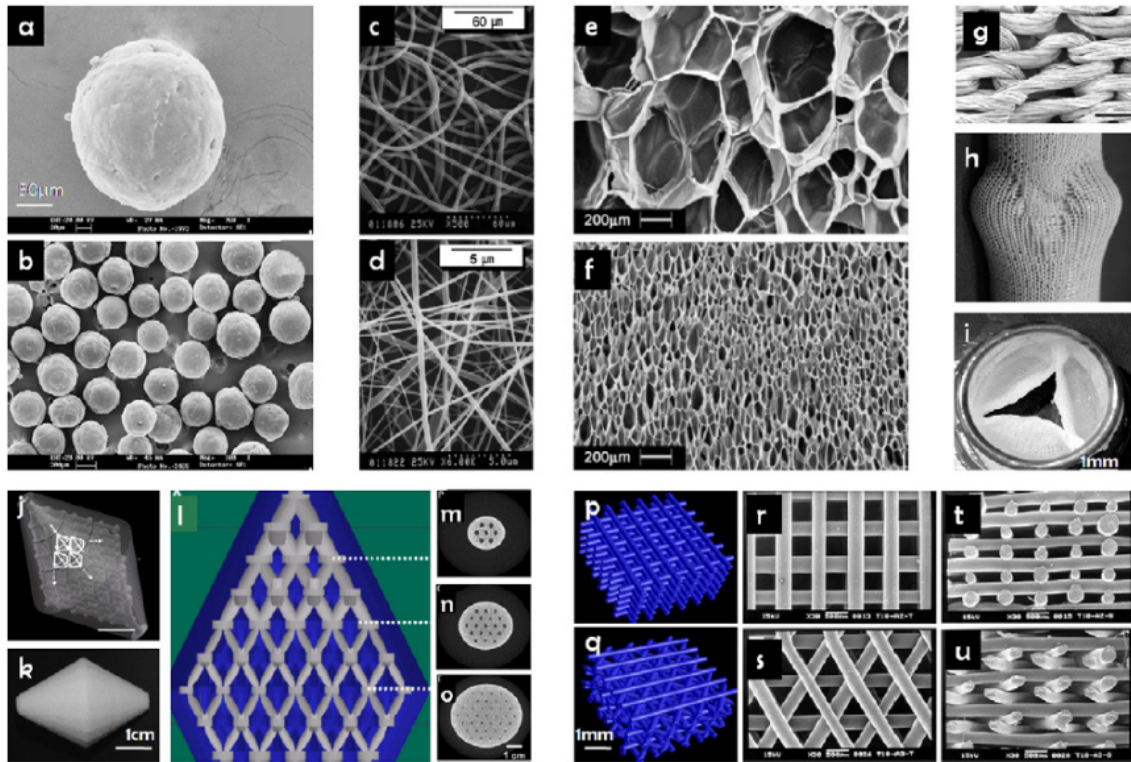


FIGURE 2.6: Structures made from PCL: Nanospheres (a, b). Nanofibres (c, d). Foams (e, f). Knitted textiles (g, h, i). Selective laser sintered scaffold (j - o). Fused deposition modeled scaffolds (p - u) (Woodruff and Hutmacher, 2010).

2.4 Functionalization of scaffolds

2.4.1 Functionalization in tissue engineering

The functionalization means that the scaffold obtains additional advantageous properties. Typically, the functionalization helps with cell adhesion and proliferation (Zeng et al., 2013), or the scaffold gains specific properties, e.g. antibacterial (Madhavan et al., 2011; Paneva et al., 2011). In general, functionalization of the scaffolds increases the biocompatibility of the scaffold and contributes to the cell-scaffold communication, triggering numerous cellular responses including proliferation and differentiation. The modifications in the scaffold can be of different types, mechanical, physical or chemical.

Mechanical improvement involves using different polymers or co-polymers (Ghasemi-Mobarakeh et al., 2008) or even different fabrication techniques to gain desired mechanical properties (Erben et al., 2015; Rampichova et al., 2018).

Physical improvement of the scaffold involves changing the surface roughness, porosity or hydrophilicity by using many different approaches (Yang et al., 2004; Jahani et al., 2015).

The chemical improvements include surface modification of micro-/nanofibrous scaffolds with drugs or other chemicals by dip-coating (Sun et al., 2014; Schneider, Günter, and Taubert, 2018; Kim et al., 2019), chemical surface deposition (Strnadová et al., 2016, Strnadová et al., 2020), or covalent bonding of the already fabricated scaffold (Bezuidenhout et al., 2010; Korzhikov-Vlakh et al., 2018). Other possibility is to blend drugs or other particles with polymer solution prior to spinning, using the solution either for direct spinning (Merrell et al., 2009) or for coaxial spinning (Mickova et al., 2012; Buzgo et al., 2013; Wang and Windbergs, 2019) or for emulsion spinning (Sinha-Ray et al., 2012; Hu et al., 2015). The chemicals can be of synthetic (Yan et al., 2014; Hu et al., 2015) or natural origin (e.g. proteins or nucleic acids) (Losi et al., 2013; Chudickova et al., 2015) and influence various cellular processes. One of the many examples of chemical modifications are conducting polymers, which are either deposited on the scaffold surface (Lee et al., 2009; Zeng et al., 2013; Strnadová et al., 2020) or are blended with the polymer solution prior to spinning (Chronakis, Grapenson, and Jakob, 2006). In neural tissue engineering the conductive polymers are believed to help differentiation of neural stem cells (Stewart et al., 2015), help the axonal elongation and spreading and to help with the transmission of the electrical signal between cells (Zhang et al., 2007; Zeng et al., 2013; Nguyen et al., 2014).

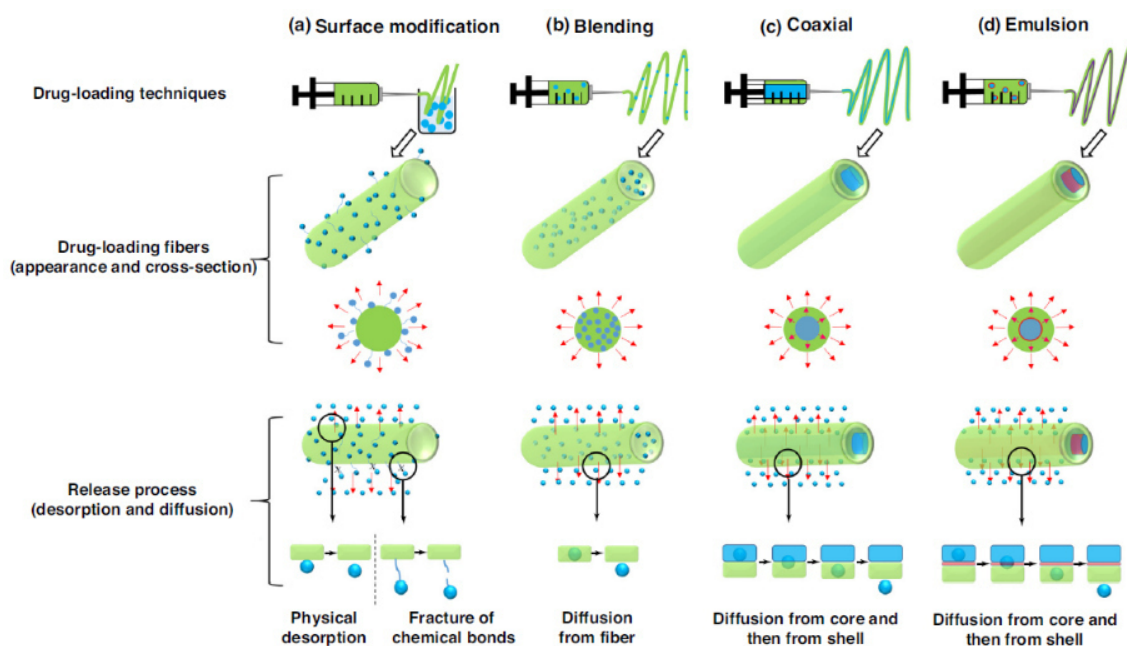


FIGURE 2.7: Drug loading and release (desorption and diffusion) from polymeric micro/nanofibers fabricated by (a) surface modification, (b) blending, (c) coaxial and (d) emulsion electrospinning. The green color stands for polymer, blue for drugs and maroon for surfactant. The red arrows represent the direction of the drug release (Zhang et al., 2017).

While the mechanical and physical changes in the scaffold usually target the biocompatibility of the scaffold and the cellular response indirectly, chemical modifications can be very specific.

Another very specific functionalization approach is the loading of scaffolds with cells (mostly the stem cells) (Dumont et al., 2018), cells' derivatives (thrombocytes) (Lukášová et al., 2019) or viruses (for the gene delivery therapy) (Park et al., 2018; Smith et al., 2019).

Depending on the targeted tissue, different types and methods of scaffold functionalization is chosen. Usually the combination of several approaches can fulfill the demands of the targeted tissue.

2.4.2 Conductive polymers

From the very beginning, polymers were considered to be insulators, until the discovery of conducting properties of π -conjugated polyacetylene (PA) using iodine as dopant in 1977. Since the discovery of conductive PA, many other conductive polymers had been reported and described. Among the most widely studied conductive polymers (CPs) belong polypyrrole (PPy), polyaniline (PANI), polythiophene (PT) or polyacetylene (PA), of which only PA is non-cyclic

polymer (Fig. 2.8). The other listed polymers are aromatic CPs and are much more stable due to their aromatic structure.

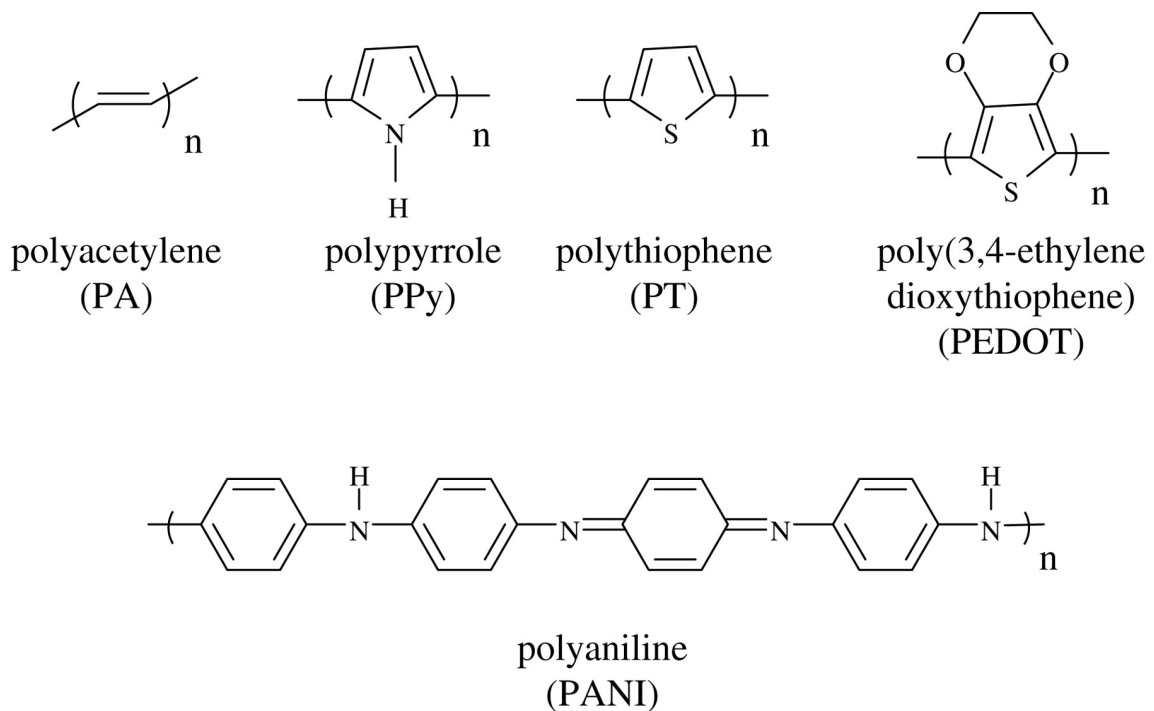


FIGURE 2.8: Chemical structure of representatives of CPs (Guimard, Gomez, and Schmidt, 2007).

Their conductivity varies in the range of tens to thousands of $S \cdot cm^{-1}$ and is influenced by the type of dopant, method of synthesis and temperature, length of polymer chain and crystallinity, etc. (Fig. 2.9, table 2.5, 2.6) (Guimard, Gomez, and Schmidt, 2007; Wan, 2008).

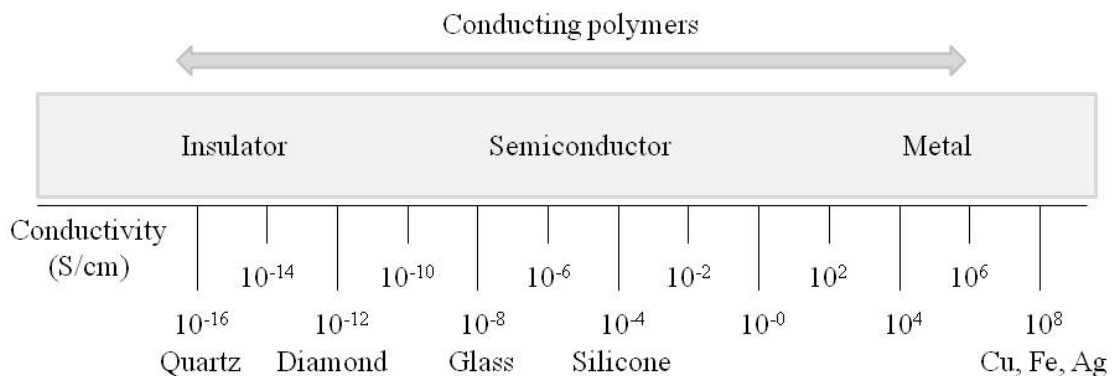


FIGURE 2.9: Schematic illustration of conductivity distribution (Guimard, Gomez, and Schmidt, 2007) [12].

TABLE 2.5: Conductivity of common CPs (Guimard, Gomez, and Schmidt, 2007).

Conducting polymer	Maximum conductivity [$\text{S}\cdot\text{cm}^{-1}$]
Polyacetylene (PA)	200 - 1000
Polypyrrole (Ppy)	40 - 200
Polythiophene (PT)	10 - 100
Polyaniline (PANI)	5

TABLE 2.6: Doping levels and conductivities of a variety of CPs. Film: electrochemically polymerized films; pp: pressed pellet from chemically synthesized powder (Guimard, Gomez, and Schmidt, 2007) [12].

Polymer	Dopant (X^-)	Structure	Conductivity ($\text{S}\cdot\text{cm}^{-1}$)
Polypyrrole (PPy)	CF_3SO_3^-	$(\text{C}_4\text{H}_3\text{N})X_{0.3}$	150 (film)
			10 (pp)
Polypyrrole (PPy)	ClO_4^-	$(\text{C}_4\text{H}_3\text{N})X_{0.3}$	100 (film)
			10 (pp)
Polythiophene (PT)	SO_3SF_3^-	$(\text{C}_4\text{H}_2\text{S})S_{0.3}$	10-20 (pp)
			None
Poly(3-methylthiophene)	BF_4^- or PF_6^-	$(\text{C}_4\text{H}_2\text{S})X_{0.06}$	0.02 (pp)
			None
Poly(3-methylthiophene)	SO_3CF_3^-	$(\text{C}_5\text{H}_4\text{S})X_{0.3}$	30-50 (pp)
			None
Poly(3,4-dimethylthiophene)	PF_6^-	$(\text{C}_6\text{H}_6\text{S})X_{0.12}$	1 (pp)
			None
Polyfuran	SO_3CF_3^-	$(\text{C}_4\text{H}_2\text{O})X_{0.3}$	20-50 (pp)
Polyazulene	ClO_4^-	$(\text{C}_{10}\text{H}_6)X_{0.25}$	10^{-2} - 10^{-1} (pp)

2.4.3 Polypyrrole

Polypyrrole was first discovered in 1968 by Dall'olio and his co-workers and was called pyrrole black. It took more than 10 years (1979) until Diaz and Kanazawa were able to electrochemically synthesized highly conductive and stable PPy. Nowadays, both methods, i.e. chemical and electrochemical, are used to synthesize PPy.

The most common chemical synthesis is the radical polymerization. The electrochemical oxidation involves the polymerization of pyrrole monomers on an anodic electrode in the presence of electrolyte salt and suitable solvent in the form of thin film. The electrochemical polymerization yields high conductive PPy films, it is fast and easy.

Chemical oxidation of pyrrole is performed in the presence of oxidizing agent and dopant dissolved in a solvent. As a result of a chemical polymerization, PPy powder is formed (which adheres to surfaces as well). The powder has lower conductivities than the film prepared by electrochemical polymerization, but is more suitable for mass production with controllable PPy properties. However, chemical synthesis is very sensitive to polymerization conditions as concentration and type of dopant and oxidizing agent, reaction temperature and time, stoichiometry or used solvent (Skothiem and Reynolds, 2007).

2.4.4 Advantages of conductive polymers for tissue engineering

Conducting polymers have wide variety of possible applications, ranging from the technical, i.e. chemical sensors, solar cells, polymeric batteries, electrochromic displays, light emitting diodes, to the biotechnological, i.e. biosensors, neural probes, drug delivery, bio-actuators up to tissue engineering (Table 2.7) (Ramakrishnan, 1997; Guimard, Gomez, and Schmidt, 2007; Ziadan, 2012). Great advantage of CPs is the possibility of their modulation by modification of the synthesis conditions (different dopants and their concentration, copolymerization, covalent modification of monomer) and thus modulation of their final properties, i.e. conductivity, biocompatibility, hydrophobicity, surface roughness, 3D geometry, or redox stability (Guimard, Gomez, and Schmidt, 2007). On the other hand, these possible modifications lead to enormous variety of PPy-derived products and thus the literature in this scientific field is very extensive and the results are often incomparable.

TABLE 2.7: Conducting polymers in biological applications (Guimard, Gomez, and Schmidt, 2007).

Application	Description of application	Advantages of conducting polymers	Limitations of conducting polymers	Polymers currently explored
Tissue engineering	Biocompatible, biodegradable scaffolds contain stimuli to enhance tissue regeneration	<ul style="list-style-type: none"> • Biocompatibility • Good conductivity • Possible modification to include chemical cues 	<ul style="list-style-type: none"> • Not biodegradable • Not highly porous • Hydrophobicity 	<ul style="list-style-type: none"> • PPy and derivatives • PANI • PT and derivatives • Novel CPs
Neural probes	Implantable electrodes for recording or stimulating neurons, primarily in the brain	<ul style="list-style-type: none"> • Biocompatibility • Good conductivity • Good stability • Electrochemical synthesis on metal electrodes • Increased surface area (decreased impedance) • Ability to entrap biomolecules in films 	<ul style="list-style-type: none"> • Decreased electrical contact at interface 	<ul style="list-style-type: none"> • PPy • PEDOT
Biosensors	Devices containing biomolecules as sensing elements, integrated with electrical transducers	<ul style="list-style-type: none"> • Possible surface modification • Efficient electric charge transfer from biorestrictions • synthesis on metal electrodes 	<ul style="list-style-type: none"> • Hydrophobicity can denature entrapped proteins • Diffusion barriers for entrapped enzymes 	
Drug Delivery	Devices for storage and controlled release of drugs	<ul style="list-style-type: none"> • Ability to entrap biomolecules • Controlled release with reduction • Biocompatibility • Good conductivity 	<ul style="list-style-type: none"> • Hydrophobicity can denature entrapped proteins • Rapid release 	<ul style="list-style-type: none"> • PPy • PEDOT
Bio-actuators	Devices to create mechanical force that could be used as "artificial muscle" - type actuators	<ul style="list-style-type: none"> • Can control depant uptake/ release (control volume) • Lightweight • Work at body temp. and with body fluids 	<ul style="list-style-type: none"> • Short-term redox stability • Delamination of CP films • Response limited by ion mobility 	<ul style="list-style-type: none"> • PPy • PANI • Polymer-carbon nanotube composites

There are many factors influencing the behavior of cells in contact with CP. It is assumed that, among the others, probably the most important factors are the chosen dopant, the level of conductivity, oxidation level of polymer or the thickness of polymer film, which are again related to synthesis of the polymer. For example, a reducing potential applied on PPy causes an expulsion of negative ions, in the case of small dopants, or, the uptake of positive ions from medium in the case of large dopants. In the case of Na^+ , which can be scavenged from medium when electrical current is applied, it is speculated that it affects protein adsorption to the scaffold surface and cell cycle. It is assumed that the local release of cations or anions influences the ionic transport across the neighboring cell membranes (Guimard, Gomez, and Schmidt, 2007 ; Balint, Cassidy, and Cartmell, 2014). The information about the effect of CPs on biological tissues also differ with the cell line used for *in vitro* tests and the field of tissue engineering, ranging from wound healing system, muscle or bone tissue engineering up to the probably most promising field of neural tissue engineering (Ateh, Navsaria, and Vadgama, 2006; Ravichandran et al., 2010).

The well-known fact about the cells is that they possess a membrane potential, where the inside of the cell is more negative than the outside. The potential outside the cell is called zero potential, thus the value of membrane potential is usually ranging from -60 to -100 mV (Matthews, 2002). This potential is maintained in the resting cell and is also called the resting potential (Paul, 1975). The cells can decrease and increase the membrane potential if it is necessary by uptake or distribution of ions through membrane. The cells can even control or rectify current flow. All these processes are influenced by electrical signals. One of the most electrically-active cells, among the skeletal muscle cells or heart, are the cells of nervous system. Nerve cells undergo electrical changes when stimulated. The neural impulse then travels along the axon as a wave, which is maintained by depolarization and repolarization of membrane potential. Briefly, the neural cell receives the signal, which causes the Na^+ channels to open, Na^+ enters the cell, which moves the potential to -55 mV. This shift drives further influx of Na^+ and causes depolarization of membrane potential to $+30$ mV. At this point the K^+ channels open and the repolarization occurs. At the end of repolarization the membrane potential shifts up to -90 mV, which is called hyper-polarization and it prevents the neuron from receiving another signal (Ghasemi-Mobarakeh et al., 2011).

The signal can be either chemical, which is the case of transmission of the neural signal in nervous system, or artificial electrical stimulation. It was also reported that cells generate electrical field during basic cellular behavior as cell division, migration or differentiation (McCaig and Zhao, 1997; Zhao, Forrester, and McCaig, 1999; Stewart et al., 2015; Snyder, DeJulius, and Willits, 2017). Thus, applying electric current into biological systems can influence many cellular processes, but the exact mechanisms are still poorly understood. In the case of neural cells it was reported that application of electric current stimulates the neurite extension and direction of their outgrowth (Zhang et al., 2007; Chang et al., 2013; Nguyen et al., 2014). There are several theories that explain the effect of electric stimulation on neural regeneration as the redistribution of cytoplasmic material, accumulation of surface molecules responsible for neurite growth and cell adhesion, increase in gene expression and protein synthesis (Patel and Poo, 1982; Siskin et al., 1989; Kimura et al., 1998). The increased absorption of fibronectin to electrically stimulated PPy surface was also reported (Kotwal and Schmidt, 2001). Another study described upregulated mitochondrial activity in fibroblasts when treated by constant electric field (Ghasemi-Mobarakeh et al., 2011).

Among different conducting polymers used in tissue engineering, polypyrrole was reported as the least immunogenic (Guimard, Gomez, and Schmidt, 2007; Balint, Cassidy, and Cartmell, 2014). *In vitro* and *in vivo* biocompatibility of polypyrrole was proven by many authors (Williams and Doherty, 1994; Wang et al., 2004). On the other hand, polypyrrole is a non-biodegradable and quite brittle polymer and little is known about its behavioral after the long-term implantation *in vivo*. It may induce chronic inflammation, which would require surgical removal. There are several approaches to address the drawbacks of the non-biodegradability of CPs. The most widely used methods are the blending of CPs with biodegradable polymers, chemical modification of the polymer's backbone with ionizable or hydrolysable side groups, or synthesis of very small chains of CPs, that would undergo gradual erosion and further renal clearance (Guo, Glavas, and Albertsson, 2013; Balint, Cassidy, and Cartmell, 2014).

To enhance the biocompatibility of CPs, the physico-chemical, electrical and mechanical properties of CPs can be modified by various functionalization techniques. For example, the neural electrodes' functionality can be improved by changing the roughness or porosity (Yang et al., 2004, Yang and Martin, 2004b, Yang and Martin, 2004a) or by the incorporation of cell adhesion peptides (Cui et al., 2001), proteins (Buchko, Kozloff, and Martin, 2001) or anti-inflammatory drugs (Abidian, Kim, and Martin, 2006). There are countless techniques of the surface modifications of CPs. One very interesting approach was applied by the group of prof. Stibor (Lukasek et al., 2019). The pyrrole monomers were chemically modified by cyclodextrines (CDs) prior to the polymerization reaction. The Py-CD is mixed with the plain pyrrole in desired ratio in the polymerization reaction, introducing the CD into the PPy backbone. The used ratio defines the concentration of CDs in the scaffold. Cyclodextrines are naturally occurring glucose-based cyclic oligosaccharides. The cavity of CDs is able to harbor lipophilic guests in the aquatic environment. Such property enables e.g the sequestration of growth factors (Grier et al., 2018) or even the drug release during cell culturing (Prabaharan and Jayakumar, 2009). This is very versatile functionalization, because it can be used for any tissue just by using tissue-specific biomolecules which will be entrapped within the CDs. However, the most relevant use of such scaffolds is for the electrically active tissues such as neural tissue due to the PPy backbone.

Chapter 3

Materials and methods

The aim of this work was to prepare scaffold made of highly oriented fibers, which would be further functionalized by polypyrrole and to test such scaffold for biocompatibility *in vitro*. This scaffold was then used for fabrication of novel composite spinal cord bridge implant, which was tested *in vitro* and *in vivo* on mice. Its biocompatibility was evaluated in terms of the immunogenicity and axon infiltration and myelination.

3.1 Materials and equipment

3.1.1 List of chemicals

3-(4,5-dimethylthiazol-2-yl)-2,5-diphenyltetrazolium bromide (MTT)	Sigma Aldrich
4',6-diamidin-2-fenylindol (DAPI)	Sigma Aldrich
5/0 Chromic gut	CP Medical
50x B27	Gibco
Acetic acid	Penta
Acetone	Penta
antibiotics	Lonza
Baytril (enrofloxacin)	VetOne
Chloroform	Penta, Sigma Aldrich
D-(+)-Glucose	Sigma Aldrich
Dextran from <i>Leuconostoc</i> spp.	Sigma Aldrich
DMEM (high glucose)	Lonza
D-Sucrose	Sigma Aldrich
Ethanol	Penta, Sigma Aldrich
FeCl ₃	Sigma Aldrich
Fetal bovine serum	Biosera

Flouromount G	Southern Biotech
Formic acid	Penta
Gelfoam®	Pfizer
Glutaraldehyde	Sigma Aldrich
Glutaraldehyde 25%	Sigma Aldrich
Glycogen	Ambion
HCl	Penta
Hoechst 33342	Thermo Fisher Scientific
Isopropylalcohol	Penta
KCl	Penta
KH ₂ PO ₄	Penta
Lactate Ringer solution	VetOne
Laminin (10 µg / ml)	Sigma Aldrich
L-Glutamine	Biosera
L-glutamine (GlutaMAX 100x)	Gibco
Methanol	Penta
Na ₂ HPO ₄ ·12H ₂ O	Penta
NaCl	Penta, Fisher Scientific
NaHCO ₃	Sigma Aldrich
NaOH	Sigma Aldrich
Neural growth factor 2.5S (100 µg / ml, murine)	Invitrogen
Neurobasal medium, w/o L-glutamine	Gibco
Normal Donkey Serum	Jackson ImmunoResearch
Normal Goat Serum	Vector Laboratories
Paraformaldehyde	Sigma Aldrich
Penicilin /streptomycin (10,000 U / ml)	Gibco
Phalloidin-FITC	Sigma Aldrich
Polyamide-6, Ultramid B27	BASF
Polycaprolactone, M _n 45,000	Sigma Aldrich
Polycaprolactone, M _n 80,000	Sigma Aldrich
Poly-lactide-co-glycolide acid, M _n 75,000 - 85,000	Polyscitech
Polyvinylacohol, M _w 130,000, MOWIOL 20-98	Merck
p-toluensulfonic acid	Sigma Aldrich
Pyrrole	Sigma Aldrich
Reflex 7 wound clips, 203 - 1000, 7 mm	Cellpoint Scientific
Sudan Black, high purity biological stain	Acros Organics

Tissue-Tek O.C.T.	Sakura
Triton X-100	Sigma Aldrich
Trizma hydrochloride solution 10x, pH 7,4	Sigma Aldrich
TRIzol™ Reagent	Thermo Fisher Scientific
Tween® 20	Sigma Aldrich

3.1.2 Primary antibodies

Mouse anti- β -tubulin	Abcam
Goat anti-arginase	Santa Cruz Biotechnology
Rat anti-F4/80	Abcam
Rabbit anti-NF200	Sigma Aldrich
Goat anti-MBP	Santa Cruz Biotechnology
Chicken anti-P0	Aves Lab

3.1.3 Secondary antibodies

AF555 goat anti-mouse IgG	Life Technologies
CF555 donkey anti-goat IgG	Invitrogen
AF647/633 goat anti-rat IgG	Invitrogen
CF555 donkey anti-rabbit IgG	Sigma Aldrich
CF488 donkey anti-goat IgG	Invitrogen
CF633 donkey anti-chicken IgY	Sigma Aldrich

3.1.4 Primers

18s rRNA forward; 5'-GCAATTATTCCCCATGAACG-3'	Invitrogen
18s rRNA reverse; 5'-GGCCTCACTAAACCATCCAA-3'	Invitrogen
MHC II forward; 5'-GACGCTCAACTTGTCCCAAA-3'	Invitrogen
MHC II reverse; 5'-GCAGCCGTGAACTTGTTGA-3'	Invitrogen
iNOS forward; 5'-CCCTTCAATGGTTGGTACAT-3'	Invitrogen
iNOS reverse; 5'-ACATTGATCTCCGTGACAGC-3'	Invitrogen
CD86 forward; 5'-TTGTGTGTGTTCTGGAAACG-3'	Invitrogen
CD86 reverse; 5'-AACTTAGAGGCTGTGTTGCT-3'	Invitrogen
Arginase 1 forward; 5'-GAACACGGCAGTGGCTTTA-3'	Invitrogen
Arginase 1 reverse; 5'-TGCTTAGCTCTGTCTGCTTT-3'	Invitrogen
CD206 forward; 5'-TCTTTGCCTTTCCAGTCTC-3'	Invitrogen
CD206 reverse; 5'-TGACACCCAGCGGAATTC-3'	Invitrogen
Cytochrome C forward, 5'-GAGGCAAGCATAAGACTGGA-3'	Invitrogen
Cytochrome C reverse; 5'-TACTCCATCAGGGTATCCTC-3'	Invitrogen

Caspase 3 forward; 5'-CCTCAGAGAGACATTCATGG-3'	Invitrogen
Caspase 3 reverse; 5'-GCAGTAGTCGCCTCTGAAGA-3'	Invitrogen

3.1.5 Commercial kits

iScript™ cDNA Synthesis Kit	Bio-Rad
iQ™ SYBR® Green Supermix	Bio-Rad
Direct-zol™ RNA MiniPrep Plus	Zymo Research

3.1.6 Cell cultures and animals

3T3 mice fibroblasts, Swiss Albino	ATCC
C57Bl6 mice	Charles River

3.1.7 Polymer solutions

Polymers	Composition	Notes
PCL, M_n 80,000	<ul style="list-style-type: none"> • PCL, M_n 80,000 • Chloroform 	<ul style="list-style-type: none"> • Solutions of 4%, 6%, 8%, 12%, 16% and 20% polymer by weight • Dissolve O/N on magnetic stirrer • Do not store
PCL, M_n 45,000	<ul style="list-style-type: none"> • PCL, M_n 45,000 • Chloroform • Acetone • Acetic acid 	<ul style="list-style-type: none"> • Solutions of 8 %, 12 %, 16 %, 20 %, 24 %, 28 % and 32 % polymer by weight • Dissolve in the solution of chloroform, acetone, acetic acid mixed in the ratio of 8:1:1 • Dissolve O/N on magnetic stirrer • Do not store

PVA, M_w 130,000	<ul style="list-style-type: none"> • PVA, M_w130,000 • Distilled water 	<ul style="list-style-type: none"> • Solutions of 8 %, 12 %, 16 %, 20 %, 24 % and 28 % polymer by weight • Dissolve O/N on magnetic stirrer • Do not store
PA-6	<ul style="list-style-type: none"> • PA-6, Ultramid B27 • Acetic acid • Formic acid 	<ul style="list-style-type: none"> • Solutions of 8 %, 12 %, 16 %, 20 % polymer by weight • Dissolve in the solution of acetic and formic acid mixed in the ratio of 1:1 • Dissolve O/N on magnetic stirrer • Do not store

3.1.8 Cultivation media and solutions

Medium / solution	Composition	Notes
DMEM medium	<ul style="list-style-type: none"> • 88 ml DMEM (high glucose) • 10 ml Fetal bovine serum (FBS) • 1 ml L-Glutamine • 1 ml Antibiotics • 20 μl 7.5 % NaHCO_3 	<ul style="list-style-type: none"> • NaHCO_3 is filter-sterilized (0.2 μm) • FBS is inactivated for 30 min at 55 °C • All components mixed together and filter-sterilized (0.2 μm filter) in a flow hood. • Store at 4 °C • Warm up to 37 °C prior to use

Neurobasal medium	<ul style="list-style-type: none"> • 10 ml Neurobasal medium, w/o L-Glutamine • 200 μl 50x B27 • 100 μl L-Glutamine (Glu-taMAX 100x) • 2.5 μl Neural Growth Factor 2.5S (100 μg /ml, murine) • 50 μl Penicilin / Streptomycin (10,000 U / ml) 	<ul style="list-style-type: none"> • Mix all components • Filter-sterilize (0.2 μm filter) in a flow hood • Make fresh before use • Warm up to 37 °C before use
Phosphate Buffered Saline (PBS)	<ul style="list-style-type: none"> • 8 g NaCl • 0.2 g KCl • 3.63 g $\text{Na}_2\text{HPO}_4 \cdot 12\text{H}_2\text{O}$ • 0.24 g KH_2PO_4 • Distilled water (up to 1000 ml total) 	<ul style="list-style-type: none"> • Dissolve in 800 ml of dH₂O on magnetic stirrer • Adjust pH to 7.4 by HCl • Adjust volume to 1000 ml • Filter through filter paper • Sterilize by autoclave • Store at room temperature

3.1.9 Solutions for biological experiments

Solutions	Composition	Notes
MTT solution	<ul style="list-style-type: none"> • 0.1 g 3-(4,5-dimethylthiazol-2-yl)-2,5-diphenyltetrazolium bromide (MTT) • 50 ml PBS 	<ul style="list-style-type: none"> • Dissolve MTT in PBS • Heat up to 37 °C if needed • Filter-sterilize (0.2 μm filter) in a flow hood • Store at 4 °C • Warm up to 37 °C prior to use

Phalloidin-FITC	<ul style="list-style-type: none"> • 1 mg Phalloidin-FITC • 1 ml PBS 	<ul style="list-style-type: none"> • Dissolve Phalloidin-FITC in PBS to make a STOCK solution (1 mg / ml) • Store at -20 °C • Dilute 1:1000 in PBS prior to use
Isopropylalcohol (IPA)	<ul style="list-style-type: none"> • 50 ml IPA • 20 µl concentrated HCl 	<ul style="list-style-type: none"> • Mix throughoutly • Store at RT
Glutaraldehyde	<ul style="list-style-type: none"> • 5 ml 25% Glutaraldehyde • 45 ml PBS 	<ul style="list-style-type: none"> • Mix throughoutly • Store at RT
DAPI solution	<ul style="list-style-type: none"> • 1 mg 4',6-diamidin-2-fenylindol (DAPI) • 1 ml PBS 	<ul style="list-style-type: none"> • Dissolve DAPI in PBS to make a STOCK solution • Dilute 1:1000 in PBS prior to use
Paraformaldehyde	<ul style="list-style-type: none"> • 40 g Paraformaldehyde • 100 ml 10x PBS • 200 - 1000 µl 1M NaOH • 750 ml Deionized water 	<ul style="list-style-type: none"> • Heat dH₂O to 60 - 65 °C on magnetic stirrer / heater • Dissolve paraformaldehyde in pre-heated water while stirring • Continue stirring and add NaOH until the solution is no more cloudy • Remove from heat • Add PBS • Filter the solution • Make up total volume to 1000 ml by adding dH₂O • Store at 4 °C, longer storage at -20 °C

1x TRIS	<ul style="list-style-type: none"> • 100 ml Trizma hydrochloride solution 10x, pH 7,4 • 8,5 g NaCl • MilliQ water 	<ul style="list-style-type: none"> • Adjust the volume to 1 l with MilliQ water • Add 8,5 g NaCl to 1 l of solution • Mix throughoutly • Store at RT
---------	--	--

3.1.10 List of equipment

See System for WCA	Advex Instruments, Czech Republic
Cryostat Microm HM525	Thermo Fisher Scientific
Cycler C1000 Touch Thermal Cycler	Bio-Rad
Fluorescent microscope, AxioObserver	Zeiss
Fluorescent microscope, Nikon Eclipse Ti-e Manipulator	Nikon Technical University of Liberec
Multimeter, Agilent 34401A	Agilent
Multimeter, HP 34401A	HP
Multimeter, HP 4339B	HP
Multimeter, Keithley 614 Electrometer	Keithley
NanoDrop™ Spectrophotometer	Thermo Fisher Scientific
Pressure vessel	Custom made
S 25 N - 8 G ST Dispersion Tool	IKA Dispensers
SEM, Nova 200 Nanolab	FEI
SEM, Quanta 3D	FEI
SEM, Vega3 SB Easy Probe	Tescan
Spectrophotometer ELx808	BioTek
T25 Digital ULTRA-TURRAX® homogenizer	IKA Dispensers
Tensile testing machine, LabTest 2.010	LaborTech
Tensiometer, PocketDyne	Krüss
Thermal cycler, BIO-RAD C1000 Touch	Bio-Rad
Viscometer, HAAKE RotoVisco 1	Thermo Scientific

3.1.11 Software

Image analysis	ImageJ	National Institute of Health
	NIS Elements software	Nikon
	Zen Pro	Zeis
	MATLAB	MathWorks
Instrumental software	See System E	Advex Instruments
	isiMotion system	isiMotion
	Gen5 software	BioTek
	LabTest software	LaborTech
Data analysis	GraphPad Prism 6	GraphPad
	Microsoft Excel	Microsoft

3.2 Methods

3.2.1 Drawing fibers and their characterization

3.2.1.1 Preparation of polymer solutions

The PCL (M_n 80,000) solutions were prepared in the concentrations of 4 %, 6 %, 8 %, 12 %, 16 % and 20 % by weight in chloroform. The PCL (M_n 45,000) solutions were prepared in the concentration of 8 %, 12 %, 16 %, 20 %, 24 %, 28 % and 32 % by weight in the solution of chloroform, ethanol and acetic acid in the ratio of 8:1:1. The PVA (M_w 130,000, MOWIOL 20-98) solutions were prepared in the concentrations of 8 %, 12 %, 16 %, 20 %, 24 % and 28 % by weight in distilled water. The polyamide-6 (PA6; Ultramid B27) solutions were prepared in the concentrations of 8 %, 12 %, 16 %, 20 % by weight in the solution of acetic acid and formic acid in the ratio of 1:1. Depending on the type of the experiment, different polymer solutions were used. Solutions were prepared the day before use in the volume of 10 ml up to 100 ml for drawing or for measuring the solution properties, respectively. All solutions were mixed on magnetic stirrer over night at room temperature.

3.2.1.2 Solution characterization

All solutions were analyzed by rotational viscometer and by surface tensiometer. The viscosity of PCL, M_n 80,000 was measured three times per individual concentration using the HAAKE RotoVisco 1 viscometer with 35/1 Ti L plate at the linearly increasing shear rate (10 – 60 s⁻¹).

The surface tension was measured several times (at least five times) per individual concentration using the PocketDyne tensiometer.

Mean values of all measurements were used for further processing.

3.2.1.3 Drawing samples

All fibrous samples were drawn by the Manipulator using a plastic tip (OKI International). The polymer solution was dosed once per cycle (on both sides) at a constant pressure and time just before the tip touched the surface. The syringe with the tip was attached to the moving element perpendicular to the underlay. The motion program consisted of the circular interpolation with a 0.1 s break at the dead point.

For the experiment studying the drawing spinnability of various polymers at different concentrations were chosen following polymers, PCL M_n 45,000, PVA M_n 13,000 and PA-6. All solutions of the PCL, M_n 45,000 (8 %, 12 %, 16 %, 20 %, 24 %, 28 % and 32 %), the PVA (8 %, 12 %, 16 %, 20 %, 24 % and 28 %) and PA-6 (8 %, 12 %, 16 % and 20 %) were drawn using a 20G plastic tip. Constant pressure of 25 kPa and time of 1 ± 0.4 s was used for dosing. All solutions were drawn with the acceleration of $0.5 \text{ m}\cdot\text{s}^{-1}$ and the velocity of $1 \text{ m}\cdot\text{s}^{-1}$. The length of the fiber was set to 0.18 m. Fiber drawing was carried out under ambient conditions: room temperature 20 - 25 °C, relative humidity 30 – 35 %.

The influence of the velocity and solution concentration on the fiber diameter was studied and evaluated. For the evaluation of the impact of the drawing conditions on the fiber morphology, all solutions of PCL, M_n 80,000 (4 %, 6 %, 8 %, 12 %, 16 % and 20 %) were drawn using the 25G plastic tip. Constant pressure of 60 kPa and time of 0.6 s was used for dosing. The established velocities, i.e. 0.1, 0.5, 1, 2 and $3 \text{ m}\cdot\text{s}^{-1}$, were used to study the morphology of resultant fibers. The length of the fiber was set to 0.18 m. Fiber drawing was carried out under ambient conditions: room temperature 20 – 25 °C, relative humidity 30 – 35 %.

For the *in vitro* and *in vivo* experiments the chosen polymer (PCL, M_n 80,000) concentration was 12 % and the drawing speed was $2 \text{ m}\cdot\text{s}^{-1}$. The rest of the parameters was set as mentioned above. The fibers were either fixed within the fixation ring (*in vitro* experiments, WCA measurement) or within the Teflon frame (*in vivo* experiments and conductivity measurement).

3.2.1.4 Fiber characterization and image analysis

For the fiber morphology analysis, the samples were observed by SEM. For the image analysis on the Tescan SEM the samples were sputter coated with gold (7 nm). The cross-section of the fibers was done either in the liquid nitrogen with a scalpel or by the SEM (FEI Nova 200 Nanolab), where a thin layer of platinum was deposited on the side of the cut and the fibers were subsequently cut by a laser. Fiber diameter was measured by NIS Elements software. Other image analyses were done in ImageJ.

3.2.1.5 Mechanical testing of drawn fibers

The mechanical properties were measured (Hauzerová, 2018) using the tensile testing machine LabTest 2.010 with the 1N sensor. The tensile strength measurement was done according to the standard ČSN EN ISO 5079 (Textiles - Fibers - Determination of breaking force and elongation at break of individual fibers; identical with EN ISO 5079:1995). Each sample was measured until failure. 15 to 20 measurements were done for each sample.

The samples for testing the breaking force and the elongation at break were prepared by drawing (chapter 3.2.1.3) from PCL M_n 80,000. 200 fibers were drawn into a bundle of 0.2 m of length on a plastic underlay. The bundles were collected from the underlay with tweezers and attached into the upper grip. The bundle was pre-loaded with 0.1 g weight to even the fibers and attached into the bottom grip. The weight was removed. The tested gauge length was set to 30 mm, the strain rate was 20 mm \times min⁻¹. The measurement was controlled using the LabTest software.

The force value and the gauge length was used to calculate the tension σ (equation 1) and the relative elongation ϵ (equation 1) at brake.

$$\begin{aligned}\sigma &= \frac{\vec{F}}{s} \\ \sigma &= \frac{\vec{F}}{t}\end{aligned}\tag{3.1}$$

Equation. 1: Tension and the specific tension of the tested sample (Neckář and Dipayan, 2012)

The tension is the force F , where F is the function of area s . When testing the fibrous materials we use the specific tension, where the force F is the function of fiber fineness t .

$$\epsilon = \frac{\Delta l}{l_0} \quad (3.2)$$

Equation. 2: Relative elongation of the sample (Neckář and Dipayan, 2012)

The elongation, or deformation, is the increase in the sample's length Δl compared to the initial length l_0 (here 10 mm).

The linear area was used to calculate the Young's modulus (E) according to the equation:

$$E = \frac{\sigma}{\epsilon} \quad (3.3)$$

3.2.1.6 Functionalization of the fibers by polypyrrole

The prepared PCL scaffolds were subsequently functionalized by a thin layer of conductive polypyrrole (PPy). The polymerization reaction of pyrrole (10 mM) was maintained for three days at room temperature in the presence of FeCl_3 (23 mM) and *p*-toluenesulfonic acid (11 mM) under constant stirring. After the polymerization, samples were washed and sonicated in methanol and dH_2O . Samples were dried and stored in vacuum desiccator at RT. The fibers' morphology was evaluated using scanning electron microscope.

3.2.1.7 Water contact angle (WCA) measurement

Samples for the WCA analysis were prepared by drawing 300 fibers from 12% solution of PCL M_n 80,000 as described in chapter 3.2.1.3. The fibers were fixed within the fixation ring (Fig. 3.1). Two sets of samples were analyzed, plain PCL fibers and PPy-coated PCL fibers (coated with PPy according to the protocol, chapter 3.2.1.6). The 3 μl droplet of dH_2O was pipetted on the sample and the image of the droplet was captured using Advex Instruments See System camera right after pipetting the water on the sample. The WCA was measured using See System software. The WCA was measured on five samples per each condition, measuring two or more droplets per sample.



FIGURE 3.1: Measuring the WCA on the drawn samples fixed within the fixation ring.

3.2.1.8 Conductivity measurements

Conductivity was measured by different approaches. First, bundles of fibers were drawn by Manipulator (chapter 3.2.1.3). The bundles contained either 100 or 200 fibers depending on the experiment. The fibers were fixed within a Teflon frame (Fig. 3.2, inner diameter 4 x 4 cm) and coated with polypyrrole.

Experiment at the Department of Material Engineering, TUL

The first measurement was done using a multimeter (Agilent 34401A and HP 4339B) at the Department of Material Engineering (Technical University of Liberec). The bundle of 100 fibers was fixed between two clamps in defined distances (from 1 to 5 cm) and the change in the resistance was measured.

Experiment at the Department of Material Science, TUL

For the second experiment (Krabicová, 2017), bundles of 200 fibers (2,000 fibers total) were fixed within a Teflon frame in between an aluminum foil. The aluminum foil was connected to a multimeter (HP 34401A) with automated range and the resistance was measured.



FIGURE 3.2: Polypyrrole-coated PCL fibers made by drawing, fixed within a Teflon frame in between an aluminum foil.

Experiment at the Department of Surface and Plasma Science, Charles University in Prague

The third measurement was done at the Charles University in Prague (Faculty of Mathematics and Physics, Department of Surface and Plasma Science). The bundles of 100 fibers were used. The resistance was measured by multimeter Keithley 614 Electrometer in the range up to 200 G Ω .

3.2.2 Biological testing

3.2.2.1 Drawing fibers for the *in vitro* and *in vivo* experiments

The 12% PCL solution (M_n 80,000) was drawn using the 25G plastic tip and the drawing speed 2 m·s⁻¹. Constant pressure of 60 kPa and time of 0.6 s was used for dosing. The length of the fiber was set to 0.18 m. Fiber drawing was carried out under ambient conditions: room temperature 20 – 25 °C, relative humidity 30 – 35 %. The fibers were either fixed within the fixation ring (*in vitro* experiments) or within the teflon frame (PPy-samples for *in vivo* experiments).

3.2.2.2 *In vitro* experiments - oriented fibers

The *in vitro* samples were prepared from the 12% PCL using the velocity of $2 \text{ m}\cdot\text{s}^{-1}$. The prepared structures were fixed within a supporting ring (Fig. 4.17). The size of the fixation ring is designed to fit in 24-well cultivation plate and allows better manipulation with the fibers as well as it keeps the scaffold in the designed pattern. The fixation ring was made by injection molding from PMMA at TUL.

Two sets of experiments were carried out. The first experiments were focused on the direction of cell growth. For these experiments two types of scaffolds were prepared varying in the orientation of fibers. Fibers were ordered either in one or in two directions (Fib I, Fib II) (Fig. 3.3 A,B). Fib I and Fib II samples were prepared using 1,000 repeats per 0.01 m (Y) or twice 500 repeats per 0.01 m (X and Y), respectively.

The second set of experiments was focused on the evaluation of biocompatibility of the functionalized fibers. Fib I samples were used for the functionalization experiments. For these experiments, two types of scaffolds were prepared, which differed in the surface modification - plain PCL fibers and PPy-coated PCL fibers (Fig. 3.3 C).

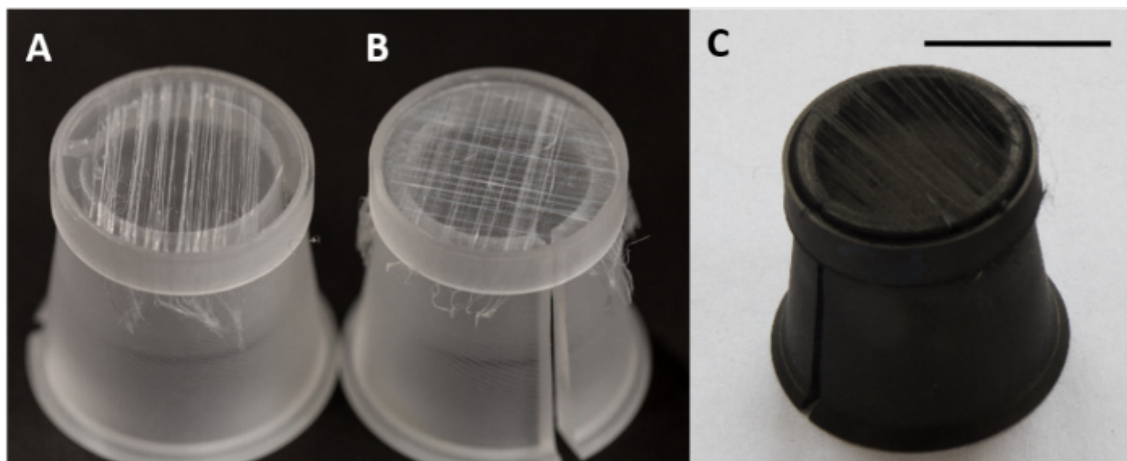


FIGURE 3.3: Macroscopic picture of *in vitro* samples fixed within a supporting ring – (A) fibers ordered in one (Fib I) or (B) two directions (Fib II). (C) *in vitro* sample ordered in one direction functionalized by polypyrrole. Scale bar: 1 cm

The prepared scaffolds were sterilized in 70% ethanol for 30 minutes and washed several times in phosphate buffer saline (PBS, pH 7.4), followed by one wash with complete DMEM medium prior to cell seeding.

3T3 mice fibroblasts were used for the *in vitro* experiments. Cells were seeded in the concentration of $1\cdot 10^5$ per well in 24-well plates and were maintained

in Dulbecco's Modified Eagle's Medium (DMEM) supplemented with 10% (v/v) fetal bovine serum (FBS) and 1% (v/v) penicillin / streptomycin / amphotericin B. Cells were cultured in an incubator (37 °C, 5% CO₂). The medium was changed three times a week and the second passage was used for the *in vitro* experiments.

Cell viability and proliferation was measured by MTT assay on day 1, 3, 7, 14 and 21 after cell seeding. 50 µl of MTT solution and 150 µl of DMEM was added to all the samples and the samples were incubated for three hours at 37 °C, 5% CO₂. After the incubation period the fixation rings were disassembled and the fibers were collected and deposited in to the new 24-well plate. The formazan crystals were dissolved in 200 µl of acidic isopropyl alcohol and the absorbance was measured at 570 nm with the reference wavelength at 650 nm using the ELx808 spectrophotometer with Gen5 software. The solutions were diluted prior to the measurement when the absorbance exceeded 1. The final absorbance is related to the dilution.

Within all testing days, the samples were analyzed by scanning electron microscopy. All the samples were washed with PBS prior to fixation to remove unattached cells. The scaffolds were fixed with 2.5% glutaraldehyde. After the fixation the samples were washed with PBS and then dried up with up-grading concentration of ethanol (60 %, 70 %, 80 %, 90 %, 95 % and 100 %). After the drying, the samples were sputter-coated with gold and were analyzed by scanning electron microscope (VEGA3 SB easy probe).

The samples were analyzed by fluorescent microscopy within all testing days as well. All the samples were washed with PBS prior to fixation to remove unattached cells. The scaffolds were fixed with ice-cold methanol. After the fixation the samples were rinsed with PBS. Next, the samples were either stained with DAPI or with DAPI together with phalloidin-FITC, depending on the experiment. The Fib I and Fib II samples tested for the direction of cell growth were stained with DAPI only and were incubated for 15 minutes with DAPI at room temperature in the dark. The Fib I samples functionalized with polypyrrole were stained with phalloidin-FITC and DAPI. First, the cells were permeabilized in 0.1% Triton for 5 minutes at room temperature (RT). After permeabilization the samples were washed with PBS and stained with phalloidin-FITC (1 mg/ml stock solution diluted 1:1000 in PBS) for 30 minutes at RT. Then the samples were washed with PBS and stained with DAPI for 5 minutes at RT. After incubation period, the samples were rinsed with PBS and analyzed by the fluorescent microscope.

3.2.2.3 Fabrication of *in vivo* scaffolds for *in vitro* testing

New composite scaffold was designed for the *in vivo* experiments. The well established method of spinal cord bridge production was used (Thomas et al., 2013). The bridges were developed and tested in the laboratory of professor Shea (University of Michigan, USA). They are made from PLGA (poly-lactide-co-glycolide acid) microparticles. Briefly, PLGA microspheres are mixed with salt crystals (sodium chloride) of defined size (63 - 106 μm). Dextran with glucose and sucrose and with distilled water are mixed in extra beaker. This mixture is boiled and caramelized. From the caramelized sugar are drawn fibers of the diameter of 150 to 250 μm . The microsphere mixture together with the sugar fibers are placed into a specific mold to make a half-cylinder with evenly distributed sugar fibers (7 fibers per mold). The mold is placed into a pressure vessel and the bridge is foamed in a CO_2 atmosphere under a high pressure (> 5,5 MPa) for 16 to 24 hours. After the foaming, the bridges are cut into a specific length and washed with deionized water to wash out the sugar fibers and salt crystals. After drying out the bridges are sorted under the microscope. The resulting bridges are porous with 6 to 7 longitudinal channels (Fig. 3.4 A). The channels, which are around 150 μm in diameter, allow the cell infiltration through a specific region of the implant, however, the channels itself do not actively guide the cells since the size of the channels is larger compared to the cells and their axons. The channels lined with the fibers were prepared to increase the neural cell infiltration as well as the infiltration of axons into the bridge. The original method was modified to place the oriented fibers into the channels. The polymer fibers are stucked to the sugar fibers, thus resulting in the deposition of the polymer fibers along the channels (Fig. 3.4 B). Three different types of scaffolds were made, one with no fibers (plain PLGA bridge; NoF), one with PCL fibers (PCL) and one with PCL-PPy fibers (PCL coated with polypyrrole; PCL-PPy).

To be able to test this scaffolds *in vitro*, the shape of the bridge had to be modified. The *in vitro* scaffolds were flat from both sides (top and bottom) and had a block shape with just one or two channels with or without fibers (Fig. 3.4 C,D).

3.2.2.4 *In vitro* testing of the *in vivo* implants

The *in vitro* samples were sterilized by 70% ethanol for several minutes and washed with distilled water. Then the samples were incubated with laminin (10 $\mu\text{g}/\text{ml}$) for one hour. After the incubation the samples were washed with Neurobasal medium. The samples were dried before the seeding of the DRGs.

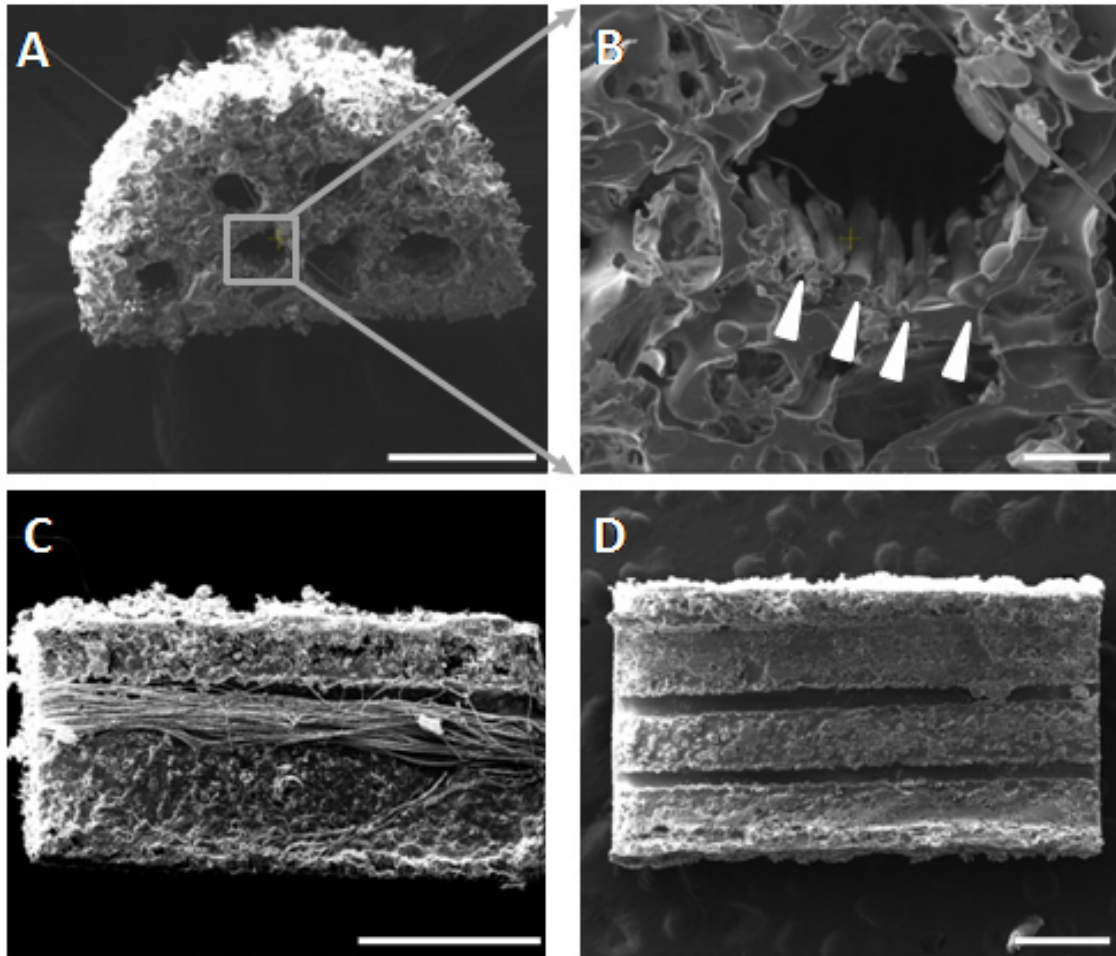


FIGURE 3.4: SEM images of the *in vivo* (A, B) and *in vitro* (C, D) scaffolds. (A) A transversal section of multiple-channel bridge (scale bar 400 μm). (B) Magnification of one particular bridge channel (arrows pointing at the aligned fibers; scale bar 50 μm). (C) *in vitro* sample with oriented PCL-PPy fibers (scale bar 1 mm). (D) *In vitro* samples with channels only (scale bar 500 μm).

The dorsal root ganglia (DRGs) were isolated from two days old mice pups (C57Bl6). The DRGs were washed and kept in the HBSS buffer (Hanks' Balanced Salt Solution) before use. The DRGs were placed on the scaffold specifically under the microscope so that the DRG covered the channel. The DRGs were kept dry for another two minutes and after the incubation the medium was added (Neurobasal medium supplemented with B27, L-glutamine, Penicillin / Streptomycin and NGF).

The medium was changed every other day. After 7 days of incubation the samples were fixed in 4% paraformaldehyde and they were stained using the primary antibody against β -tubulin (mouse anti- β -3-tubulin, 1:1000) and AF555 goat anti-mouse IgG as secondary antibody (1:1000). Nuclei were stained with Hoechst

(Hoechst 33342, 1:2000) (Table 3.12). The samples were observed under the inverted fluorescent microscope (AxioObserver) using a 10x dry objective and analyzed by ImageJ.

TABLE 3.12: Sudan Black and β -3-tubulin staining

WASHING	1x 2 min 1x TRIS
FIXING	10 min at RT in cold (4°C) 4% paraformaldehyde
WASHING	2 x 5 min in 1x TRIS
BLOCKING	4 hr at RT in 0,12 g of Sudan Black / 40 ml 70% ethanol (filtered)
WASHING	3 x 5 min in 1x TRIS with 0,1% Triton X-100
BLOCKING	In 10% NGS in 1x TRIS with 0,1% Triton X-100 for 1 hr at RT
PRIMARY	Mouse anti- β 3t 1:1000 in 10% NGS in 1x TRIS with 0,1% Triton X-100
INCUBATION	O/N at 4°C (let samples warm up for 30 min before continuing)
WASHING	3 x 5 min in 1x TRIS with 0,1% Triton X-100
SECONDARY	AF555 goat anti-mouse IgG 1:1000 in 1% NGS in 1x TRIS with 0,1% Triton X-100
INCUBATION	60 min at RT
WASHING	3 x 5 min in 1x TRIS with 0,1% Triton X-100
COUNTERSTAINING	Hoechst 33342 1:2000 in 1x TRIS for 2 min
WASHING	1 x 5 min in 0,1% Triton X-100 in 1x TRIS, 2 x 5 min in 1x TRIS

3.2.2.5 Surgeries and sample collection

All animals housing conditions, surgical procedures, and postoperative care was conducted according to IACUC guidelines at the University of Michigan, Michigan, USA. Four weeks old female mice aged 6 - 8 weeks (C57Bl6) were anesthetized using isoflurane (2%). Mice received a T9 laminectomy, followed by a left-sided double lateral hemisection and removal of a unilateral 1 - 1.1 mm segment of the spinal cord to enable bridge implantation into the resulting gap. The length of the bridge was greater than the length of the hemisection to ensure good apposition of the multichannel bridge to the spared rostral and caudal

spinal cord. The bridges were sterilized by 70% ethanol and washed by distilled water prior to implantation. PLGA multichannel bridges were implanted into the gap immediately after SCI. After the bridge implantation, the dorsal surface of the spinal cord above the injury site was covered with gelfoam, the muscle sutured with 5/0 chromic gut, and the skin closed using wound clips. Postoperative care included administration of Baytril (enrofloxacin 2.5 mg/kg, once a day for 2 weeks), buprenorphine (0.1 mg/kg twice a day for 3 days), and lactate ringer solution (5 ml/100g, once a day for 5 days). Bladders were expressed twice daily until function recovered, and mice monitored daily thereafter.

46 mice were used for this study, one mouse died and two mice had to be euthanized. No animals were excluded from the histological assessments or RNA isolation. The bridges were explanted after 2 or 8 weeks. Bridges isolated after 2 weeks were either used for RNA isolation with subsequent qPCR, or were deep-frozen into a mounting media and sectioned transversally in 12 μm thick slices (cryostat Microm HM525). The slices were collected from rostral to caudal end of bridge in series of 7 slides (series named A, B, C, etc.; resulting in A1 to A7 slides), gradually 1 slice per slide (from A1 to A7), until 3 slices per slide were collected (Fig. 3.5). This technique let to the distance of 72 μm (6 \times 12 μm) in collected tissue on one slide. The bridges isolated after 8 weeks were only collected for sectioning. The sections were fixed and subjected to immunohistochemistry.

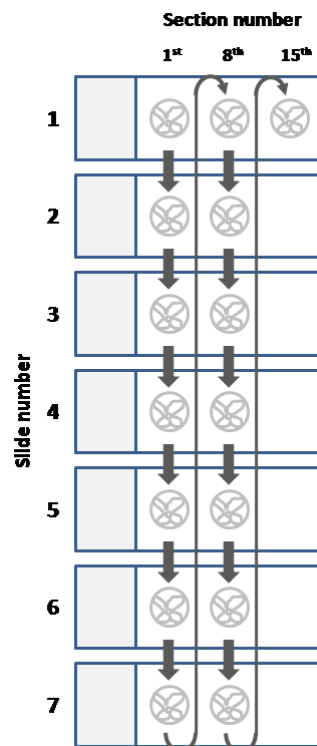


FIGURE 3.5: Diagram of the section deposition on the slides.

3.2.2.6 RNA isolation

Upon retrieval, the samples were deep frozen on dry ice. Four mice per each condition (NoF, PCL, PCL-PPy, control = no bridge) were euthanized except for the bridge with PCL fibers, where only three mice survived. Samples were homogenized by IKA T25 Digital Ultra Turrax homogenizer with S 25 N - 8 G ST dispenser in 1 ml of TRIZOL Reagent. RNA was isolated using TRIZOL Reagent according to the protocol. After the isolation, the RNA was purified by Direct-ZOL™ RNA MiniPrep Plus. The RNA concentration and purity was checked by NanoDrop. Isolated RNA was stored at -20 °C.

3.2.2.7 cDNA Synthesis

The cDNA was synthesized from the isolated RNA using iScript™ cDNA Synthesis Kit. For each reaction, 1 µg of RNA was used. The reverse transcription was done according to the manufacturer's protocol using BIO-RAD C1000 Touch Thermal Cycler. The cDNA was stored in -20 °C.

3.2.2.8 qRT-PCR

The quantitative PCR (qPCR) was performed in triplicates for all samples using iQ™ SYBR® Green Supermix according to the manufacturer's protocol. The qPCR was performed on the BIO-RAD C1000 Touch Thermal Cycler. The primer sequences are listed in the table 3.13. Samples from four mice were collected for each condition (except for PCL, where one mouse died). All genes were run in triplicates.

TABLE 3.13: Gene primers' sequences used for qRT-PCR

Gene	Primer	Reference
18s rRNA forward	5'-GCAATTATCCCCATGAACG-3'	Uchida et al., 2010
18s rRNA reverse	5'-GGCCTCACTAAACCATCCAA-3'	
MHC II forward	5'-GACGCTCAACTTGTCCCAA-3'	Kigerl et al., 2010
MHC II reverse	5'-GCAGCCGTGAACCTGTTGA-3'	
iNOS forward	5'-CCCTTCAATGGTTGGTACAT-3'	Kigerl et al., 2010
iNOS reverse	5'-ACATTGATCTCCGTGACAGC-3'	
CD86 forward	5'-TTGTGTGTGTTCTGGAAACG-3'	Kigerl et al., 2010
CD86 reverse	5'-AACTTAGAGGCTGTGTTGCT-3'	
arginase forward	5'-GAACACGGCAGTGGCTTTA-3'	Kigerl et al., 2010
arginase reverse	5'-TGCTTAGCTCTGTCTGCTTT-3'	
CD206 forward	5'-TCTTTGCCTTTCCAGTCTC-3'	Kigerl et al., 2010
CD206 reverse	5'-TGACACCCAGCGGAATTTTC-3'	
cytochrome C forward	5'-GAGGCAAGCATAAGACTGGA-3'	Xu et al., 2016
cytochrome C reverse	5'-TACTCCATCAGGGTATCCTC-3'	
caspase 3 forward	5'-CCTCAGAGAGACATTCATGG-3'	Xu et al., 2016
caspase 3 reverse	5'-GCAGTAGTCGCCTCTGAAGA-3'	

qPCR started with a 3 min hot start at 95 °C followed by 40 cycles of the following: 95 °C for 10 s, 55 °C for 30s. The reaction ended with 95 °C for 10 s, 65 °C for 5 s and 95 °C for 5 s.

The $2^{-\Delta\Delta CT}$ method (Livak and Schmittgen, 2001) was used to calculate fold changes in mRNA levels for all genes compared to the negative control (mice without bridge) using 18s rRNA as the internal control gene.

3.2.2.9 Immunohistochemistry

Bridges were implanted into the mice' spinal cord for 2 (4 mice for each condition) or for 8 (6 mice for each condition) weeks. Bridges were sectioned and the sections were collected as described above. One slide from rostral, middle and caudal region was chosen per each animal. Bridge sections after 2 weeks implantations were fixed in pre-chilled 100% acetone (-20 °C) for 5 min at room temperature and stained using the following primary antibodies to detect neutrophils (goat anti-arginase 1, 1:100) and M1 macrophages (rat anti-F4/80, 1:200) and CF555 donkey anti-goat IgG (1:1000) and AF647/633 goat anti-rat IgG (1:1000) as secondary antibodies. Nuclei were stained with Hoechst (Hoechst 33342, 1:2000) (Table 3.14).

TABLE 3.14: Arginase 1, F4/80 staining

DRYING	Warm to RT
FIXING	5 min at RT in pre-chilled (-20°C for 30 min) 100% acetone
WASHING	1 x 5 min in 1x TRIS
BLOCKING	4 hr at RT in 0,12 g of Sudan Black / 40 ml 70% ethanol (filtered)
PERMEABILIZATION	10 min in 0,5% Triton X-100
WASHING	3 x 5 min in 0,1% Tween in 1x TRIS
BLOCKING	10% NDS in 0,1% Tween in 1x TRIS for 1 hr
PRIMARY	Goat anti-arginase 1 1:100 in 1% NDS in 0,1% Tween in 1x TRIS
INCUBATION	O/N at 4°C
WASHING	3 x 5 min in 0,1% Tween in 1x TRIS
SECONDARY	CF555 donkey anti-goat 1:1000 in 1% NDS in 0,1% Tween in 1x TRIS for 2 hr
WASHING	3 x 5 min in 0,1% Tween in 1x TRIS
PRIMARY	Rat anti- F4/80 1:200 in 1% NGS in 0,1% Tween in 1x TRIS
INCUBATION	O/N at 4°C
WASHING	3 x 5 min in 0,1% Tween in 1x TRIS
SECONDARY	AF647 goat anti-rat 1:1000 in 1% NGS in 0,1% Tween in 1x TRIS for 2 hr
WASHING	1 x 5 min in 0,1% Tween in 1x TRIS, 1 x 5 min in 1x TRIS, 1 x 5 min in dH ₂ O
COUNTERSTAINING	Hoechst 33342 1:2000 in dH ₂ O for 2 min
WASHING	1 x 5 min in dH ₂ O
COVERING	Fluoromount G - cover and let dry for 30 min at RT, store in 4°C

Bridges retrieved from mice after 8 weeks were fixed in cold 4% PFA for 12 min at room temperature and stained using the following primary antibodies to detect neurites (rabbit anti-NF200, 1:200), oligodendrocytes' myelin (goat anti-MBP, 1:500) and Schwann cells' myelin (chicken anti-P0, 1:250) and CF555 donkey anti-rabbit IgG (1:1000), CF488 donkey anti-goat IgG (1:1000) and CF633 donkey anti-chicken IgY (1:1000) as secondary antibodies. Nuclei were stained with Hoechst (Hoechst 33342, 1:2000) (Table 3.16).

TABLE 3.16: NFM 200, MBP, P0, staining

DRYING	Air dry section for 10 min
FIXING	12 min at RT in cold (4°C) 4% PFA
WASHING	3 x 5 min in 1x TRIS
PERMEABILIZATION	0,5% Triton X-100 in 1x TRIS for 15 min
BLOCKING	10% NDS in 0,1% Triton X-100 in 1x TRIS for 1 hr at RT
PRIMARY	Rabbit anti-NFM200 1:200, goat anti-MBP 1:500, chicken anti-P0 1:250 in 10% NDS in 0,1% Triton X-100 in 1x TRIS
INCUBATION	O/N at 4°C (let warm up for 30 min before continuing)
WASHING	2 x 5 min in 0,1% Triton X-100 in 1x TRIS
SECONDARY	CF555 donkey anti-rabbit, CF488 donkey anti-goat, CF633 donkey anti-chicken all 1:1000 in 1% NDS in 0,1% Triton X-100 in 1x TRIS
INCUBATION	90 min at RT
WASHING	1 x 5 min in 0,1% Triton X-100 in 1x TRIS
COUNTERSTAINING	Hoechst 33342 1:2000 in 0,1% Triton X-100 in 1x TRIS for 2 min
WASHING	1 x 5 min in 0,1% Triton X-100 in 1x TRIS, 1 x 5 min in 1x TRIS, 1 x 5 min in dH ₂ O
COVERING	Fluoromount G - cover and let dry for 30 min at RT, store in 4°C

Images were captured at 20x by the fluorescent microscope (AxioObserver). Stitched images were created using the Zeiss software (Zen Pro) and used for cell counting. The bridge area content was counted using ImageJ. Three tissue sections per region (rostral, middle, caudal) per animal, and four animals per condition were used for the quantification of the 2 weeks long implantations. The counting was done manually using ImageJ. Three tissue sections per region (rostral, middle, caudal) per animal, and six animals per condition were used for the quantification of the 8 weeks long implantations. The counting was semi-automated using MATLAB according to McCreedy (McCreedy et al., 2016).

3.2.3 Statistics

The obtained data were processed by Microsoft Excel. Statistical analysis was performed using GraphPad Prism 6 software. Data were analyzed either by multiple comparison analysis using one-way analysis of variance (ANOVA) or by t-test and Scheffe post-hoc analysis with a p-value < 0.05 defined as significant depending on the dataset. For all conditions, $n = 6$ mice for histological analysis of neurofilament, while $n = 4$ was used for histological analysis of immune response and qRT-PCR analysis. The fiber diameter was analyzed from $n = 100$ and higher. All values are reported as mean \pm standard deviation or standard error of the mean, noted at each analysis.

Chapter 4

Results and discussion

Drawing was used for fabrication of oriented fibers and the drawing conditions were monitored and evaluated. The most suitable conditions were used for fabrication of oriented scaffolds functionalized with polypyrrole, which were subsequently tested *in vitro* and *in vivo*. Results of these experiments were compared and discussed in context to other studies.

4.1 Drawing technology

Drawing is not particularly the method of choice for scaffold fabrication, therefore any commercially available lab - scale production device is missing. The advantage of this method is that it is possible to draw the fibers just by hand, but the samples are often inhomogeneous, because it is impossible to keep the same conditions during drawing individual fibers. To improve the drawing technology a lab-scale manipulator for drawing fibers from polymer solutions was designed and constructed. The mobile drawing element of the manipulator moves from one side to another in a repeating manner and produces single fibers one by one, laying them separately on an underlay. A basic production scheme can be seen in [4.2](#).



FIGURE 4.1: The manipulator representing the drawing movement (Strnadová et al., 2020)

The manipulator is able to move at high speeds (several $\text{m}\cdot\text{s}^{-1}$) and consists of three axes. The manipulator enables to program the trajectory of a drawing element and arrangement of fibers, and to set the speed in a wide range of velocities. This enables us to keep constant conditions during the fiber spinning, thus being able to study the influence of particular conditions on the fiber formation (solution viscosity, speed and trajectory of drawing, solvent evaporation etc.) on the properties of the fibers.

The Manipulator is a universal machine with an extendable manner of design. The core of the machine is a high precision positioning system. The machine is extendable due to an aluminum-profile building system. It is equipped with a polymer dosing device and lighting and it is possible to equip the Manipulator with additional modules, such as twisting, protective cover, etc. The machine is built on an ITEM24 construction system. To ensure its fluent motion, professional positioning axes (BAHR Modultechnik GmbH) with a synchronous belt were used. Three axes are set up to a Cartesian coordinate system, where X-Z is connected to a gantry X-shape (ELZI) system, and axis Y is doubled and joined with a synchronizing rod. Pulleys are connected to a servomotor through an elastic clutch. The servomotors possess $2 \times 0.45 \text{ Nm}$ and 0.84 Nm , at 4500 rpm nominal. The machine is controlled by isiMotion system, connected to a panel PC. The workspace dimensions are $1 \times 0.2 \times 0.2 \text{ m}$ and the repeating accuracy of this system is $\pm 0.1 \text{ mm}$. A digital dispenser (OKI International) connected

to a standard air compressor with an air accumulator is used as a polymer dosing device.

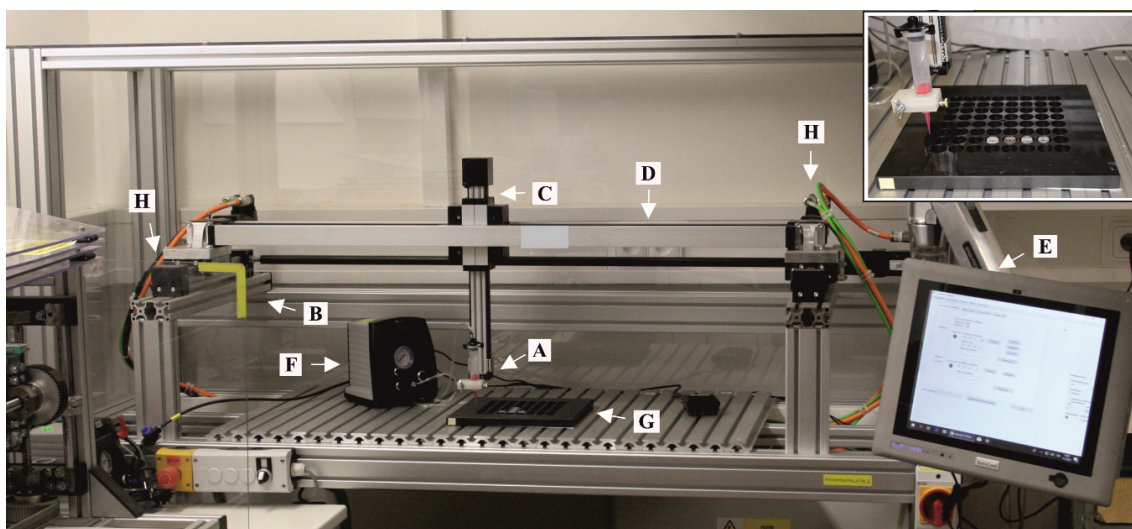


FIGURE 4.2: Image of the Manipulator. (A) the dosing system, (B - D) the positioning axes working in the X, Y and Z coordinates, (E) the computer with controlling software, (F) the dispenser, (G) the workplace, (H) the servomotors. The detail of the workplace is shown in the upper corner of the image.

Previously, the fibers were drawn for example by the tip of the STM microscope (Ondarcuhu and Joachim, 1998) resulting in a very short fibers (hundreds of micrometers long). Nain and coworkers used a glass micropipette attached to a motorized positioner, which was dosing the polymer solution continuously, but also their fibers were only several millimeters long (Nain, Amon, and Sitti, 2005; Nain, Amon, and Sitti, 2006). On the other hand, Yang (Yang et al., 2008) or Xing (Xing, Wang, and Li, 2008) used silica rod / taper to pull fibers from a polymer solution, or a polymer melt, respectively. Both obtaining fibers of tens of centimeters long. All of the authors were able to obtain fibers ranging from several micrometers to sub-100 nanometers in diameter. All of those published papers show either production of a single fiber or very simple and porous meshes fixed to an underlay. None of the previously reported structures were suitable for tissue engineering applications, because the cells would preferentially attach to the underlay. In 2015 Tokarev *et al.* (Tokarev et al., 2015) published an article about brush-spinning, which is basically drawing. They can produce highly oriented structures from nanofibers (hundreds of nanometers) up to microfibers. The structure can be very dense, the fibers can be oriented in different directions by placing the layers of the fibers on top of each other, each produced under different angle. Different 3D structures can be made as well by using various collectors. But from the nature of this method, the fibers cannot be manipulated separately to form

more complicated structure. This problem is solved by Yuan *et al.* (Yuan, Cambron, and Keynton, 2015). They developed a 3-axis robot with dispensing system, allowing them to dose the polymer at given time and location and to draw very complex structures. Compared to their machine, the Manipulator has a larger working area, thus we can produce longer fibers. It works with higher speeds of drawing, which is beneficial while drawing fiber from low polymer concentrations. It can be adjusted to draw the fibers not only from polymer solution, but also from a polymer melt or from a polymer surface.

4.2 Influence of the polymer concentration and drawing speed on the fiber diameter

The influence of extrinsic conditions on the fiber production are indisputable. Several parameters were followed during drawing as well. The PCL (M_n 80,000, Sigma Aldrich) fibers were drawn using Manipulator by established velocities (0.1, 0.5, 1, 2 and 3 $m \cdot s^{-1}$) and concentrations (4%, 6%, 8%, 12%, 16% and 20% by weight) (see chapter 3.2.1.3). From our results it is evident that under the ambient conditions the fiber diameter decreases with an increasing speed of drawing and a decreasing polymer solution concentration (Fig. 4.3). Furthermore, we found that the fiber diameter distribution decreases with an increasing speed of drawing (Fig. 4.4). The 6% PCL solution drawn at a speed of 3 $m \cdot s^{-1}$ resulted in the significantly smallest mean value of a fiber diameter ($2.51 \pm 0.12 \mu m$), whereas the 20% PCL solution drawn with the speed of 0.1 $m \cdot s^{-1}$ resulted in the significantly highest mean value of fiber diameter ($9.56 \pm 0.49 \mu m$). The lowest fiber diameter measured throughout all the samples was 190 nm for the 6% PCL at the speed of 2 $m \cdot s^{-1}$. The 6% PCL solution was also the lowest concentration capable of fiber drawing, although only at a drawing speed of 1 $m \cdot s^{-1}$ and higher (Strnadová *et al.*, 2020). Nevertheless, the fibers prepared from 12% solution have the lowest fiber diameters distribution, especially at drawing speeds above 1 $m \cdot s^{-1}$. The fibers prepared at these conditions were therefore used for cell culturing experiments.

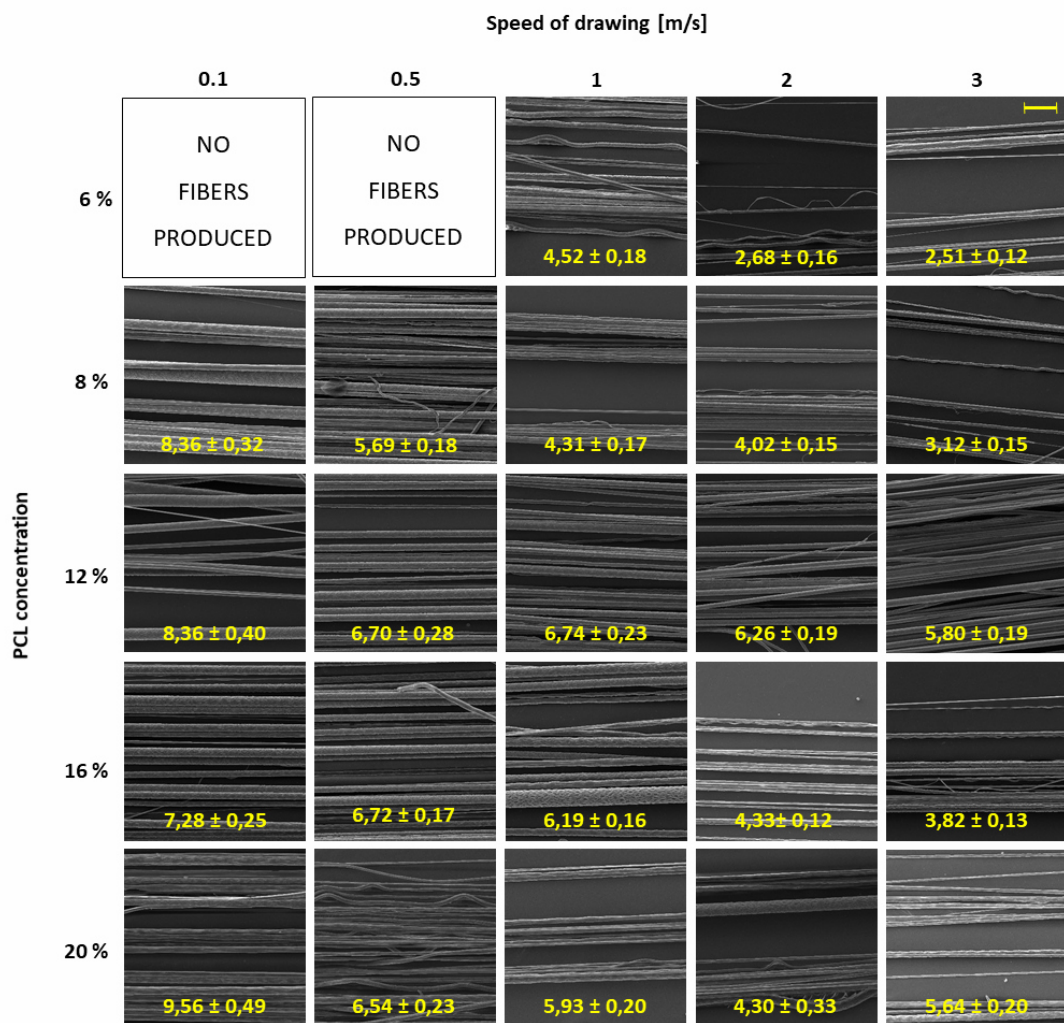


FIGURE 4.3: Diagram of the fibers' morphology depending on the speed of drawing and the polymer concentration. The fiber diameters are presented as mean in $\mu\text{m} \pm \text{SEM}$ and are marked in yellow. Scale bar: $50 \mu\text{m}$

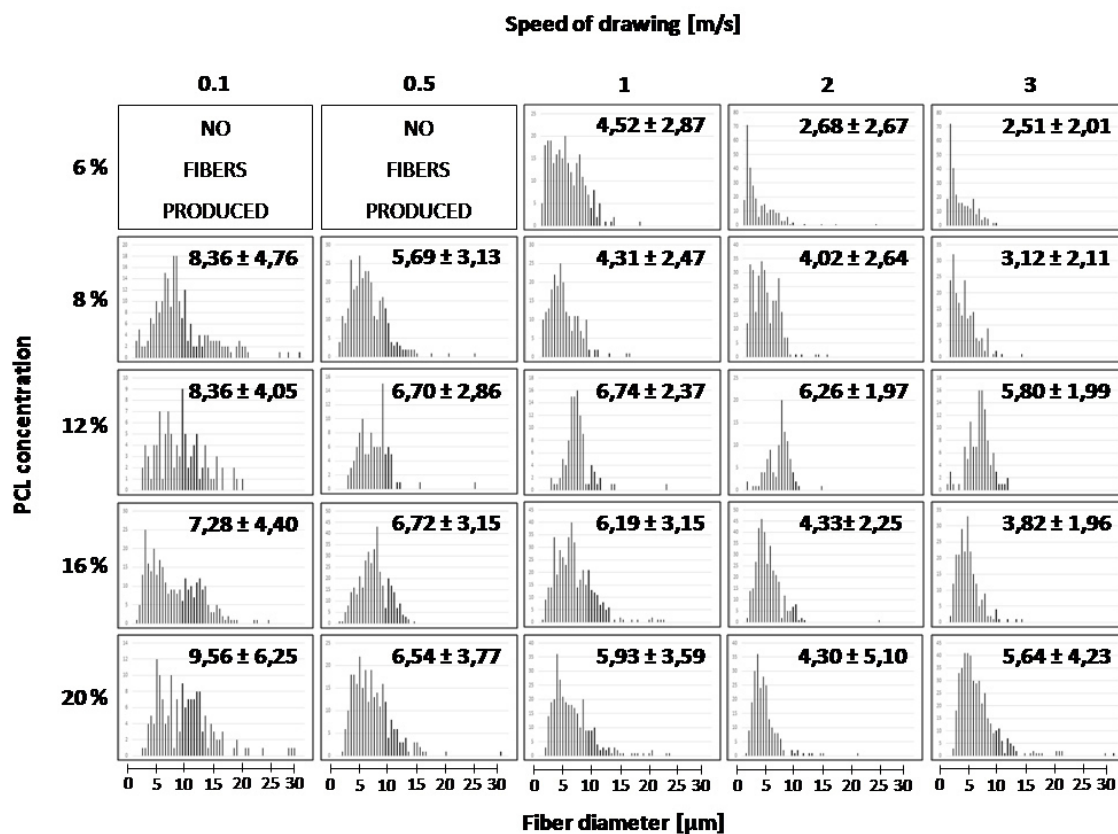


FIGURE 4.4: Histograms showing the fiber diameter distribution

There were two types of defects observed on the prepared fibers from the PCL of M_n 80,000. The fiber narrowing (Fig. 4.5) was one of the phenomena. The formation of thinner regions is significantly less frequent for fibers prepared from polymer solutions at a concentration of 12% and 16%. The SEM examinations of fibers reveal that the fibers are prone to multiple necking in some cases, which means the contraction of the fiber diameter from 1,000 nm to nearly 100 nm. The necks are not evenly spaced along the fibers. The necking and crazing was first described in the electrospun nanofibers by Zussman (Zussman, Rittel, and Yarin, 2003) as the failure mode. Therefore, we hypothesize, that the neck structure on a drawn fiber appears as a result of a fast solvent evaporation and strong stretching of solidified fibers during the fiber drawing.

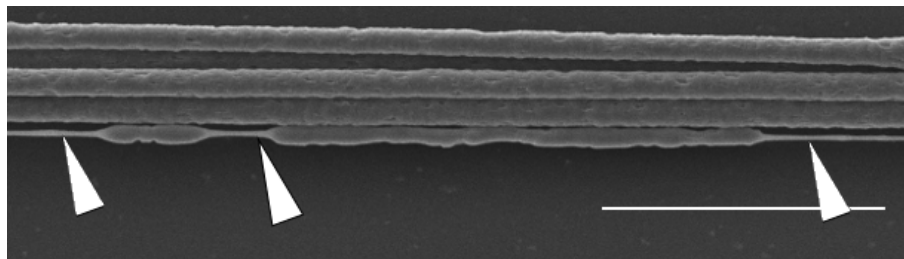


FIGURE 4.5: SEM image of the fibers drawn from the 8% PCL solution at a speed of $1 \text{ m}\cdot\text{s}^{-1}$, one of the defects (fiber necks) is indicated by arrowheads, Scale bar: $50 \mu\text{m}$.

The other type of defects observed during drawing was a nanostructured surface (Fig. 4.6). Unlike during the manual drawing of fibers, the fibers drawn by Manipulator possess nanostructured surface pattern. The pores are hundreds of nanometers wide and deep. The pores are formed by the solvent evaporation and their structure is influenced by the polymer and the solvent system used. Similar structures were described previously on electrospun fibers (Zussman, Rittel, and Yarin, 2003; Cui, Zhou, and Chang, 2010; Yang et al., 2015), and are known to be beneficial for the cell-fiber interaction and to enhance the cell adhesion (Megelski et al., 2002).

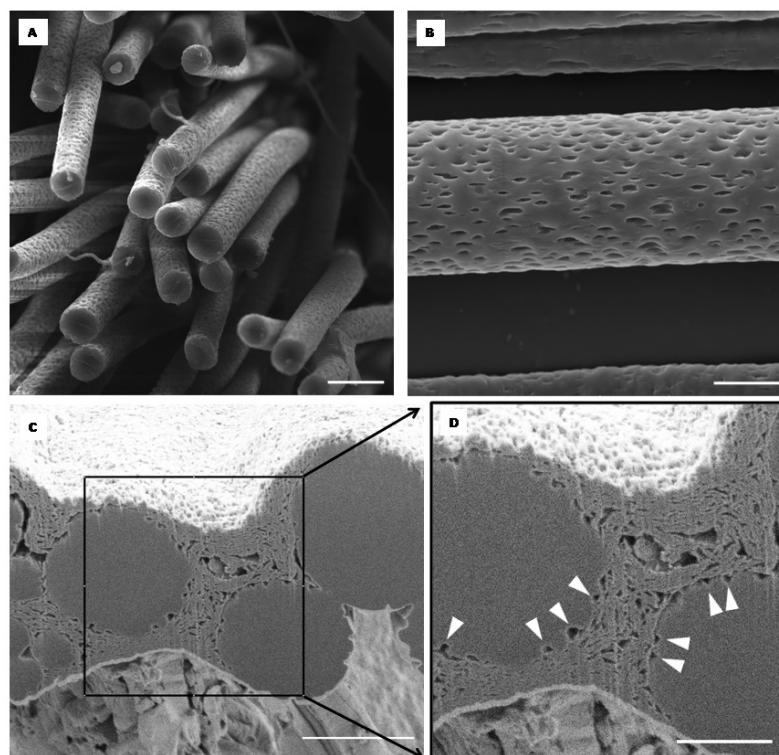


FIGURE 4.6: SEM images showing the morphology of the fibers. (A) A uniform circular cross-section (scale bar: $20 \mu\text{m}$), (B) nanostructured porous surface (scale bar: $10 \mu\text{m}$) and (C) a cross-section of the fibers (scale bar: $5 \mu\text{m}$) and (D) pore depth indicated by arrowheads (scale bar: $3 \mu\text{m}$).

Other types of polymers were drawn using Manipulator as well to show the versatility of this method (PCL (M_n 45,000, Sigma Aldrich), PVA (M_w 130,000, MOWIOL 20-98, Merck) and PA6 (Ultramid B27, BASF)). All solutions (see chapter 3.2.1.1) were drawn with the acceleration of $0.5 \text{ m}\cdot\text{s}^{-1}$ and the velocity of $1 \text{ m}\cdot\text{s}^{-1}$. Fiber diameter was typically more than one micrometer. PVA was spinnable from the concentrations above 20%. Average fiber diameters were $1,056 \pm 236 \text{ nm}$ for 20% solution, $1,838 \pm 648 \text{ nm}$ for 24% solution and $1,868 \pm 763 \text{ nm}$ for 28% solution. In case of PCL (M_n 45,000, Sigma Aldrich), concentration of 28% and higher led to fiber formation. The diameter of PCL fibers was higher than PVA fibers having the fiber diameter of $5,949 \pm 4,188 \text{ nm}$ (28%) and $4,019 \pm 1,471 \text{ nm}$ (32%). No fibers were obtained using PA6. Morphology of drawn fibers is depicted in Figure 4.7.

Compared to the fiber diameter of PCL M_n 80,000 (all used concentrations) drawn at the $1 \text{ m}\cdot\text{s}^{-1}$ speed, which was $4.31 \mu\text{m}$ and higher, the PVA had significantly lower fiber diameter (maximum mean value $1.9 \mu\text{m}$ for the highest concentration). In the case of PCL M_n 45,000, the mean values of the fiber diameter were comparable to PCL M_n 80,000. Both PVA and PCL M_n 45,000 were drawn from higher concentrations than PCL M_n 80,000 in the previous experiment. Below are shown the concentrations of polymer solutions (PVA, PCL M_n 45,000) from which it was possible to draw the fibers.

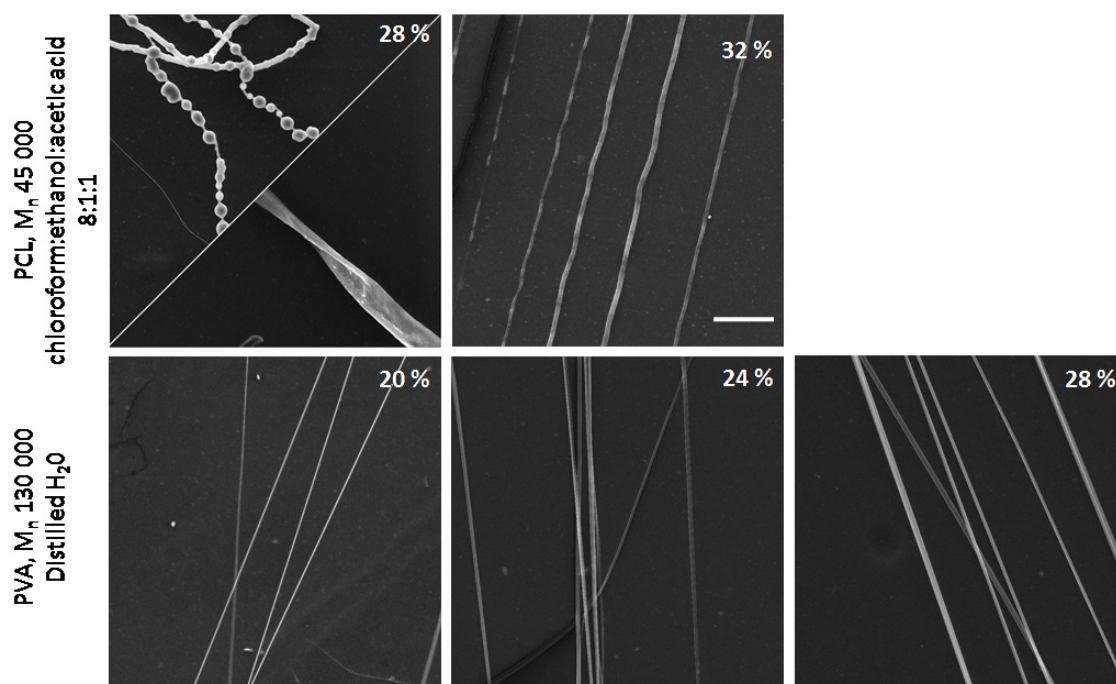


FIGURE 4.7: Images from SEM showing the drawn fibers of PCL (M_n 45,000) and PVA (M_n 130,000) at different concentrations. Scale bar: $50 \mu\text{m}$.

All three polymers (PVA, PCL M_n 45,000, PCL M_n 80,000) were of different molecular weight and were also dissolved in different solvents / solvent system. Both of these parameter influence the solubility of the polymer and the viscoelastic properties of the polymer solution and thus its spinnability and the resultant fiber appearance (Ziabicki, 1976; Koski, Yim, and Shivkumar, 2004; Reneker and Yarin, 2008). For example, the solvent system of chloroform : ethanol : acetic acid (used for PCL M_n 45,000) is mostly used for electrospinning of PCL. Acetic acid and ethanol lowers the surface tension, which enhances the spinnability of the solution via electrospinning by helping with the formation of the polymer jet by electric field. On the other hand, in the case of drawing, this feature can be undesirable. The whole process of fiber formation by drawing is significantly longer compared to electrospinning and lowering the surface tension of the solution may lead to breakage of the fluid thread, also called as Rayleigh instability (Ziabicki, 1976). This leads to lower fiber production and defects forming along the fiber (Fig. 4.7).

The defects occurring during electrospinning have been described Ziabicki, 1976; Zussman, Rittel, and Yarin, 2003; Koski, Yim, and Shivkumar, 2004; Reneker and Yarin, 2008). The breakup of the polymer jet has been shown to depend on polymer concentration and molecular weight (Koski, Yim, and Shivkumar, 2004). At low molecular weight the destabilization of the jet occurs, which leads to the beads formation. As the molecular weight increases, the polymer jet is stabilized and typical fibers are formed. As the molecular weight of the polymer grows even higher, the solvent evaporation at the jet surface is fast enough to form a skin, the fibrous structure collapses and flat ribbons instead of fibers are formed (Koski, Yim, and Shivkumar, 2004; Reneker and Yarin, 2008). As the solution concentration increases, there is a gradual shift from circular to flat fiber. In low molecular weight polymers, this shift occurs at a higher values of concentrations than in the high molecular weight polymers (Koski, Yim, and Shivkumar, 2004). These findings are in contrast what was observed during drawing. The beads and ribbons occurred simultaneously at the lower concentration of the low molecular weight PCL. We hypothesize that this discrepancy is caused by different mechanism of fiber formation during electrospinning and drawing. Drawing uses mechanical energy and the fiber is pulled from the polymer droplet. The speed of single fiber formation is incomparably slower during drawing than electrospinning. On the other hand, these defects were seen only in one experiment and more data are needed for final conclusions

4.3 Viscosity and surface tension

The viscosity and surface tension influence the fiber formation, fiber diameter and distribution. The viscosity and surface tension was measured for the PCL M_n 80,000. The viscosity grew exponentially depending on the polymer concentration and was ranging from 0.33 Pa·s for the 6% PCL up to 32.91 Pa·s for the 20% PCL (Fig. 4.8). The surface tension was ranging from 35.32 mN·m⁻¹ for the 6% PCL up to 110.64 mN·m⁻¹ for the 20% PCL (Fig. 4.8).

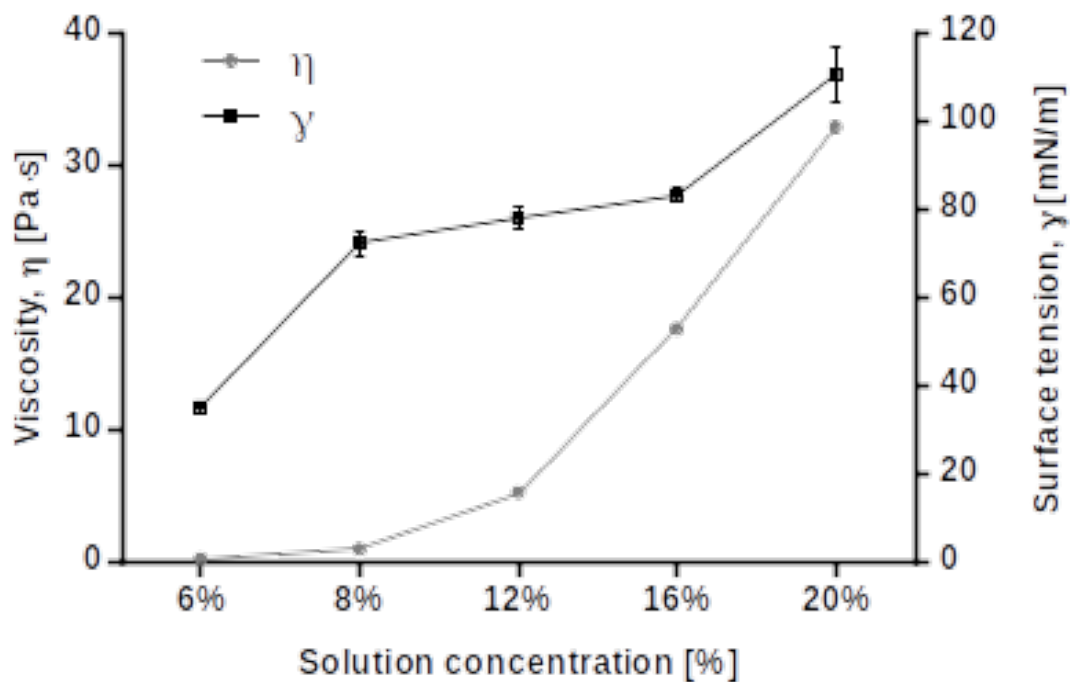


FIGURE 4.8: Comparison of viscosities and surface tensions of the polymer solutions in the dependence on solution concentration

The values of the surface tension are also not linearly arranged, but that could be caused by the inaccuracy in the measurements, as well as by the varying humidity conditions in the lab, since the measurements were not taken at the same time.

This experiment revealed the limit values for drawing under the set parameters (see chapter 3.2.1.3). The lowest concentration tested within this experiment, i.e. 6% polymer solution, which refers to value of 0.33 Pa·s for viscosity and 35.32 mN/m for surface tension, was the lowest concentration of the polymer which was possible to draw, but the limit speed of drawing was 1 m·s⁻¹. Whereas at higher concentrations (and viscosity), the speed limit of drawing was below

$0.1 \text{ m}\cdot\text{s}^{-1}$. With increasing viscosity and surface tension, the fiber diameter increases and so grows the fiber diameter distribution.

The solution viscosity and surface tension influences the spinnability of the solution. These parameters are influenced mainly by the solution concentration and its composition (polymer and its molecular weight and the solvent system) and each spinning method requires different parameters. In general, e.g. electrospinning requires lower surface tension for the fibers to be formed, whereas e.g. bubble-spinning requires higher surface tension, because first the polymer bubble needs to be formed prior to spinning

4.4 Mechanical testing

The polymeric materials used in tissue engineering are very often mechanically stressed. Mechanical properties of the implanted material are very important, because they should mimic the mechanical properties of the targeted tissue as much as possible. Not only they have to sustain the same stress as the neighboring tissue, while staying soft at the same time, but also these properties contribute to the cellular response. Mechanical properties can be tested by several approaches and they determine the breaking force and elongation at break and the collected data are used for calculations of the tension and relative elongation.

The mechanical properties were measured using the bundles of 200 drawn fibers made from PCL M_n 80,000 (see chapter 3.2.1.3). The test was done according to the standard ČSN EN ISO 5079. The diagrams show the measured force F , which is a function of the gauge length (Fig. 4.9). The diagram 4.10 shows the beginning of the measurement, thus the linear area of the curve is visible.

The Young's modulus of the 200-fiber bundle was 240.73 MPa. The force, tension and relative elongation at break were 0.1 N, 41.08 MPa and 527.89 %, respectively. All values are the mean value of all the measurements.

The tension values of the drawn samples are comparable to some results obtained from the measurement of electrospun fibers or fibers obtained by gravity spinning, which have the fiber diameter higher than 1 micrometer. The samples with the fiber diameter below 1 micrometer have the values of tensile strength up to ten times lower (Table 4.1).

It is evident from the results and also from the shape of the curve that the setup of this method of mechanical testing is not suitable. In neither case have the curves smooth shape, which is typical for testing the fibers. The instability of the tensile

TABLE 4.1: Comparison of the fibers' tension made by different spinning techniques.

Spinning Technique	Tensile Strength (MPa)	Fibers' Morphology	Reference
Electrospinning	2.2 - 9.6	Oriented fibers 350 - 550 nm	Thomas et al., 2006
Electrospinning	4.7	600 nm	Fujihara, Kotaki, and Ramakrishna, 2005
Electrospinning	40	Oriented fibers 1.4 μm	Fujihara, Kotaki, and Ramakrishna, 2005
Gravity spinning	1.8 - 9.9	147 - 190 μm	Williamson and Coombes, 2004
	8.2 - 74.3	Followed by cold drawing	Williamson and Coombes, 2004

curve and the fluctuating shape is given by the non-homogeneity of the particular fiber bundles (Fig. 4.9).

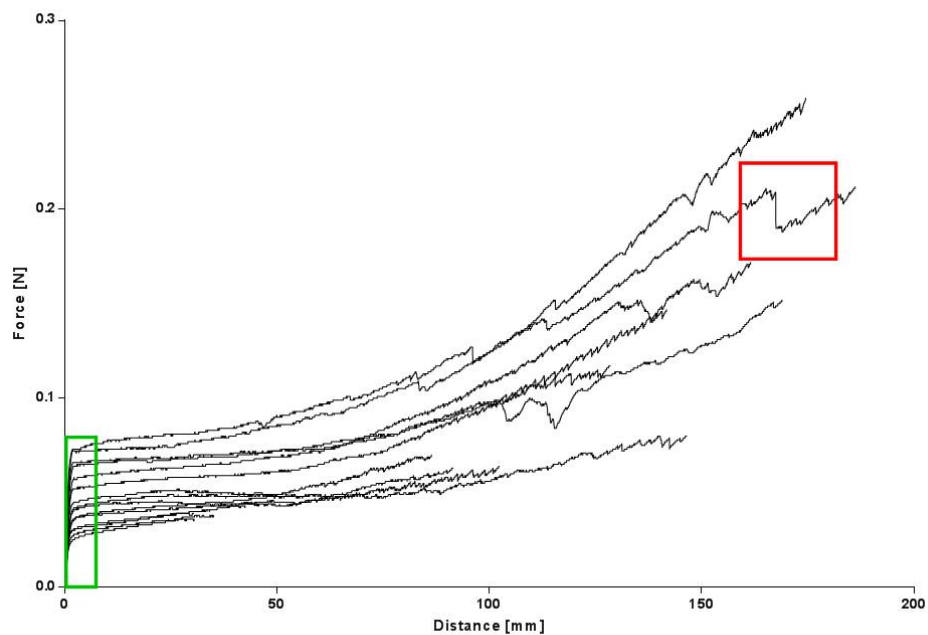


FIGURE 4.9: Diagram of the tensile curves of the individual measurements. The red rectangle shows the abnormality in the tensile measurement - the drop of the force value, which starts growing immediately again. The green rectangle shows the graph area depicted in closer detail in Fig. 4.10.

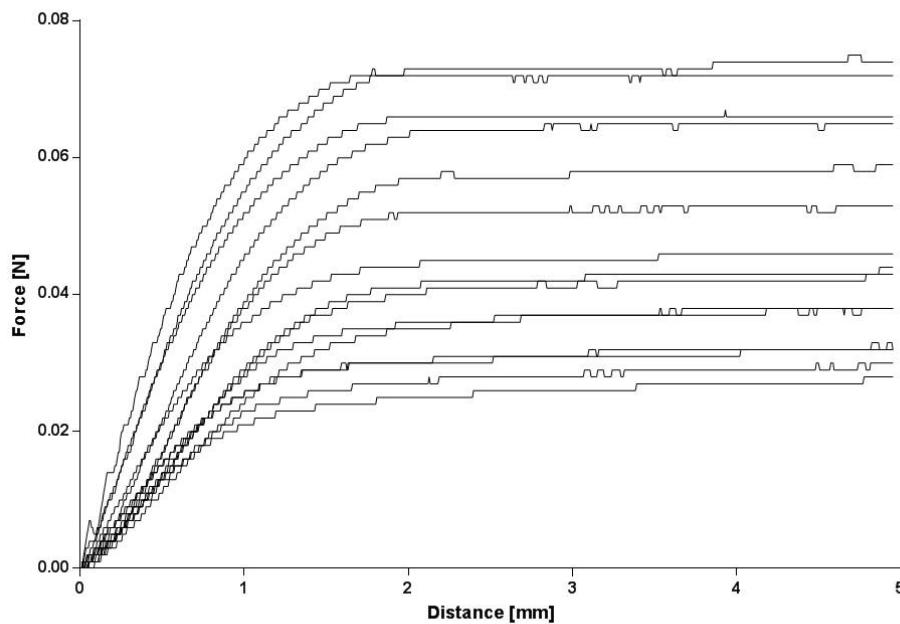


FIGURE 4.10: Diagram of the tensile curves with the emphasis on the beginning of the measurement showing the linear area of the curves, which are used for the calculations.

Also, the fiber diameter of individual fibers in the bundle is not homogeneous, both along the entire fiber length and in between the fibers in the bundle. This is not different from the electrospun fibers. But while electrospun fibers form a tissue-like structure with countless number of fibers and the whole structure is measured as one sample, the drawn samples are bundles of individual 200 fibers. That means that the mechanical properties of individual fibers in the bundle differ. This phenomenon can be observed from the shape of the curve. If there is a drop in the force value and immediately the force starts growing, that means that one or more fibers broke, but there are still many other fibers that can elongate (Fig. 4.9).

Another factor affecting the measurement is the attachment of the sample alone. The fibers are drawn in the bundle, that means that not all of the fibers are attached to the grip evenly and that increases the probability of fiber slipping between the neighboring fibers. That affects the behavior of individual fibers and of the whole bundle during the measurement.

This problem could be solved in the future by measuring the properties of individual fibers. It had been shown by Baker et al. and others (Baker et al., 2016; Neugirg et al., 2016), that mechanical properties of the individual fibers can be

tested by the tip of AFM (atomic force microscopy). The fibers measured by these authors were made from PCL and were 400 nm to 1,000 nm thick. It is questionable, whether our PCL fibers, which are usually above 1,000 nm thick would be suitable for such measurement. Otherwise, drawing is suitable method of fabrication for AFM testing. The fibers can be drawn in desired length, they are drawn separately and can be attached to the underlay. This avoids the problems of Baker *et al.* of aligning the electrospun fibers and attaching them separately to the underlay.

4.5 Functionalization of drawn scaffolds by polypyrrole

The drawn samples with fibers oriented in one direction were coated with thin layer of polypyrrole for further biological experiments (Fig. 4.11; see chapter 2.4), since PPy is widely used conducting polymer in tissue engineering and has very good stability and promotes the adhesion and proliferation of various cell types (see chapter 2.4.2) (Zeng *et al.*, 2013; Spearman *et al.*, 2015; Yang *et al.*, 2015).



FIGURE 4.11: Macroscopic image of the *in vitro* samples. Left - the PPy-coated sample.

The PPy layer was investigated under SEM (Fig. 4.12, 4.13). It is homogeneous and 50 - 100 nm thick (Fig. 4.13). The PPy layer comparably thick and smooth to other studies reported in the literature (Lee *et al.*, 2009; Yang *et al.*, 2015; Tiwari *et al.*, 2018). Moreover, drawing produces highly porous structure, which remains preserved even after the PPy coating (Fig. 4.12).

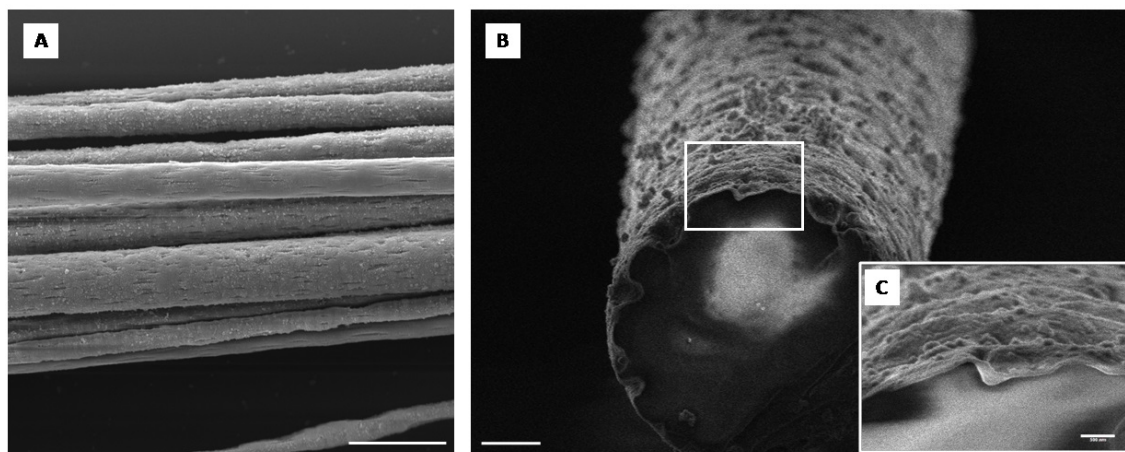


FIGURE 4.12: SEM images showing the PPy modified PCL fibers. (A) The coating of PPy is uniform and retains porous structure of the fibers. (B) The cross-section of the fiber with detailed image of the PPy layer thickness (C).

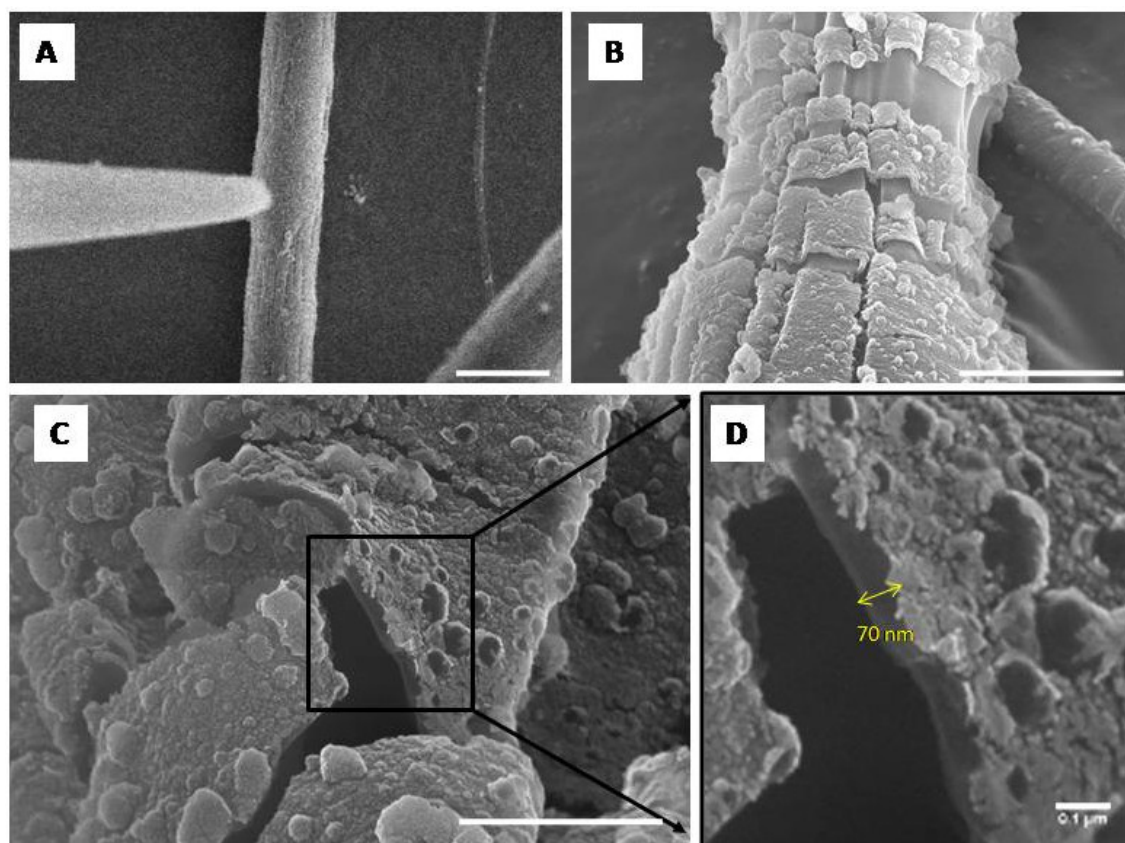


FIGURE 4.13: SEM images of PPy coated PCL fibres. The PPy layer was disrupted using the SEM (FEI Helios 650 Nanolab) retracting tip (A). (B) The disrupted PPy layer. (C, D) represent higher magnifications of the cracked PPy layer.

4.6 Conductivity measurement

The conductivity was measured by three different approaches, which differed in the used multimeter, number of fibers and the experiment setup, but used the measurement of resistivity for all approaches (see chapter 3.2.1.8). First experiment used 100 PPy-coated fibers, which were fixed between clamps in different distances (1 to 5 cm). Second experiment used 10 bundles of 200 PPy-coated fibers (2,000 fibers total) placed between aluminum foil and fixed within a Teflon frame and the resistance was measured from the aluminum foil. Third experiment was similar to the first one, but used much more sensitive multimeter.

All of the experiments were unsuccessful (the multimeters were not sensitive enough to measure the resistivity) and all our samples showed no conductivity value. On the other hand, if we use planar samples made by electrospinning from PCL and cover those by polypyrrole in the same chemical reaction, the resistance on those samples is measurable (approximately $3 \cdot 10^4 \Omega/\text{square}$) (Martínek, 2014). These data are consistent with other publications (Lee et al., 2009; Yang et al., 2015), where the fibers are prepared by electrospinning. Yang *et al.* used the four-point probe method. Their PPy layer was around 100 nm thick and they measured the conductivity from 35 to 50 mS depending on the polymerization time. Lee *et al.* measured the resistivity of the sample by placing two silver wires on the sample in the distance of 1 cm. Their PPy layer was also around 100 nm thick and the measured resistivity was ranging approximately from $9 \cdot 10^4$ to $7.5 \cdot 10^3 \Omega/\text{square}$, which refers to the conductivity of 11 to 130 $\mu\text{S}/\text{square}$. However, both experiments anyway do not correspond to the data published by Guimard *et al.* (Guimard, Gomez, and Schmidt, 2007), where the conductivity of PPy is reported to be 40 - 200 $\text{S}\cdot\text{cm}^{-1}$, depending on the method of polymerization and polymerization conditions.

Probably, the impossibility to measure the conductivity of the drawn PPy-coated fibers is due to the density of the fibers and overall appearance of the sample. Electrospinning produces fibrous mats with thousands of fibers layered over each other, whereas drawing produces separate fibers which never really form a layer even if they are drawn dense.

According to the parameters of our samples (fiber diameter, PPy layer thickness, length of the fibers), the conductivity should be around hundreds of nanoampere. Yet, after the consultation with Dr. Stejskal (Institute of Macromolecular Chemistry CAS, Conducting Polymers Department) and his experience, the conductivity on such samples as a bundle of 100 or 200 microfibers is negligible, and

therefore immeasurable. For the next experiment, much deeper discussion about the sample nature is needed to design proper drawn sample.

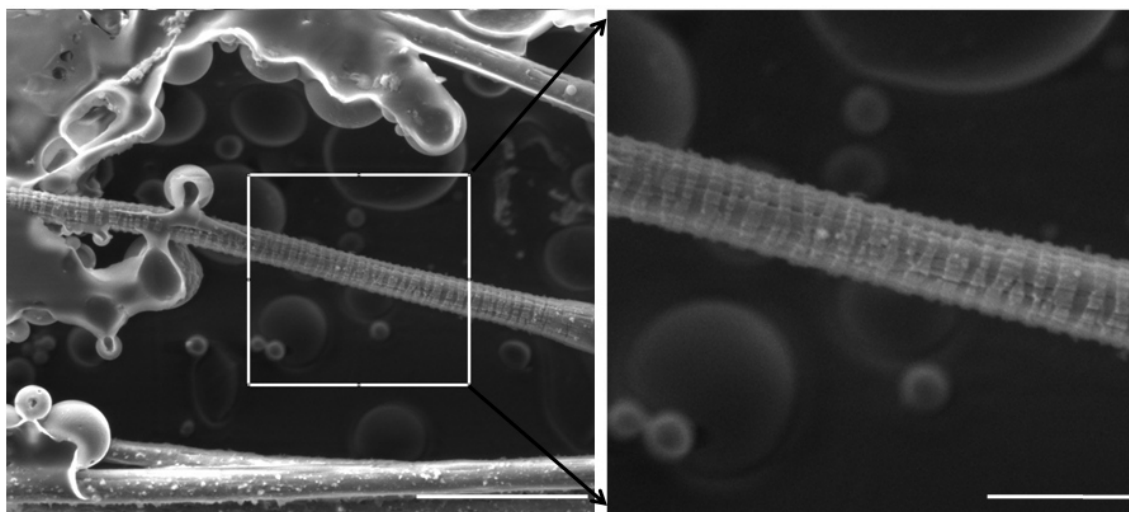


FIGURE 4.14: The SEM image of the micro fractures of the PPy layer on PCL fibers after the fiber stretching (scale bar: 30 μm) with the detailed image of the same (scale bar: 10 μm).

It is visible from Fig. 4.14 that after the fiber stretching, the homogeneous coherent layer of PPy breaks. This can be caused by inappropriate sample manipulation. Such sample disruption would cause big complications and inaccuracy in the conductivity measurement. On the other hand, such samples should not represent a big problem for the *in vitro* and *in vivo* system, because we expect the cells to elongate along the fibers, thus superimposing and connecting the gaps, which should overcome the problem of the layer conductivity.

4.7 Water contact angle

Samples for the analysis were prepared by drawing. 300 fibers from PCL M_n 80,000 were fixed within the fixation ring for the analysis and the drops were placed on the fibers as shown in Fig. 4.15 right before the measurement.

The WCA was measured on the plain PCL fibers and the PCL fibers coated with PPy (see chapter 2.4). Measured values of the WCA for both samples were above 120° . The values of WCA for plain PCL and PCL-PPy were $122.5^\circ (\pm 3.54)$ and $121.5^\circ (\pm 3.74)$, respectively (Fig. 4.15). The WCA values of both samples show no significant difference. The value of WCA for PCL is consistent with other authors (Prabhakaran et al., 2008; Jahani et al., 2015). The WCA values for PPy surfaces

vary according to the synthesis conditions (Vernitskaya and Efimov, 1997; Fonner et al., 2008; Ravichandran et al., 2010; Stewatr et al., 2015).

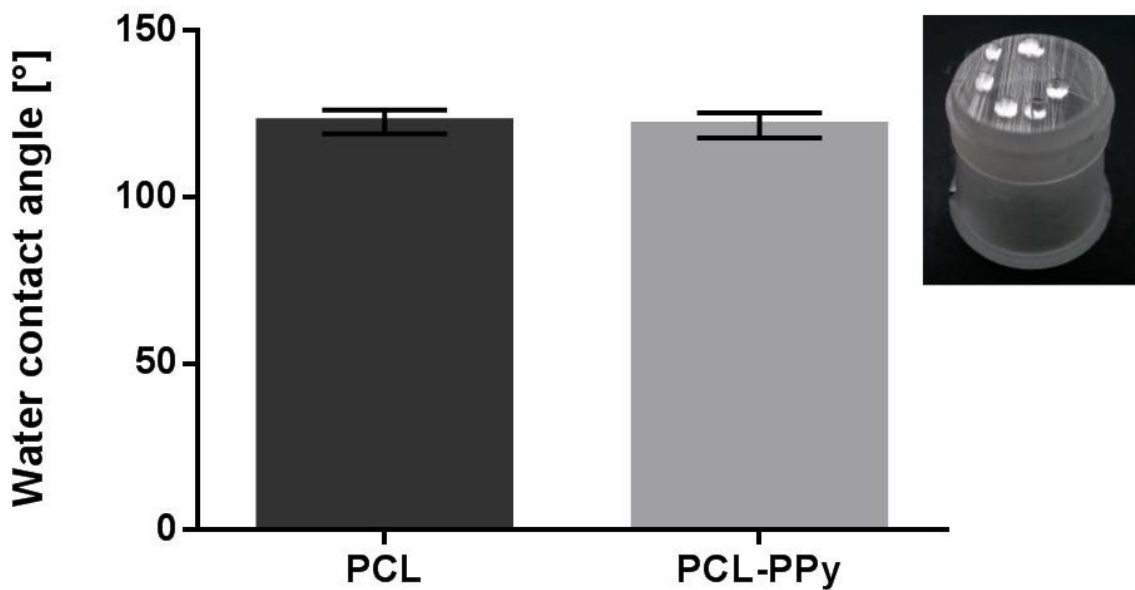


FIGURE 4.15: The diagram of water contact angles for PCL and PCL-PPy samples.

Although, PPy is mostly referred as hydrophobic (Guimard, Gomez, and Schmidt, 2007), in some cases can be prepared as hydrophilic (Fonner et al., 2008; Stewatr et al., 2015). This property is dependent on the synthesis conditions (see chapter 2.4.2), mostly the used dopants (Vernitskaya and Efimov, 1997; Fonner et al., 2008; Ravichandran et al., 2010; Stewatr et al., 2015).

Generally, it is stated that cells prefer hydrophilic surfaces to hydrophobic (Ghasemi-Mobarakeh et al., 2008; Gupta et al., 2009; Jahani et al., 2015). On the other hand, some studies suggest, that desired surface properties are specific to the cell type.

It is known that the surface roughness / porosity influences the surface properties. As the roughness increases, the hydrophobic substrate becomes more hydrophilic. For instance, a drop placed on a porous medium does not merely spread on the surface but also penetrates the depth of the support, thereby modifying its wetting properties (Gennes, Brochard-Wyart, and Quéré, 2004; Szewczyk et al., 2018). According to our porous fibers, which keep its porosity even after the PPy-coating, it is likely that this porosity contributes to the hydrophilicity of our samples (Fig. 4.16).

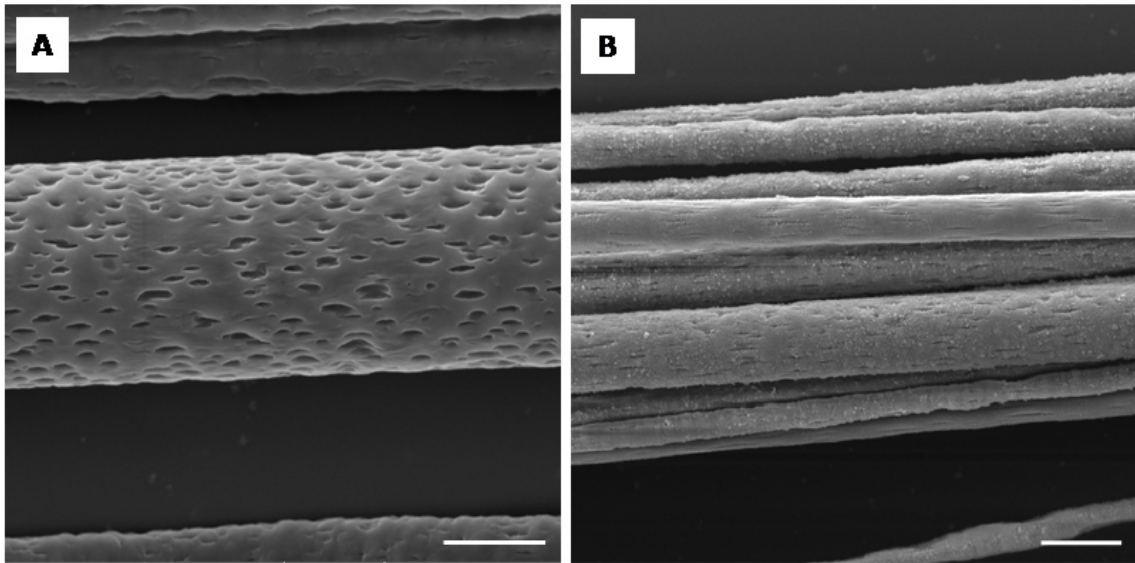


FIGURE 4.16: Comparison of the surface structure of (A) the plain PCL fibers (scale bar: 10 μm) and (B) the PPy coated fibers (scale bar: 20 μm).

On the other hand, it is to discuss, whether this method is suitable for our samples. It is evident that the drops sit on several fibers at the time and thus the density of the fibrous sample will influence the result to a large extent. Also, the water droplet will behave differently if placed on a single fiber, as it had been reported previously that the surface geometry was determining factor in wetting contact angle analysis on electrospun meshes (Szewczyk et al., 2018).

4.8 *In vitro* assessment of sample biocompatibility

4.8.1 Fibrous samples drawn in two different directions

The scaffolds made of fibers ordered either in one or in two directions (Fib I, Fib II) (Fig. 4.17) were tested *in vitro* (see chapter 3.2.2.2) and should confirm that the oriented microfibers support the oriented cell growth. The biocompatibility of these scaffolds was tested by MTT assay on day 1, 3, 7, 14 and 21 after cell seeding (showing the cell adhesion and proliferation), and by fluorescent and scanning electron microscopy. The results from the MTT assay as well as from the microscopy analysis show, that the scaffolds are capable of supporting cellular attachment and the proliferation during our *in vitro* tests (Figures 4.18, 4.19, 4.20).

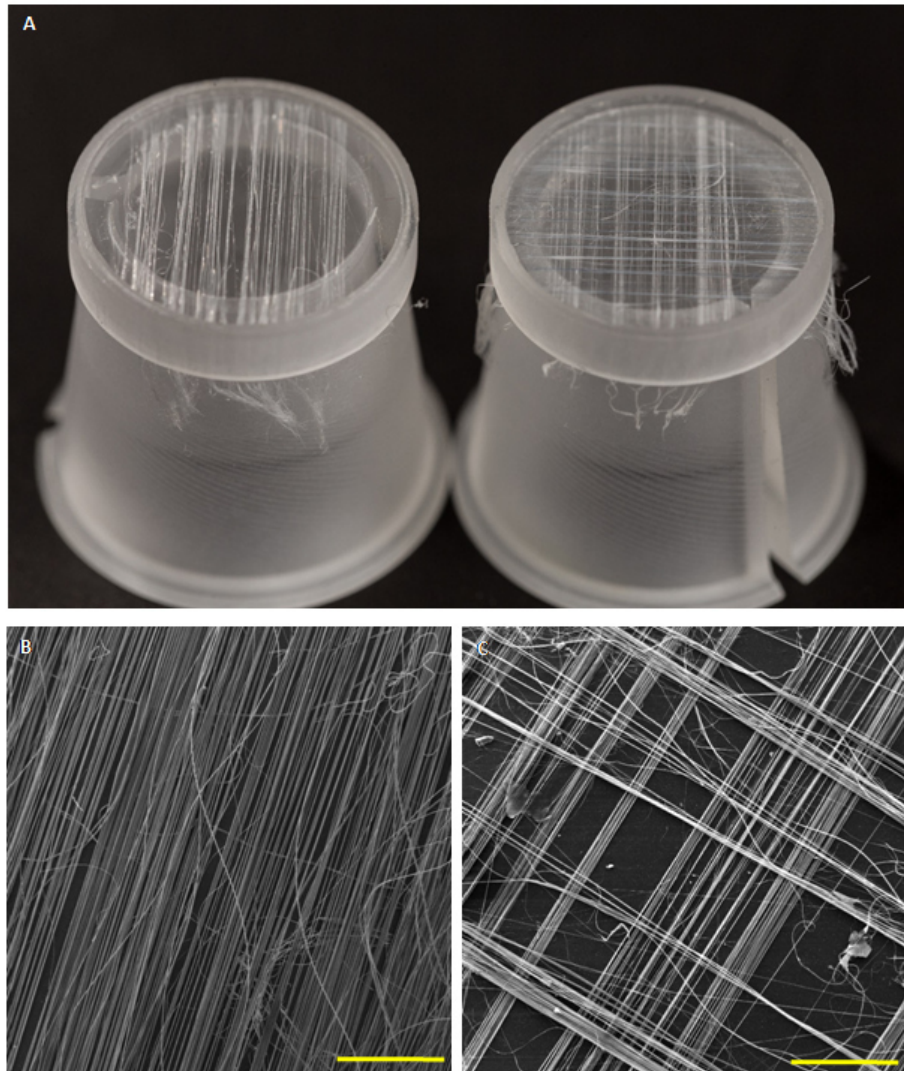


FIGURE 4.17: Images of the *in vitro* samples. (A) Macroscopic image of the fibers fixed within the fixation ring (the ring fits the well in 24-well plate), (B) and (C) SEM images of the fibers ordered in one (Fib I) or two (Fib II) directions (scale bar: 1 mm).

The data from the MTT assay reveal similar rates of cell adhesion (day 1) in both types of scaffolds (Fig. 4.18). Also during the following testing days the proliferation rate of Fib I and Fib II is comparable. This was an expected result, since the number of seeded cells was the same for both scaffolds and the cell adhesion was similar as well.

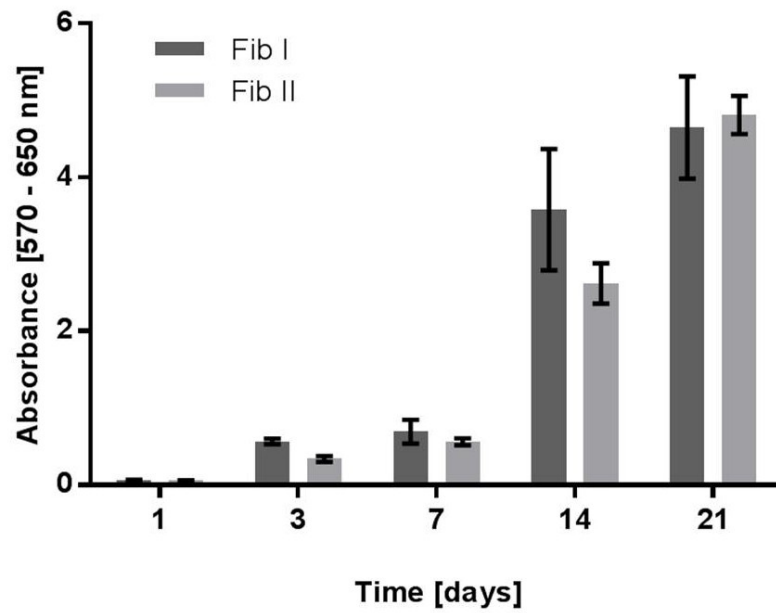


FIGURE 4.18: Results from the MTT assay showing the cell proliferation on two different scaffolds (Fib I, Fib II). Error bars representing SEM.

Fluorescent microscopy reveals very important phenomenon that the cells prefer the growth in the direction of fibers (Fig. 4.19), which can be seen from the orientation of the oval shape of cell nuclei. It had been shown previously that the cells grow in the direction of fibers (Corey et al., 2007; Wang et al., 2010; Yang et al., 2015). Wang *et al.* showed that the neurite outgrowth along the fibers was more directed and longer on the large (around 1,300 nm) and intermediate diameter (around 800 nm) fibers, which means that our microfibers are suitable for further experiments with neural cells. In addition, our samples have fibers ordered in two different directions, and the cells follow the fibers in both of them.

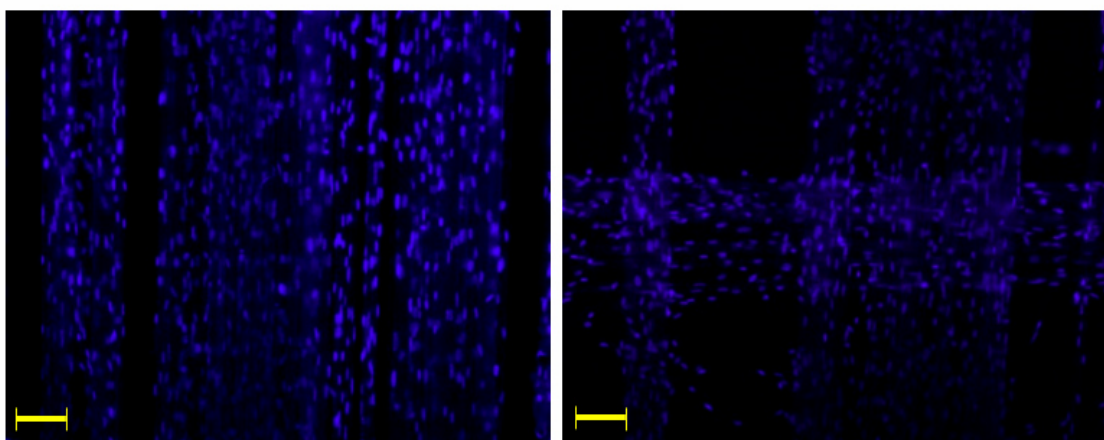


FIGURE 4.19: Images from the fluorescent microscope representing the samples Fib I and Fib II 14 days after cell seeding with mice fibroblasts. Scale bar: 100 μm .

Further, the SEM images show, that the cells are capable of overgrow the holes between the fibers of tens of micrometers in diameter (Fig 4.20).

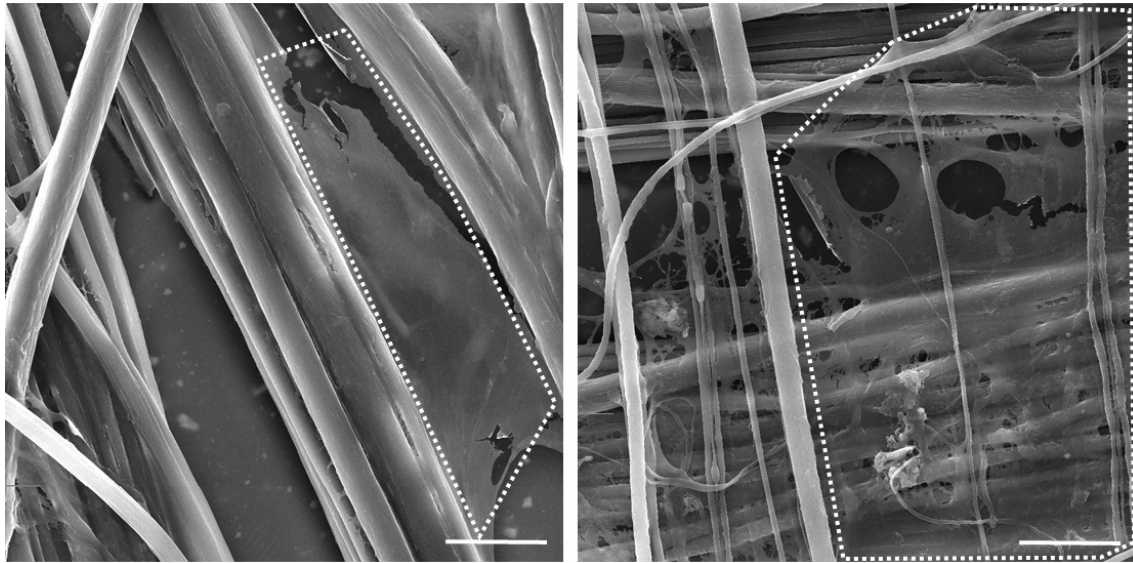


FIGURE 4.20: SEM images of the samples Fib I and Fib II 21 days after cell seeding with mice fibroblasts. Scale bar: 50 μm .

4.8.2 Fibrous samples coated with polypyrrole

The fibers oriented in one direction (Fib I) were used for further experiments. The drawn samples were coated with thin layer of polypyrrole (Fig. 4.11), since PPy is widely used conducting polymer in tissue engineering and has very good stability and promotes the adhesion and proliferation of various cell types (Zeng et al., 2013; Spearman et al., 2015; Yang et al., 2015).

The images from fluorescent microscope show very good cell adhesion on the PPy-coated fibers. The cells also proliferate within the testing days (Fig.4.21). The viability (Fig.4.22) tested by MTT assay at day 14 after cell seeding also shows higher values for the PPy-coated samples. These results are consistent with other studies (Lee et al., 2009; Yang et al., 2015) and should show, that the PPy samples are not cytotoxic and support the cell adhesion and proliferation. Moreover, according to the oval shape of the nuclei and their orientation it is evident, that the cells grow and spread along the fibers, copying the orientation of the fibers. Thus, the PPy-coated PCL fibers are suitable for the further experiments with neural cells.

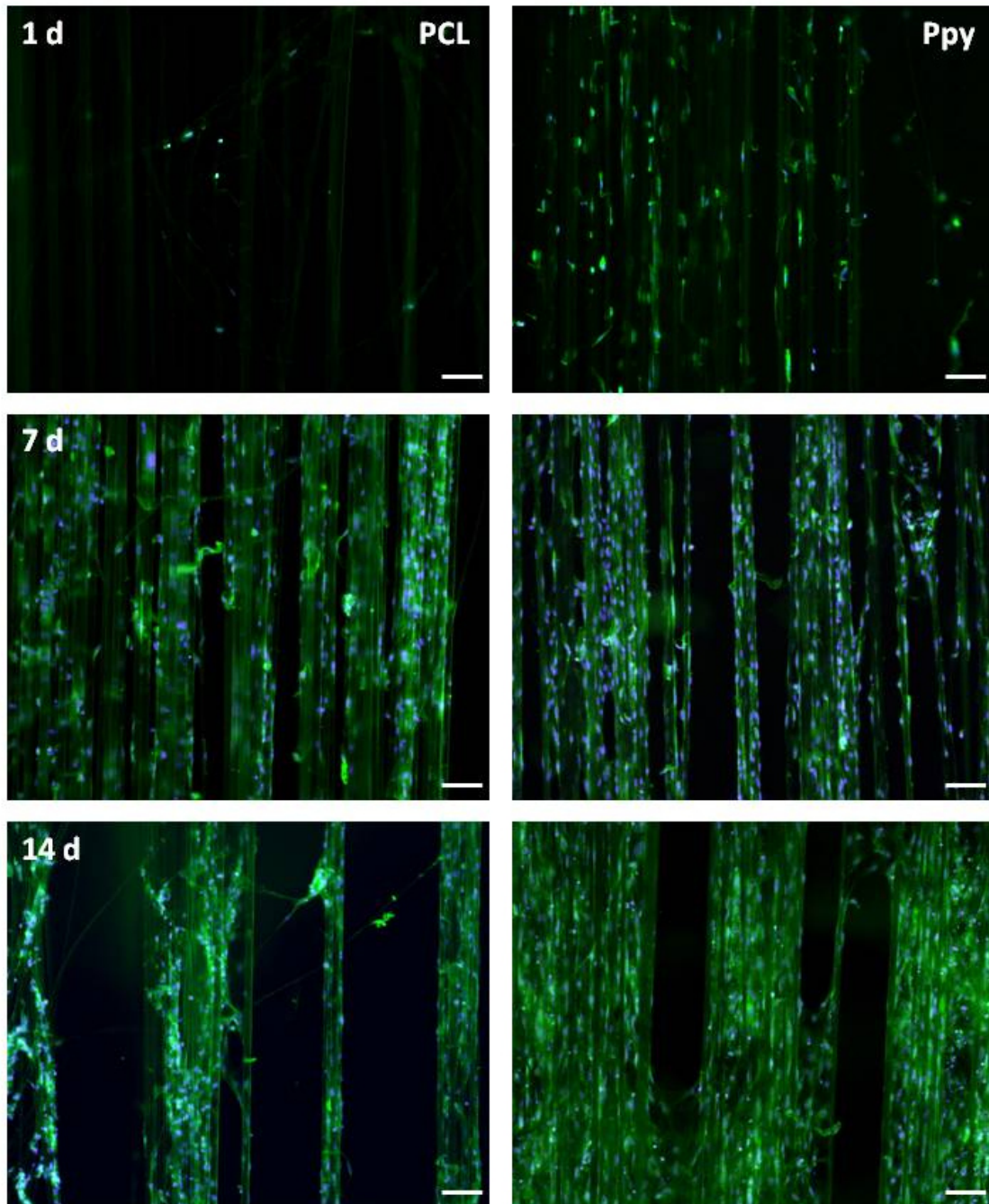


FIGURE 4.21: Images from fluorescent microscope showing the cells seeded on the plain PCL fibers (PCL) and on the PPy-coated fibers (PPy) 1, 7 and 14 days after cell seeding. Nuclei stained with DAPI (blue), cytoskeleton stained with Phalloidin-FITC (green). Scale bar: 100 μm .

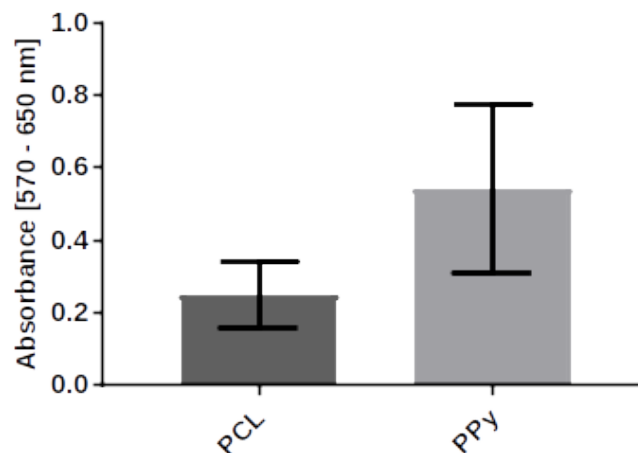


FIGURE 4.22: Diagram of the viability measured by MTT assay at day 14 after cell seeding.

4.9 *In vivo* study - development, construction and characterization of the scaffold

It had been shown previously that the aligned PPy fibers support the growth and orientation of the cells (Wang et al., 2010; Yang et al., 2015; Strnadová et al., 2020). But the problem of such scaffolds is their integrity and the implantation of such fibrous scaffolds *in vivo*. That is why new composite scaffold harboring the aligned PPy fibers was developed. This scaffold keeps the aligned structure of the fibers even after implantation.

The previously developed and tested spinal cord bridge from PLGA (Yang et al., 2009) was used as the fiber carrier. The microfibers were placed along the channels (Fig.4.23) (see chapter 3.2.2.3). The channels are around 150 μm in diameter, which allows the cell infiltration through a specific region of the implant, however, the channels itself do not actively guide the cells since the size of the channels is larger compared to the cells and their axons. The aligned PCL and PCL-PPy fibers were incorporated into the bridges to enhance the cell infiltration at a scale easily detected by cells, unlike the large channels (150 – 250 μm) that run through the bridge. Each channel was lined with a bundle of 100 fibers. The size of the *in vivo* sample was approximately 1.1 mm in length, 1.5 mm in width and 0.75 mm in height. The overall porosity is about 70 % (Thomas et al., 2013). However, some of the PCL-PPy bridges were bigger (higher) than the average size of the bridge, since it very much depends on the manual fabrication of the bridges. Also, it was often observed that the PCL-PPy fibers did not align along the whole

channel, but stayed gathered in the bundle on one side of the channel. This inhomogeneity of the samples definitely influences the final *in vivo* results, since the size of the bridge influences the side of the injury *in vivo* (can cause much severe injury after implantation). The distribution of the fibers along the channel influences the contact area of the fibers with the cells, and the bundles of PCL-PPy fibers thus have smaller area to be in contact with the cells.

In the case of the *in vitro* experiments, the samples were designed to be flat-bottomed (see chapter 3.2.2.3). The plain PLGA sample had 2 plain grooves, whereas the PCL a PCL-PPy samples had one bundle of 100 fibers incorporated into the groove. The size of the *in vitro* sample was approximately 2.6 mm in length to 1.5 mm in width.

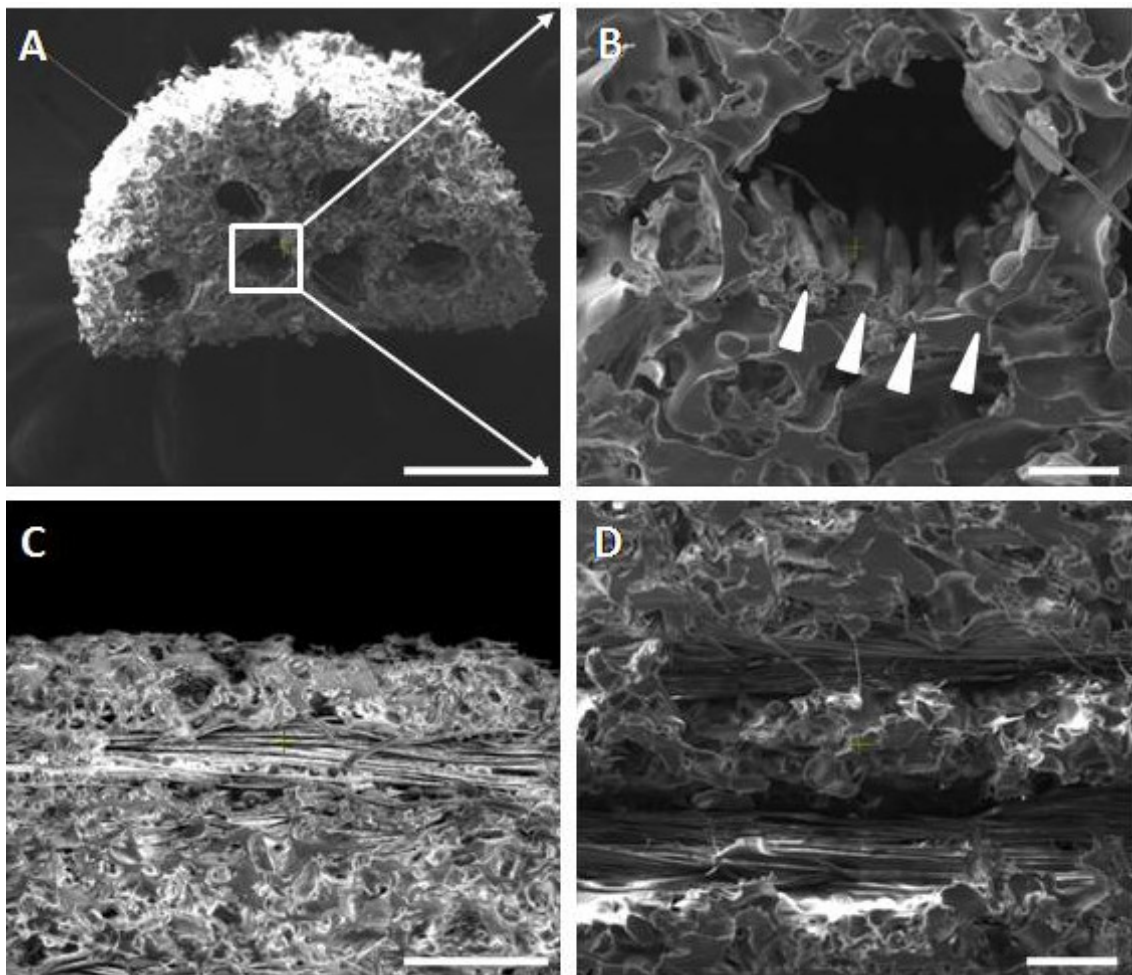


FIGURE 4.23: A – D: The SEM images of the fibers aligned along the channels.
(A) Transversal cut of the bridge (scale bar: 400 μm).
(B) Magnification of the particular channel (scale bar: 50 μm).
(C, D) Longitudinal cut of the bridge (scale bar: 200 μm (C) and 100 μm (D)).

The modified spinal cord bridges were tested *in vitro* (see chapter 3.2.2.3). The *in vitro* samples were seeded with DRGs isolated from two days old mice pups. The DRGs were placed on the scaffold specifically under the microscope so that the DRG covered the groove / fibers. After 7 days of incubation the samples were fixed in 4% paraformaldehyde and they were stained against β -tubulin (nuclei were stained with Hoechst). The samples were observed under the inverted fluorescent microscope. The axonal spread of neural cells was evaluated using the ImageJ.

The results show statistically significant decrease in the axonal length to width ration on the samples without fibers, with PCL fibers and with PPy-coated fibers. That means, that the axons of the neural cells follow rather the fibers, if available, than the plain channels. The effect is stronger if the fibers are coated with PPy (Fig. 4.24).

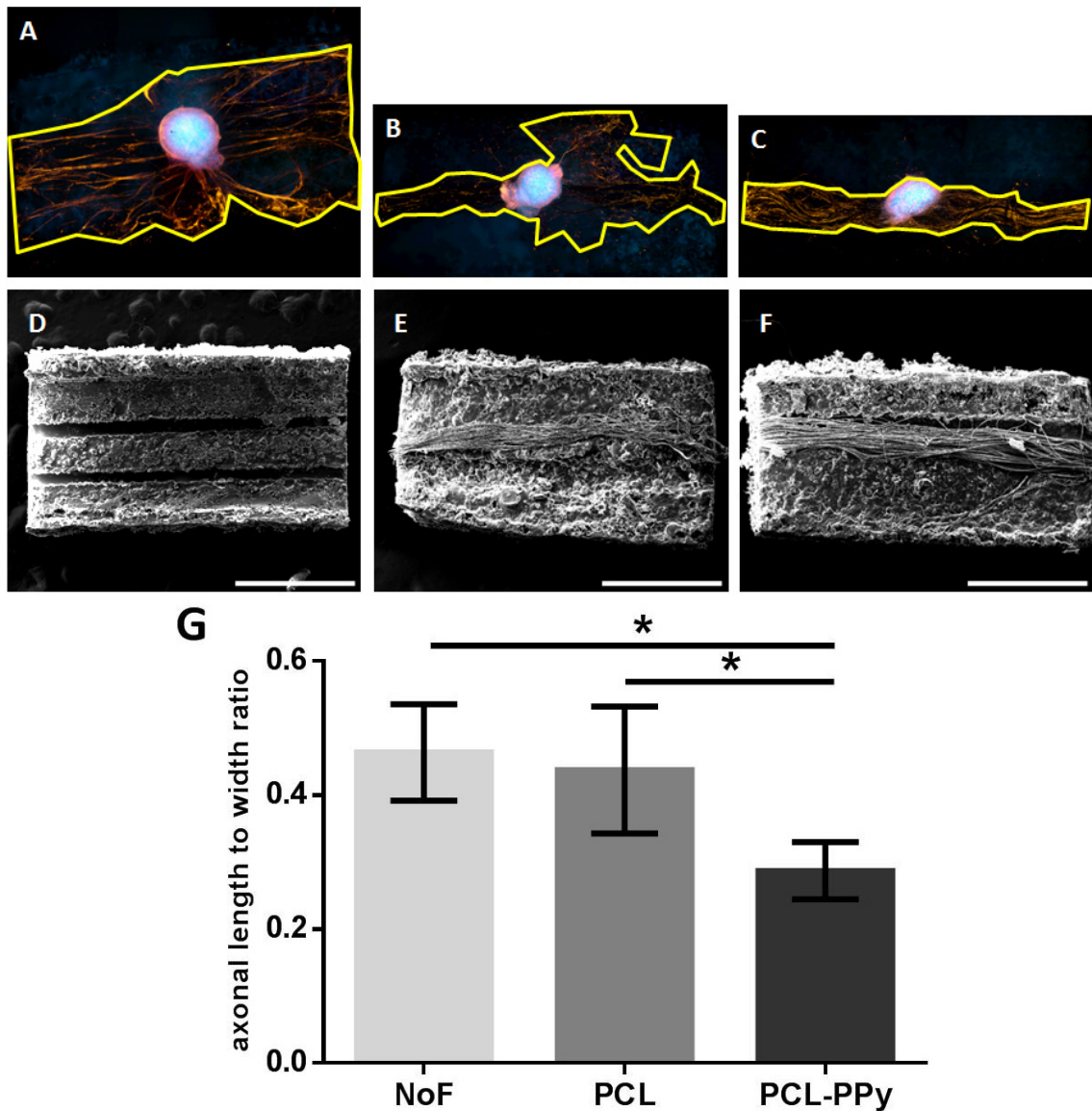


FIGURE 4.24: Axonal spread and axon elongation *in vitro*. A – C: Fluorescent images of DRGs 7 days after seeding on scaffolds. *In vitro* scaffolds with (A) no fibers, (B) PCL fibers and (C) Ppy-coated fibers. Yellow line represents the axonal spread. D - F: SEM images of the *in vitro* samples (scale bar: 1 mm). (D) sample without fibers (NoF), (E) sample with PCL fibers, (F) sample with PCL-PPy fibers. (G) Axonal length to width ratio. Data presented as mean \pm SD. * denotes $p < 0,05$.

According to these results the prepared spinal cord bridges were implanted into the mice's spinal cord after lateral hemisection at T9 (Fig. 4.25). Four weeks old female mice aged 6 - 8 weeks (C57Bl6) were used for this experiment. 46 mice total were used for this study, one mouse died and two mice had to be euthanized. The bridges were explanted after 2 or 8 weeks. Bridges isolated after 2 weeks were either used for RNA isolation with subsequent qPCR, or were deep-frozen into a mounting media and sectioned transversally in 12 μm thick slices (cryostat Microm HM525) and used for immunohistochemistry (immune response to the bridges). The slices were collected from rostral to caudal end of bridge in series of 7 slides (see Fig. 3.5, chapter 3.2.2.6). The bridges isolated after 8 weeks were only collected for sectioning. The sections were fixed and subjected to immunohistochemistry (cell infiltration into the bridges). For RNA isolation, four mice per each condition (NoF, PCL-PPy, control = no bridge) were euthanized and three mice euthanized with bridges with PCL fibers. For immunohistochemistry, four mice were euthanized for each condition after 2-week implantations and six mice were euthanized for each condition after 8-week implantations.

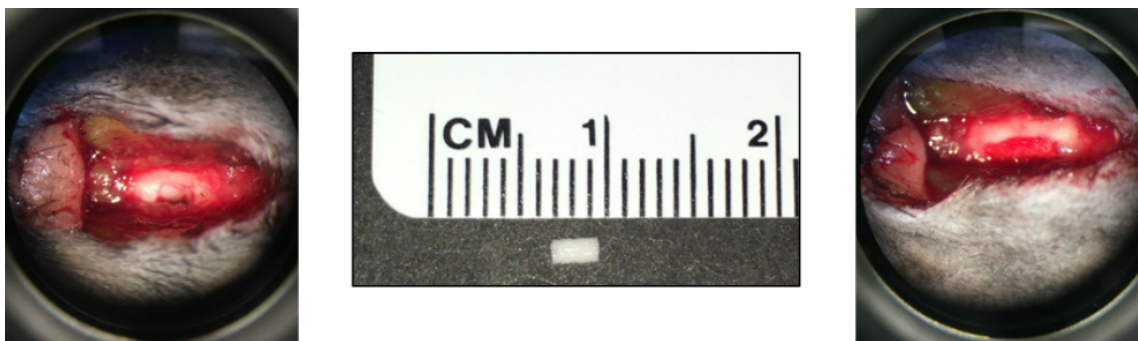


FIGURE 4.25: Lateral hemisection at T9 spinal cord region (left) and hemisection after the bridge implantation (right). The bridge implanted into the hemisection is depicted in the middle. The images are illustrative. The samples used for the *in vivo* study were half the size of the depicted bridge.

The samples were explanted 2 and 8 weeks after implantation. The 2-week time-point samples were tested for the immune response by immunostaining followed by fluorescent microscopy (Fig. 4.26) and by RT-PCR (Fig. 4.27). The images from the fluorescent microscope show similar immune response in all tested samples (bridges without fibers, with PCL fibers and with PPy-coated fibers). The immune response evaluated with immunostaining primarily evaluated pro-inflammatory M1 macrophages (F4/-80⁺ cells) and anti-inflammatory M2 macrophages (F4/-80⁺ Arginase1⁺ cells), as both are necessary at this time point for clearing cellular debris and laying down matrix for attachment of infiltrating cells. Together, the absence of qualitative differences in macrophage populations suggests

that the inclusion of the PCL fibers or PPy-coated fibers do not exacerbate the immune reaction to the bridges making them suitable for further evaluation.

The results from the RT-PCR show the expression of immunogenic markers compared to the control SHAM mice (mice with laminectomy only). There is significant increase in CD86 in non-fibrous samples compared to SHAM samples, and moderate increase in MHC II and iNOS, which suggests the activation of pro-inflammatory M1 immune response. The CD86 marker is significantly lower in the PPy-coated samples compared to the non-fibrous samples, but it is comparable to SHAM samples, with the iNOS expression lower than SHAM mice. Also, the Arginase 1 marker is significantly higher in the both fibrous samples (PCL and PPy-coated fibers) compared to SHAM and non-fibrous sample, which suggests the activation of the pro-healing M2 immune response. Other pro-inflammatory markers as MHC II, iNOS, CD206 and apoptotic markers cytochrome C and caspase 3 from all samples are comparable to the SHAM samples, suggesting the non-immunogenicity of the bridge samples.

These findings support our immunostaining results demonstrating that the addition of the PCL fiber or PPy-coated fibers do not lead to increase immunogenicity, but rather they increase pro-healing immune cell infiltration compared to the bridge alone. PPy is considered as the least immunogenic from the all conducting polymers used in tissue engineering (Guimard, Gomez, and Schmidt, 2007; Bendrea, Cianga, and Cianga, 2011). Still there are some reports of its immunogenicity, mostly after electrical stimulation (Williams and Doherty, 1994; Wang et al., 2004). Also it had been shown that the biocompatibility is dependent on the synthesis method, the conditions and used dopants. The biocompatibility is dependent on the washing step of the PPy layers before cell seeding (Ateh, Navsaria, and Vadgama, 2006; Fonner et al., 2008).

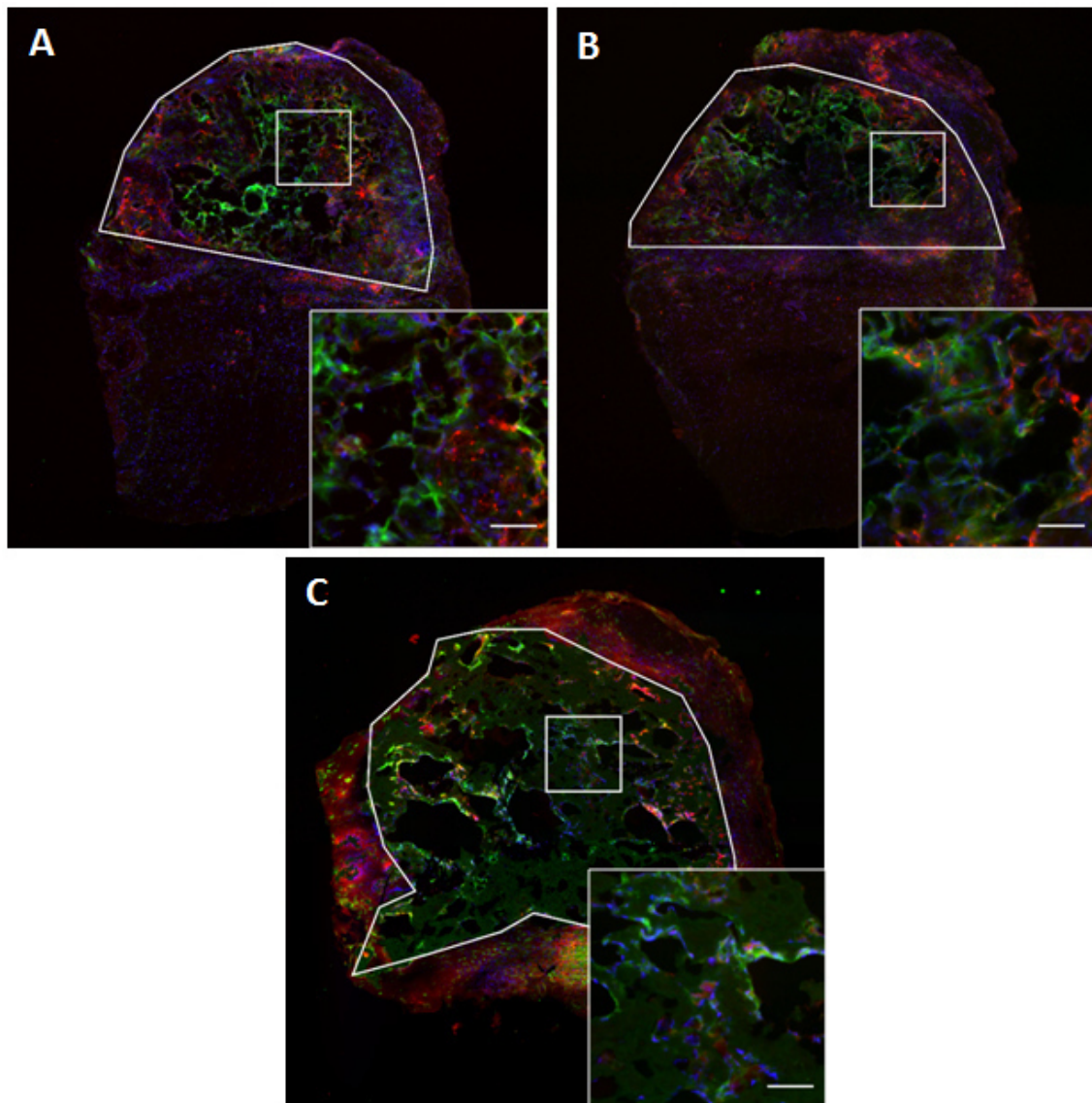


FIGURE 4.26: Immune response to the bridges with PCL / PPy fibers. F4/80 and Arginase1 fluorescence (Arginase 1 in red, F4/80 in green, nuclei in blue) at 2 weeks after bridge implantation. (A) Plain bridge, (B) bridge with PCL fibers, (C) bridge with PPy fibers. The bridges with PCL / PPy fibers do not reveal any excessive immune response compared to the plain bridge. Scale bar: 50 μm .

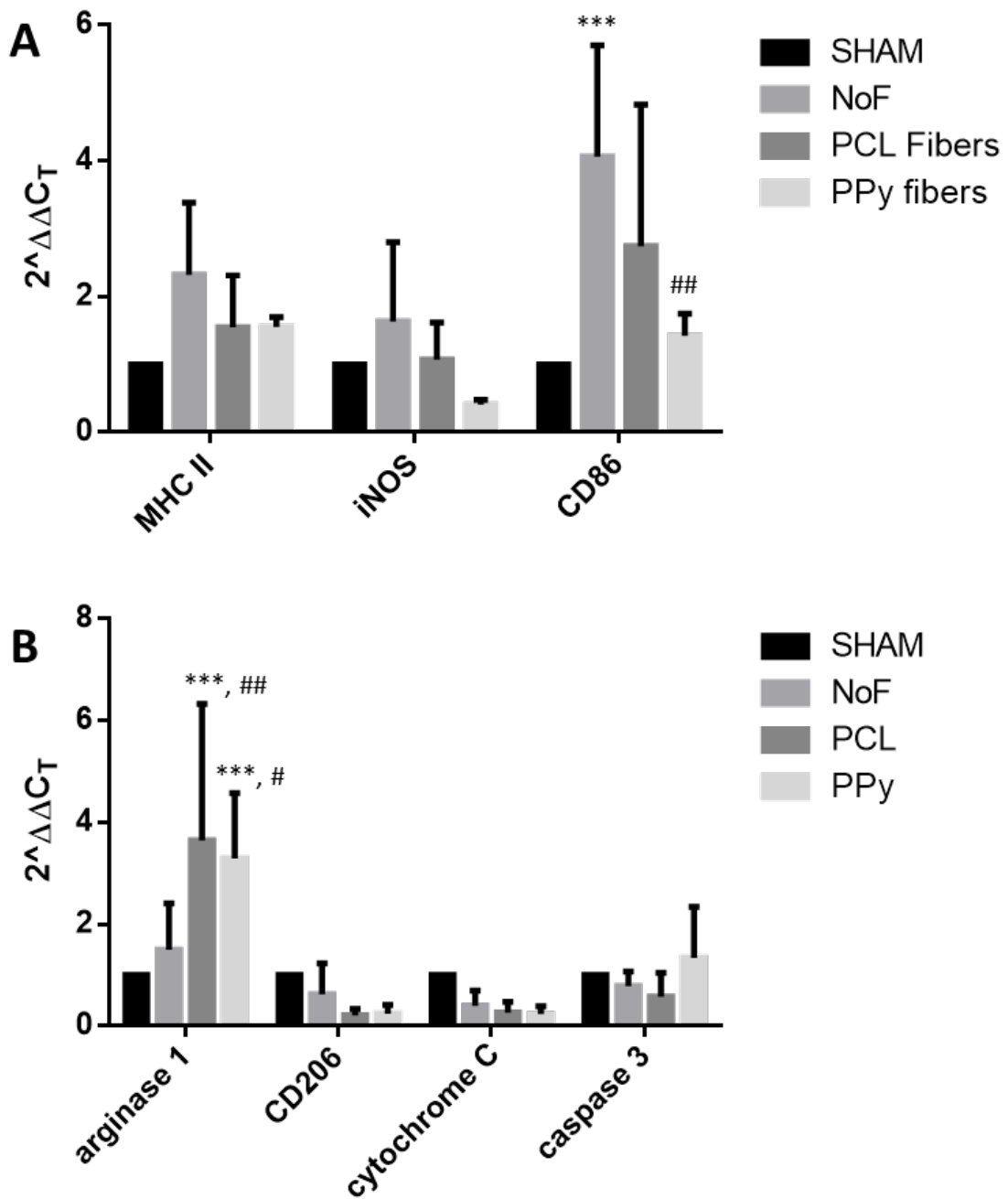


FIGURE 4.27: Quantification of immune response using qPCR. Samples collected 2 weeks after implantation. (A) qPCR data for M1 (A) and M2 and inflammation markers (B). *** denotes $p < 0,001$ vs. SHAM, ## denotes $p < 0,01$ vs. NoF, # denotes $p < 0,05$ vs. NoF.

The 8-week timepoint samples were tested for the axonal infiltration into the spinal cord bridge and for the axonal myelination by immunostaining (Fig. 4.28).

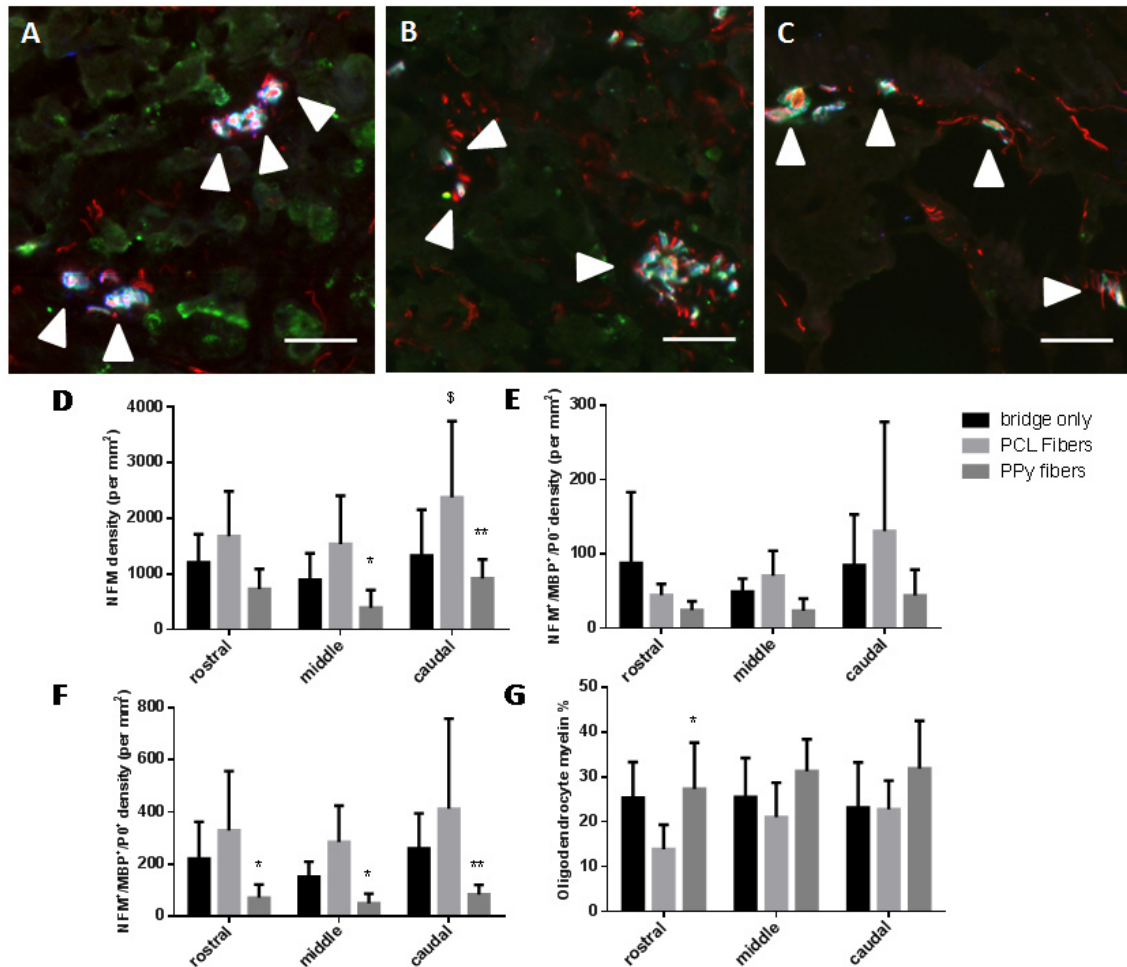


FIGURE 4.28: Axon infiltration and myelination 8 weeks after injury. Immunofluorescence from bridges of Schwann cell (NFM⁺/MBP⁺/P0⁺: red/green/blue, respectively) and oligodendrocyte (NFM⁺/MBP⁺/P0⁻) derived myelin fibers from bridge with no fibers (A), PCL (B) and PPy fibers (C). White arrow show fibers wrapped by Schwann cell-derived myelin. Brightness and contrast were adjusted for clarity. Density of axons (D), oligodendrocytes (E), Schwann cells (F), and percentage of oligodendrocyte derived myelinated axons (G) in bridge with no fibers, PCL and PPy fibers conditions (mean +/- SD). Scale bar: 50 μ m. ** denotes $p < 0.01$ vs. PCL bridge, * denotes $p < 0.05$ vs. PCL bridge, \$ denotes $p < 0.05$ vs. bridge only.

Axons (NFM density) were present throughout the bridges (Fig. 4.29 - D) 8 weeks after SCI under all experimental conditions. NFM-positive axons were typically observed in small groups or bundles as previously reported for multichannel PLG bridges (Tuinstra et al., 2013; McCreedy et al., 2016). The plain bridges had a mean of axons approximately 1,100 axons / mm². The bridges with PCL fibers show higher axon infiltration compared to control (plain bridges) with the mean of approximately 2,000 axons / mm², but the difference was statistically significant only in the caudal region. The PPy-PCL laden bridges had the mean of axon

infiltration approximately 600 axons / mm². However, these findings are statistically significant only for the middle and caudal region compared to PCL bridge. About 20% of these axons are myelinated, 75% of this myelin is derived from the Schwann cells (Fig. 4.27 G). The myelination of axons is important, because it allows the neural cells to conduct the nervous impulses. In the peripheral nervous system it is the Schwann cells who are responsible for the myelination of axons. Nevertheless, it is expected that Schwann cell - derived myelin is less effective for CNS function (Zhang et al., 2013). The number of infiltrating axons as well as the percentage of myelination is comparable to other studies (Dumont et al., 2018; Smith et al., 2019).

The lower axonal infiltration into the bridges with PPy-coated fibers compared to bridges with PCL fibers or compared to control is not consistent with the *in vitro* experiment. That could be caused by several factors. First, the PPy-coated fibers tend to form bundles. That results in the non-homogeneous distribution of the PPy-coated fibers around the channel perimeter, thus the surface area and therefore the contact surface of the PPy-coated fibers is much lower than in the case of PCL fibers. Second, the bridges with PPy-coated fibers were visibly bigger (Fig. 4.28) in perimeter than the control bridges and the bridges with PCL fibers. That resulted in the compression of the remaining half of the spinal cord, causing more severe injury, which is harder to heal. More experiments with more precise samples with emphasis on the fiber distribution would be needed, however, these results suggest that the inclusion of fibers within the bridge channels can improve regenerative outcomes following spinal cord injury.

On the other hand, despite these shortcomings, the bridges with PCL-PPy fibers do not reveal any excessive immune response compared to other two types of samples and the cell infiltration is comparable to bridges without fibers.

4.10 Using drawing for the biocompatibility assessment of fibrous materials

Another project where the drawing is used as a very unique method of scaffold fabrication is the biocompatibility assessment of polymeric materials. Drawing serves as the tool for fabrication of specific scaffold - polymeric grid of defined parameters. Such scaffold is seeded with cells. The biocompatibility is evaluated using the live cell imaging technology (cooperation with the Faculty of Fisheries and Protection of Waters, University of South Bohemia in České Budějovice). The time the cells need to over-grow the grid is compared between the materials (Fig. 4.29).

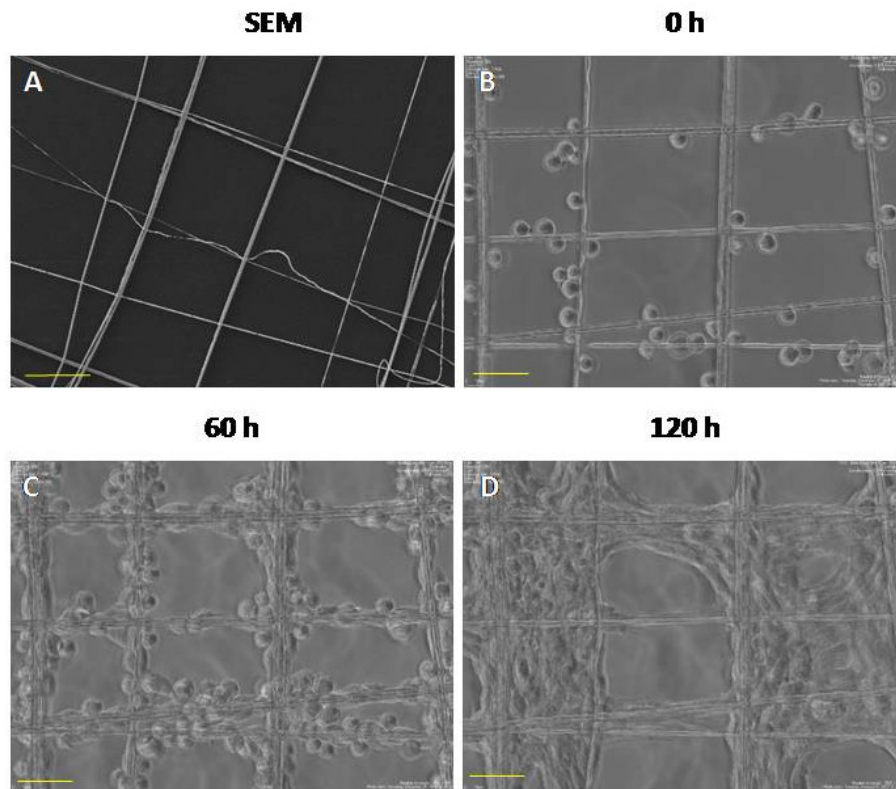


FIGURE 4.29: Using the polymer grid made by drawing for the biocompatibility assessment. (A) SEM - image of the grid from the scanning electron microscope (scale bar: 200 μm). (B – D) Following the behavior of the cell culture in time by live cell imaging; 0 hours - beginning of the experiment (B), and after 60 (C) and 120 (D) hours.

The advantage of this method is that we observe the cells' behavior in time. We can study the movement of individual cells on the fiber (until they start to multiply to big numbers), cell division, how they grow on the scaffold and the overall dynamics of the cell culture until it fills all the gaps between the fibers.

It is new and unique method how to study the cellular response to the material. Other methods of scaffold fabrication are not suitable for live cell imaging, because the cells itself are invisible if attached to the material using optical microscope. The only way how to visualize the cells on such materials is fluorescent staining and imaging. The fluorescent dyes often influence at least some part of the cell cycle, thus influencing the cellular response to the material. Moreover, the immunostaining requires fixation of the cells prior to staining (so-called end point assay), thus, there is different sample for each testing day. This may lead to inconsistent results e.g. due to the cell seeding inaccuracy. Second option is to use the commercially available ready-to-use fluorescent cell lines, which express fluorescent protein gene sequences as free cytoplasmatic proteins. This feature is advantageous because the gene expression is permanent and thus we can use the same sample every testing day, or, we could use such cell line for the live cell imaging as well. Problem with this approach is that the expression of such fluorescent protein is unnatural and may as well influence the behavior of the cell line. The comparison to the non-transfected cell line would be necessary.

4.11 Using drawing for the fabrication of hernia meshes

Thanks to the possibility of manipulation with single fiber during drawing we can prepare various fibrous patterns. This feature opens up new possibilities of application. One of them is definitely the hernia, or rather the hernia meshes. One such project was conducted at our Department (Department of Nonwovens and Nanofibrous Materials; Nanofibrous materials for tissue engineering, reg. no. CZ.1.05/3.1.00/14.0308). The hernia meshes were prepared by drawing from PCL. The results showed that these hernia meshes improved the healing process and the mechanical properties of the incision site.

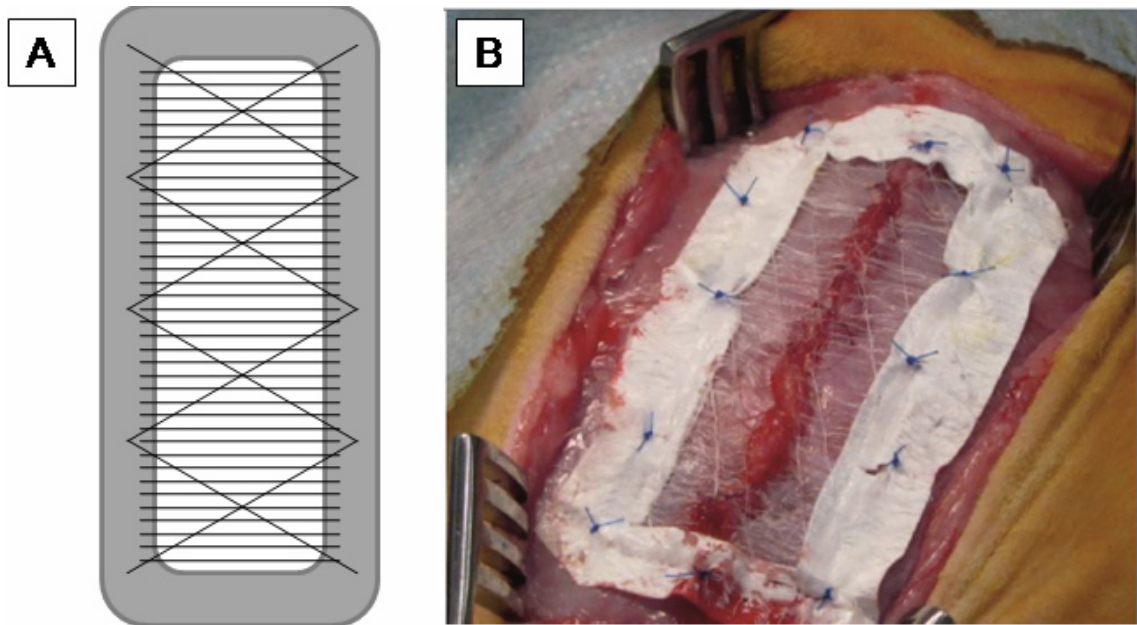


FIGURE 4.30: Hernia meshes prepared by drawing implanted into rabbits *in vivo* after abdominal incision. (A) Proposed hernia mesh, the frame (in gray) is made by electro-spinning from PCL, the mesh itself is made by drawing from PCL. The fibers are mainly oriented in one direction, with a few slant fibers for support, (B) Implanted hernia mesh *in vivo* on the suture after the abdominal incision.

Chapter 5

Conclusion

Drawing is a unique method to produce precise fibrous structures. To ensure stable drawing conditions, a new drawing machine called Manipulator was used. Several polymers were used to for drawing to show the versatility of this spinning method. Finally, drawing was used for the fabrication of scaffolds for tissue engineering and these scaffolds were tested *in vitro* and *in vivo*.

- Fiber production by drawing is dependent on the polymer concentration, molecular weight and speed of drawing. These parameters also influence the fiber diameter. It had been shown using the PCL M_n 80,000, that under ambient conditions the fiber diameter decreases with an increasing speed of drawing and a decreasing polymer solution concentration. Furthermore, the fiber diameter distribution decreases with increasing the speed of drawing. With decreasing polymer concentration, higher speed of drawing is necessary to prepare the fibers.
- Also high molecular weight PVA and low molecular weight PCL was possible to spun with drawing, although much higher concentrations had to be used. That is due to the solubility of these polymers in their solvents and also due to the chosen molecular weight.
- During drawing, formation of some common defects was observed. Almost all of the drawn fibers are porous. The pores are hundreds of nanometers wide and deep. The pores are formed by the solvent evaporation and their structure is influenced by the polymer and the solvent system used. Similar structures were described previously on electrospun fibers, and are known to be beneficial for the cell-fiber interaction and to enhance the cell adhesion. Other defects found were necking as a result of a fast solvent evaporation

and strong stretching of solidified fibers during the fiber drawing, and formation of beads and ribbons, which are influenced by the molecular weight of the polymer and the polymer solution concentration.

- Mechanical testing revealed that the tension values of the drawn samples are comparable to some results obtained from the measurement of electrospun fibers or fibers obtained by gravity spinning, which have the fiber diameter higher than 1 micrometer. The results also revealed that more suitable method for measuring the mechanical properties of drawn fiber would be beneficial.
- WCA measurement shows that both samples have the WCA higher than 120°. The value of WCA for PCL is consistent with other authors. The WCA values for PPy surfaces vary according to the synthesis conditions.
- The conductivity was measured by three different approaches, but all of the experiments were unsuccessful and all our samples showed no conductivity value. The failure of those experiments is probably given by the overall appearance of our samples. First, the PPy layer is very thin (70 nm), second, the samples contained only 100 or 200 fibers which is in this case very little number.
- The *in vitro* experiments of the oriented fibers show that all the samples are capable of supporting cell adhesion and proliferation during our experiment. Also, the results confirm that the cells prefer the growth in the direction of fibers.
- The *in vitro* experiment of the PPy-coated fibers very good biocompatibility of the PPy-coated fibers. These fibers were subsequently used for the preparation of the novel composite spinal cord bridges.
- New composite spinal cord bridge was developed using previously tested PLGA bridges as matrix for harboring aligned PCL and PPy-coated fibers.
- The new spinal cord bridges were tested *in vitro* for the axonal spread of neural cells. The results show that the oriented fibers support the guidance of neurite outgrowth. This phenomenon is even more pronounced, if the fibers are coated with PPy.
- The new spinal cord bridges were successfully implanted into mice for *in vivo* experiments. The bridges were implanted into mice spinal cord after lateral hemisection. After two and eight weeks the samples were explanted and subjected to further analysis. The assessment of the pro-inflammatory

and apoptotic markers after two weeks of implantations were comparable to the SHAM samples, suggesting the non-immunogenicity of the fibrous bridge samples. Moreover, the expression levels of Arginase 1 was significantly higher in the both fibrous bridges compared to SHAM and non-fibrous sample, which suggests the activation of the pro-healing M2 immune response.

- Samples explanted 8 weeks post surgery were evaluated for the axon infiltration and axonal myelination. The bridges with PCL fibers show higher axon infiltration compared to control. About 20 % of these axons are myelinated, 75 % of this myelin is derived from the Schwann cells. The axonal infiltration into the bridges with PPy-coated fibers is lower compared to bridges with PCL fibers or compared to control. This result is not consistent with the *in vitro* experiment. That could be caused by several factors. First, the PPy-coated fibers tend to form bundles. That results in the non-homogeneous distribution of the PPy-coated fibers around the channel perimeter, thus the surface area and therefore the contact surface of the PPy-coated fibers is much lower than in the case of PCL fibers. Second, the bridges with PPy-coated fibers were visibly bigger in perimeter than the control bridges and the bridges with PCL fibers. That resulted in the compression of the remaining half of the spinal cord, causing more severe injury, which is harder to heal. The obtained results show, that the oriented fibers enhance the axon infiltration and that the combination of the currently available approaches with new functionalization methods will be the method of choice for neural tissue engineering.
- Drawing appears to be a suitable tool also for other applications such as fabrication of hernia meshes or development of new and unique method for the biocompatibility evaluation of polymer scaffolds.

This work proved that drawing is very unique and suitable method for fabrication of specific fibrous scaffolds for tissue engineering. The obtained results will help us to precisely control the fiber morphology in the future, design different patterns of scaffolds and fulfill the needs of tissue engineering, where other non-woven methods are often inadequate. Moreover, this technique can be used to study the real-time dynamics of the population and the cell - material interactions (cytocompatibility), for which other spinning techniques are inadequate.

Bibliography

- Abidian, Mohammad Reza, Dong Hwan Kim, and David C. Martin (2006). "Conducting-polymer nanotubes for controlled drug release". In: *Advanced Materials* 18 (4), pp. 405–409. DOI: [10.1002/adma.200501726](https://doi.org/10.1002/adma.200501726).
- Adeli-Sardou, Mahboobeh et al. (2019). *Controlled release of lawsone from polycaprolactone/gelatin electrospun nano fibers for skin tissue regeneration*. Vol. 124. Elsevier B.V, pp. 478–491. DOI: [10.1016/j.ijbiomac.2018.11.237](https://doi.org/10.1016/j.ijbiomac.2018.11.237).
- Ando, Shuichi et al. (1999). "PLGA microspheres containing plasmid DNA: Preservation of supercoiled DNA via cryopreparation and carbohydrate stabilization". In: *Journal of Pharmaceutical Sciences* 88 (1), pp. 126–130.
- Arcaute, Karina, Brenda K. Mann, and Ryan B. Wicker (2010). "Fabrication of off-the-shelf multilumen poly(Ethylene glycol) nerve guidance conduits using stereolithography". In: *Tissue Engineering - Part C: Methods* 17 (1), pp. 27–38. DOI: [10.1089/ten.tec.2010.0011](https://doi.org/10.1089/ten.tec.2010.0011).
- Ateh, D D, H A Navsaria, and P Vadgama (2006). "Polypyrrole-based conducting polymers and interactions with biological tissues". In: *Journal of the Royal Society Interface* 3, pp. 741–752. DOI: [10.1098/rsif.2006.0141](https://doi.org/10.1098/rsif.2006.0141).
- Bacakova, Lucie et al. (2019). "Nanofibrous Scaffolds for Skin Tissue Engineering and Wound Healing Based on Synthetic Polymers". In: *Applications of Nanobiotechnology*. DOI: [10.5772/intechopen.88602](https://doi.org/10.5772/intechopen.88602).
- Bacakova, Marketa et al. (2017). "Protein nanocoatings on synthetic polymeric nanofibrous membranes designed as carriers for skin cells". In: *International Journal of Nanomedicine* 12, pp. 1143–1160. DOI: [10.2147/IJN.S121299](https://doi.org/10.2147/IJN.S121299).
- Badrossamay, Mohammad R. et al. (2014). "Engineering hybrid polymer-protein super-aligned nanofibers via rotary jet spinning". In: *Biomaterials* 35 (10), pp. 3188–3197. DOI: [10.1016/j.biomaterials.2013.12.072](https://doi.org/10.1016/j.biomaterials.2013.12.072).

- Baker, Stephen R. et al. (2016). "Determining the mechanical properties of electrospun poly- ϵ -caprolactone (PCL) nanofibers using AFM and a novel fiber anchoring technique". In: *Materials Science and Engineering C* 59, pp. 203–212. DOI: [10.1016/j.msec.2015.09.102](https://doi.org/10.1016/j.msec.2015.09.102).
- Balint, Richard, Nigel J Cassidy, and Sarah H Cartmell (2014). "Conductive polymers: Towards a smart biomaterial for tissue engineering". In: *Acta Biomaterialia* 10 (6), pp. 2341–2353. DOI: [10.1016/j.actbio.2014.02.015](https://doi.org/10.1016/j.actbio.2014.02.015).
- Bendrea, Anca-Dana, Luminita Cianga, and Ioan Cianga (2011). "Review paper : Progress in the Field of Conducting Polymers for Tissue Engineering Applications". In: *Journal of Biomaterials Applications* 26, pp. 3–84. DOI: [10.1177/0885328211402704](https://doi.org/10.1177/0885328211402704).
- Bergsma, J. E. et al. (1995). "Late degradation tissue response to poly(l-lactide) bone plates and screws". In: *Biomaterials* 16 (1), pp. 25–31. DOI: [10.1016/0142-9612\(95\)91092-D](https://doi.org/10.1016/0142-9612(95)91092-D).
- Bezuidenhout, Deon et al. (2010). "Covalent surface heparinization potentiates porous polyurethane scaffold vascularization". In: *Journal of Biomaterials Applications* 24 (5), pp. 401–418. DOI: [10.1177/0885328208097565](https://doi.org/10.1177/0885328208097565).
- Bostman, O. et al. (1990). "Foreign-body reactions to fracture fixation implants of biodegradable synthetic polymers". In: *Journal of Bone and Joint Surgery - Series B* 72 (4), pp. 592–596. DOI: [10.1302/0301-620x.72b4.2199452](https://doi.org/10.1302/0301-620x.72b4.2199452).
- Boys, Charles Vernon (1887). "On the Production, Properties, and some suggested Uses of the Finest Threads". In: *Proceedings of the Physical Society of London* 9 (8), pp. 8–19. DOI: [10.1088/1478-7814/9/1/303](https://doi.org/10.1088/1478-7814/9/1/303).
- Buchko, Christopher J., Kenneth M. Kozloff, and David C. Martin (2001). "Surface characterization of porous, biocompatible protein polymer thin films". In: *Biomaterials* 22 (11), pp. 1289–1300. DOI: [10.1016/S0142-9612\(00\)00281-7](https://doi.org/10.1016/S0142-9612(00)00281-7).
- Buzgo, M et al. (2013). "Controlled dual drug release by coaxial electrospun fibers - Impact of the core fluid on drug encapsulation and release". In: *Nanomedicine* 8 (7), pp. 1137–1154. DOI: <https://doi.org/10.2217/nmm.12.140>.
- Carvalho, Marta S et al. (2019). "Materials Science & Engineering C Co-culture cell-derived extracellular matrix loaded electrospun micro fibrous scaffolds for bone tissue engineering". In: *Materials Science & Engineering C* 99, pp. 479–490. DOI: [10.1016/j.msec.2019.01.127](https://doi.org/10.1016/j.msec.2019.01.127).

- Cebotari, Serghei et al. (2002). "Construction of autologous human heart valves based on an acellular allograft matrix". In: *Circulation* 106 (13 SUPPL.). DOI: [10.1161/01.cir.0000032900.55215.85](https://doi.org/10.1161/01.cir.0000032900.55215.85).
- Ceozzo, Kathleen et al. (2006). "Polyglycolic acid-induced inflammation: Role of hydrolysis and resulting complement activation". In: *Tissue Engineering* 12 (2), pp. 301–308. DOI: [10.1089/ten.2006.12.301](https://doi.org/10.1089/ten.2006.12.301).
- Chan, B P and K W Leong (2008). "Scaffolding in tissue engineering : general approaches and tissue-specific considerations". In: *European Spine Journal* 17, pp. 467–479. DOI: [10.1007/s00586-008-0745-3](https://doi.org/10.1007/s00586-008-0745-3).
- Chang, Yu Jung et al. (2013). "Electrical stimulation promotes nerve growth factor-induced neurite outgrowth and signaling". In: *Biochimica et Biophysica Acta - General Subjects* 1830 (8), pp. 4130–4136. DOI: [10.1016/j.bbagen.2013.04.007](https://doi.org/10.1016/j.bbagen.2013.04.007).
- Chronakis, Ioannis S, Sven Grapenson, and Alexandra Jakob (2006). "Conductive polypyrrole nanofibers via electrospinning : Electrical and morphological properties". In: *Polymer* 47, pp. 1597–1603. DOI: [10.1016/j.polymer.2006.01.032](https://doi.org/10.1016/j.polymer.2006.01.032).
- Chudickova, Milada et al. (2015). "Targeted neural differentiation of murine mesenchymal stem cells by a protocol simulating the inflammatory site of neural injury". In: *Journal of tissue engineering and regenerative medicine*. DOI: [10.1002/term](https://doi.org/10.1002/term).
- Corey, Joseph M et al. (2007). "Aligned electrospun nanofibers specify the direction of dorsal root ganglia neurite growth". In: *Journal of Biomedical Materials Research Part A* 83 (3), pp. 636–654. DOI: [10.1002/jbm.a](https://doi.org/10.1002/jbm.a).
- Cui, Wenguo, Yue Zhou, and Jiang Chang (2010). "Electrospun nanofibrous materials for tissue engineering and drug delivery". In: *Science and Technology of Advanced Materials* 11 (1), pp. 1–11. DOI: [10.1088/1468-6996/11/1/014108](https://doi.org/10.1088/1468-6996/11/1/014108).
- Cui, Xinyan et al. (2001). "Surface modification of neural recording electrodes with conducting polymer/biomolecule blends". In: *Journal of Biomedical Materials Research* 56 (2), pp. 261–272. DOI: [10.1002/1097-4636\(200108\)56:2<261::AID-JBM1094>3.0.CO;2-I](https://doi.org/10.1002/1097-4636(200108)56:2<261::AID-JBM1094>3.0.CO;2-I).
- Dai, Ying et al. (2012). "Characterizing the Effects of VPA , VC and RCCS on Rabbit Keratocytes onto Decellularized Bovine Cornea". In: *Plos One* 7 (11), pp. 1–10. DOI: [10.1371/journal.pone.0050114](https://doi.org/10.1371/journal.pone.0050114).

- Dhandayuthapani, Brahatheeswaran et al. (2011). "Polymeric Scaffolds in Tissue Engineering Application : A Review". In: *International Journal of Polymer Science* 2011. DOI: [10.1155/2011/290602](https://doi.org/10.1155/2011/290602).
- Duan, Huichuan et al. (2013). "Engineering of epidermis skin grafts using electrospun nanofibrous gelatin / polycaprolactone membranes". In: *International Journal of Nanomedicine* 8, pp. 2077–2084.
- Dumont, Courtney M et al. (2018). "Spinal Progenitor-Laden Bridges Support Earlier Axon Regeneration Following Spinal Cord Injury". In: *Tissue Engineering: Part A* 24, pp. 1588–1602. DOI: [10.1089/ten.tea.2018.0053](https://doi.org/10.1089/ten.tea.2018.0053).
- Dumont, Courtney M et al. (2019). "Aligned hydrogel tubes guide regeneration following spinal cord injury". In: *Acta Biomaterialia* 86, pp. 312–322. DOI: [10.1016/j.actbio.2018.12.052](https://doi.org/10.1016/j.actbio.2018.12.052).
- Ebersole, Gregory C et al. (2012). "Development of novel electrospun absorbable polycaprolactone (PCL) scaffolds for hernia repair applications". In: *Surgical Endoscopy* 26 (10), pp. 2717–2728. DOI: [10.1007/s00464-012-2258-8](https://doi.org/10.1007/s00464-012-2258-8).
- Erben, Jakub et al. (2015). "The combination of meltblown and electrospinning for bone tissue engineering". In: *Materials Letters* 143, pp. 172–176. DOI: [10.1016/j.matlet.2014.12.100](https://doi.org/10.1016/j.matlet.2014.12.100).
- Erben, Jakub et al. (2016). "The combination of meltblown technology and electrospinning – The influence of the ratio of micro and nano fibers on cell viability". In: *Materials Letters* 173, pp. 153–157. DOI: [10.1016/j.matlet.2016.02.147](https://doi.org/10.1016/j.matlet.2016.02.147).
- Fonner, John M et al. (2008). "Biocompatibility implications of polypyrrole synthesis techniques". In: *Biomedical M* 3 (3), pp. 1 –25. DOI: [10.1088/1748-6041/3/3/034124](https://doi.org/10.1088/1748-6041/3/3/034124).
- Freiberg, S and X X Zhu (2004). "Polymer microspheres for controlled drug release". In: *International Journal of Pharmaceutics* 282 (1-2), pp. 1–18. DOI: [10.1016/j.ijpharm.2004.04.013](https://doi.org/10.1016/j.ijpharm.2004.04.013).
- Fu, Yinxin et al. (2014). "Human urine-derived stem cells in combination with polycaprolactone/gelatin nanofibrous membranes enhance wound healing by promoting angiogenesis". In: *Journal of Translational Medicine* 12 (1), pp. 1–14. DOI: [10.1186/s12967-014-0274-2](https://doi.org/10.1186/s12967-014-0274-2).
- Fuchs, Andreas et al. (2019). "A new multilayered membrane for tissue engineering of oral hard- and soft tissue by means of melt electrospinning writing and

- film casting - An in vitro study". In: *Journal of Cranio-Maxillofacial Surgery* 47 (4), pp. 695–703. DOI: [10.1016/j.jcms.2019.01.043](https://doi.org/10.1016/j.jcms.2019.01.043).
- Fujihara, K., M. Kotaki, and S. Ramakrishna (2005). "Guided bone regeneration membrane made of polycaprolactone/calcium carbonate composite nanofibers". In: *Biomaterials* 26 (19), pp. 4139–4147. DOI: [10.1016/j.biomaterials.2004.09.014](https://doi.org/10.1016/j.biomaterials.2004.09.014).
- Fullana, Matthew J and Gary E Wnek (2012). "Electrospun collagen and its applications in regenerative medicine". In: *Drug Delivery and Translational Research* 2, pp. 313–322. DOI: [10.1007/s13346-012-0087-x](https://doi.org/10.1007/s13346-012-0087-x).
- Gennes, Pierre-Gilles de, Françoise Brochard-Wyart, and David Quéré (2004). *Capillarity and Wetting Phenomena: Drops, Bubbles, Pearls, Waves*. Springer, New York, NY, p. 291. DOI: <https://doi.org/10.1007/978-0-387-21656-0>.
- Ghasemi-Mobarakeh, Laleh et al. (2008). "Electrospun poly(-caprolactone)-gelatin nanofibrous scaffolds for nerve tissue engineering". In: *Biomaterials* 29, pp. 4532–4539.
- Ghasemi-Mobarakeh, Laleh et al. (2011). "Application of conductive polymers , scaffolds and electrical stimulation for nerve tissue engineering". In: *Journal of tissue engineering and regenerative medicine* 5 (4), pp. 17–35. DOI: [10.1002/term.383](https://doi.org/10.1002/term.383).
- Giménez, Virna M.Martín et al. (2020). "Synthesis, physicochemical characterisation and biological activity of anandamide/?polycaprolactone nanoparticles obtained by electrospraying". In: *IET Nanobiotechnology* 14 (1), pp. 86–93. DOI: [10.1049/iet-nbt.2019.0108](https://doi.org/10.1049/iet-nbt.2019.0108).
- Grier, William K. et al. (2018). "Incorporating β -cyclodextrin into collagen scaffolds to sequester growth factors and modulate mesenchymal stem cell activity". In: *Acta Biomaterialia* 76, pp. 116–125. DOI: [10.1016/j.actbio.2018.06.033](https://doi.org/10.1016/j.actbio.2018.06.033).
- Grijalvo, Santiago et al. (2019). "Alginate Hydrogels as Scaffolds and Delivery Systems to Repair the Damaged Spinal Cord". In: *Biotechnology Journal* 14 (12), pp. 1–8. DOI: [10.1002/biot.201900275](https://doi.org/10.1002/biot.201900275).
- Gu, Fuxing et al. (2008). "Polymer Single-Nanowire Optical Sensors". In: *Nano Letters* 8 (9), pp. 2757–2761. DOI: [10.1021/nl8012314](https://doi.org/10.1021/nl8012314).

- Guimard, Nathalie K, Natalia Gomez, and Christine E Schmidt (2007). "Conducting polymers in biomedical engineering". In: *Progress in Polymer Science* 32, pp. 876–921. DOI: [10.1016/j.progpolymsci.2007.05.012](https://doi.org/10.1016/j.progpolymsci.2007.05.012).
- Gunatillake, Pathiraja A., Raju Adhikari, and N. Gadegaard (2003). "Biodegradable synthetic polymers for tissue engineering". In: *European Cells and Materials* 5, pp. 1–16. DOI: [10.22203/eCM.v005a01](https://doi.org/10.22203/eCM.v005a01).
- Guo, Baolin, Lidija Glavas, and Ann Christine Albertsson (2013). "Biodegradable and electrically conducting polymers for biomedical applications". In: *Progress in Polymer Science* 38 (9), pp. 1263–1286. DOI: [10.1016/j.progpolymsci.2013.06.003](https://doi.org/10.1016/j.progpolymsci.2013.06.003).
- Gupta, Deepika et al. (2009). "Aligned and random nanofibrous substrate for the in vitro culture of Schwann cells for neural tissue engineering". In: *Acta Biomaterialia* 5 (7), pp. 2560–2569. DOI: [10.1016/j.actbio.2009.01.039](https://doi.org/10.1016/j.actbio.2009.01.039).
- Hausherr, T C et al. (2018). "Bone Reports Effect of temporal onsets of mechanical loading on bone formation inside a tissue engineering scaffold combined with cell therapy". In: *Bone Reports* 8, pp. 173–179. DOI: [10.1016/j.bonr.2018.04.008](https://doi.org/10.1016/j.bonr.2018.04.008).
- Hauzerová, Šárka (2018). "Příprava a charakteristika polyesterových orientovaných vláken metodou drawing". PhD thesis. Technical University of Liberec, p. 81.
- Hopkins, Richard A (2005). *Tissue engineering of heart valves: Decellularized valve scaffolds*. DOI: [10.1161/CIRCULATIONAHA.104.527820](https://doi.org/10.1161/CIRCULATIONAHA.104.527820).
- Horakova, J. et al. (2018). "Electrospun vascular grafts fabricated from poly(L-lactide-co-ε-caprolactone) used as a bypass for the rabbit carotid artery". In: *Biomedical Materials* 13 (6). DOI: [10.1088/1748-605X/aade9d](https://doi.org/10.1088/1748-605X/aade9d).
- Hu, Jue et al. (2015). "Drug-loaded emulsion electrospun nanofibers: Characterization, drug release and in vitro biocompatibility". In: *RSC Advances* 5 (121), pp. 100256–100267. DOI: [10.1039/c5ra18535a](https://doi.org/10.1039/c5ra18535a).
- Jahani, Hoda et al. (2015). "Controlled surface morphology and hydrophilicity of polycaprolactone toward selective differentiation of mesenchymal stem cells to neural like cells". In: *Journal of Biomedical Materials Research Part A* 103 (5), pp. 1875–1881. DOI: [10.1002/jbm.a.35328](https://doi.org/10.1002/jbm.a.35328).

- Kessick, Royal, John Fenn, and Gary Tepper (2004). "The use of AC potentials in electrospraying and electrospinning processes". In: *Polymer* 45, pp. 2981–2984. DOI: [10.1016/j.polymer.2004.02.056](https://doi.org/10.1016/j.polymer.2004.02.056).
- Khil, Myung-seob et al. (2003). "Electrospun Nanofibrous Polyurethane Membrane as Wound Dressing". In: *Journal of Biomedical Materials Research Part B: Applied Biomaterials* 67 (2), pp. 675–679.
- Kigerl, Kristina A et al. (2010). "NIH Public Access". In: 29 (43), pp. 13435–13444. DOI: [10.1523/JNEUROSCI.3257-09.2009](https://doi.org/10.1523/JNEUROSCI.3257-09.2009). Identification.
- Kim, Jueun et al. (2019). "Fabrication and characterization of bioresorbable drug-coated porous scaffolds for vascular tissue engineering". In: *Materials* 12 (9), pp. 9–11. DOI: [10.3390/ma12091438](https://doi.org/10.3390/ma12091438).
- Kim, Tae Hyoung and Tae Gwan Park (2004). "Critical effect of freezing / freeze-drying on sustained release of FITC-dextran encapsulated within PLGA microspheres". In: *International Journal of Pharmaceutics* 271, pp. 207–214. DOI: [10.1016/j.ijpharm.2003.11.021](https://doi.org/10.1016/j.ijpharm.2003.11.021).
- Kimura, K. et al. (1998). "Gene expression in the electrically stimulated differentiation of PC12 cells". In: *Journal of Biotechnology* 63 (1), pp. 55–65. DOI: [10.1016/S0168-1656\(98\)00075-3](https://doi.org/10.1016/S0168-1656(98)00075-3).
- Korzhikov-Vlakh, Viktor et al. (2018). "Novel pathway for efficient covalent modification of polyester materials of different design to prepare biomimetic surfaces". In: *Polymers* 10 (12). DOI: [10.3390/polym10121299](https://doi.org/10.3390/polym10121299).
- Koski, A., K. Yim, and S. Shivkumar (2004). "Effect of molecular weight on fibrous PVA produced by electrospinning". In: *Materials Letters* 58 (3-4), pp. 493–497. DOI: [10.1016/S0167-577X\(03\)00532-9](https://doi.org/10.1016/S0167-577X(03)00532-9).
- Kotwal, Arundhati and Christine E. Schmidt (2001). "Electrical stimulation alters protein adsorption and nerve cell interactions with electrically conducting biomaterials". In: *Biomaterials* 22 (10), pp. 1055–1064. DOI: [10.1016/S0142-9612\(00\)00344-6](https://doi.org/10.1016/S0142-9612(00)00344-6).
- Krubicová, Ilona (2017). "Příprava a charakteristika vlákenného nosiče pro náhradu nervové tkáně". PhD thesis. Technical University of Liberec, p. 77.
- Krchová, S. et al. (2014). "Nanovlákná v hojení kožních ran". In: *Česká dermatovenerologie* 4 (4), pp. 234–240.

- Kriz, J et al. (2017). "Incidence of acute spinal cord injury in the Czech Republic: A prospective epidemiological study 2006-2015". In: *Spinal Cord* 55 (9), pp. 870–874. DOI: [10.1038/sc.2017.20](https://doi.org/10.1038/sc.2017.20).
- Laporte, Laura De, Anna Yan, and Lonnie D Shea (2009). "Local gene delivery from ECM coated poly (lactide co glycolide) multiple channel bridges after spinal cord injury". In: *Biomaterials* 30 (12), pp. 2361–2368. DOI: [10.1016/j.biomaterials.2008.12.051](https://doi.org/10.1016/j.biomaterials.2008.12.051).
- LaPres, Jason (2009). *The Nervous System: Neural Tissue*.
- Lee, Jae Y et al. (2009). "Polypyrrole-coated electrospun PLGA nanofibers for neural tissue applications". In: *Biomaterials* 30 (26), pp. 4325–4335. DOI: [10.1016/j.biomaterials.2009.04.042](https://doi.org/10.1016/j.biomaterials.2009.04.042).
- Lerman, Max J et al. (2019). "Development of surface functionalization strategies for 3D-printed polystyrene constructs". In: *Society for Biomaterials*. DOI: [10.1002/jbm.b.34347](https://doi.org/10.1002/jbm.b.34347).
- Li, Dan et al. (2003). "Electrospinning of Polymeric and Ceramic Nanofibers as Uniaxially Aligned Arrays". In: *Nano Letters* 3 (8), pp. 1167–1171. DOI: [10.1021/nl034425](https://doi.org/10.1021/nl034425).
- Li, Jun and Guilherme Lepski (2013). "Cell Transplantation for Spinal Cord Injury : A Systematic Review". In: *BioMed Research International* 2013, pp. 1 –32. DOI: [10.1155/2013/786475](https://doi.org/10.1155/2013/786475).
- Li, Zhen et al. (2019). "High efficiency fabrication of chitosan composite nanofibers with uniform morphology via centrifugal spinning". In: *Polymers* 11 (10). DOI: [10.3390/polym11101550](https://doi.org/10.3390/polym11101550).
- Liu, Shu-liang et al. (2013). "Assembly of Oriented Ultrafine Polymer Fibers by Centrifugal Electrospinning". In: *Journal of Nanomaterials* 2013 (1), pp. 1–9. DOI: [10.1155/2013/713275](https://doi.org/10.1155/2013/713275).
- Liu, Ting et al. (2012). "Nanofibrous Collagen Nerve Conduits for Spinal Cord Repair". In: *Tissue Engineering: Part A* 18 (9-10), pp. 1057–1066. DOI: [10.1089/ten.tea.2011.0430](https://doi.org/10.1089/ten.tea.2011.0430).
- Livak, Kenneth J and Thomas D Schmittgen (2001). "Analysis of Relative Gene Expression Data Using Real- Time Quantitative PCR and the 2^{-C_T} Method". In: *Methods* 408, pp. 402–408. DOI: [10.1006/meth.2001.1262](https://doi.org/10.1006/meth.2001.1262).

- Losi, Paola et al. (2013). "Fibrin-based scaffold incorporating VEGF- and bFGF-loaded nanoparticles stimulates wound healing in diabetic mice". In: *Acta Biomaterialia* 9 (8), pp. 7814–7821. DOI: [10.1016/j.actbio.2013.04.019](https://doi.org/10.1016/j.actbio.2013.04.019).
- Lukasek, J. et al. (2019). "Cyclodextrin-Polypyrrole Coatings of Scaffolds for Tissue Engineering". In: *Polymers* 11 (459), pp. 1–11. DOI: [10.3390/polym11030459](https://doi.org/10.3390/polym11030459).
- Lukášová, V. et al. (2019). "Needleless electrospun and centrifugal spun poly-ε-caprolactone scaffolds as a carrier for platelets in tissue engineering applications - A comparative study with hMSCs". In: *Materials Science Engineering C* 97, pp. 567–575.
- Macaya, D. and M. Spector (2012). "Injectable hydrogel materials for spinal cord regeneration: A review". In: *Biomedical Materials* 7 (1). DOI: [10.1088/1748-6041/7/1/012001](https://doi.org/10.1088/1748-6041/7/1/012001).
- Madhavan, Ragaseema V. et al. (2011). "Silver nanoparticle impregnated poly (ε-caprolactone) scaffolds: Optimization of antimicrobial and noncytotoxic concentrations". In: *Tissue Engineering - Part A* 17 (3-4), pp. 439–449. DOI: [10.1089/ten.tea.2009.0791](https://doi.org/10.1089/ten.tea.2009.0791).
- Martínek, Michal (2014). "Modifikované vodivé nanomateriály na bázi heterocyklů". PhD thesis, pp. 1–110.
- Matthews, Gary G. (2002). *Cellular Physiology of Nerve and Muscle*. Malden, MA USA: Blackwell Publishing Ltd. DOI: [10.1002/9781118687864](https://doi.org/10.1002/9781118687864).
- McCaig, C D and M Zhao (1997). "Physiological electrical fields modify cell behaviour." In: *BioEssays* 19 (9), p. 826. DOI: [10.1002/bies.950190912](https://doi.org/10.1002/bies.950190912).
- McCreedy, Dylan A et al. (2016). "Semi-automated counting of axon regeneration in poly (lactide co -glycolide) spinal cord bridges". In: *Journal of Neuroscience Methods* 263, pp. 15–22. DOI: [10.1016/j.jneumeth.2016.01.021](https://doi.org/10.1016/j.jneumeth.2016.01.021).
- Mckinley, Gareth H and Tamarapu Sridhar (2002). "Filament-Stretching Rheometry of Complex Fluids". In: *Annual Review of Fluid Mechanics* 34, pp. 375–415. DOI: [10.1146/annurev.fluid.34.083001.125207](https://doi.org/10.1146/annurev.fluid.34.083001.125207).
- Megelski, Silke et al. (2002). "Micro- and nanostructured surface morphology on electrospun polymer fibers". In: *Macromolecules* 35 (22), pp. 8456–8466. DOI: [10.1021/ma020444a](https://doi.org/10.1021/ma020444a).

- Meng, Chao et al. (2011). "Quantum-Dot-Doped Polymer Nanofibers for Optical Sensing". In: *Advanced Materials* 23 (33), pp. 3770–3774. DOI: [10.1002/adma.201101392](https://doi.org/10.1002/adma.201101392).
- Merrell, Jonathan G et al. (2009). "Curcumin Loaded Poly(ϵ -Caprolactone) Nanofibers: Diabetic Wound Dressing with Antioxidant and Anti-inflammatory Properties NIH Public Access Author Manuscript". In: *Clin Exp Pharmacol Physiol* 36 (12), pp. 1149–1156. DOI: [10.1111/j.](https://doi.org/10.1111/j.)
- Meyer, U (2009). "The History of Tissue Engineering and Regenerative Medicine in Perspective". In: *Fundamentals of tissue engineering and regenerative medicine*, pp. 1–12.
- Mickova, A. et al. (2012). "Core/shell nanofibers with embedded liposomes as a drug delivery system". In: *Biomacromolecules* 13 (4), pp. 952–962. DOI: [10.1021/bm2018118](https://doi.org/10.1021/bm2018118).
- Mikos, Antonios G et al. (1993). "Laminated three-dimensional biodegradable foams for use in tissue engineering". In: *Biomaterials* 14 (5).
- Mironov, Vladimir et al. (2003). "Organ printing: Computer-aided jet-based 3D tissue engineering". In: *Trends in Biotechnology* 21 (4), pp. 157–161. DOI: [10.1016/S0167-7799\(03\)00033-7](https://doi.org/10.1016/S0167-7799(03)00033-7).
- Mooney, David J et al. (1996). "Novel approach to fabricate porous sponges of poly(D,L-lactic-co-glycolic acid) without the use of organic solvents". In: *Biomaterials* 17, pp. 1417–1422.
- Mothe, Andrea J and Charles H Tator (2013). "Review of transplantation of neural stem / progenitor cells for spinal cord injury". In: *International Journal of Developmental Neuroscience* 31 (7), pp. 701–713. DOI: [10.1016/j.ijdevneu.2013.07.004](https://doi.org/10.1016/j.ijdevneu.2013.07.004).
- Murray, JE, JP Merrill, and JH Harrison (1955). "Renal homotransplantation in identical twins". In: *Surgical forum* 6, pp. 432–436.
- Nain, Amrinder S, Cristina Amon, and Metin Sitti (2005). "Polymer Micro / Nanofiber Fabrication using Micro / Nanopipettes". In: *Proceedings of 2005 5th IEEE Conference on Nanotechnology* 1, pp. 366–369. DOI: [10.1109/NANO.2005.1500772](https://doi.org/10.1109/NANO.2005.1500772).

- Nain, Amrinder S, Cristina Amon, and Metin Sitti (2006). "Proximal Probes Based Nanorobotic Drawing of Polymer Micro / Nanofibers". In: *IEEE Transaction on Nanotechnology* 5 (5), pp. 499–510. DOI: [10.1109/TNANO.2006.880453](https://doi.org/10.1109/TNANO.2006.880453).
- Nain, Amrinder S et al. (2006). "Drawing suspended polymer micro- / nanofibers using glass micropipettes". In: *Applied Physics Letters* 89, pp. 183103–183105. DOI: [10.1063/1.2372694](https://doi.org/10.1063/1.2372694).
- Nair, Lakshmi S and Cato T Laurencin (2007). "Biodegradable polymers as bio-materials". In: *Progress in Polymer Science (Oxford)* 32 (8-9), pp. 762–798. DOI: [10.1016/j.progpolymsci.2007.05.017](https://doi.org/10.1016/j.progpolymsci.2007.05.017).
- Neckář, Bohuslav and Das Dipayan (2012). *Theory of Structure and Mechanics of Fibrous Assemblies*. Woodhead Publishing India, p. 310.
- Neergaard-Petersen, Søs et al. (2013). "Fibrin Clot Structure and Platelet Aggregation in Patients with Aspirin Treatment Failure". In: *Plos One* 8 (8), pp. 1–8. DOI: [10.1371/journal.pone.0071150](https://doi.org/10.1371/journal.pone.0071150).
- Neugirg, Benedikt R. et al. (2016). "AFM-based mechanical characterization of single nanofibres". In: *Nanoscale* 8 (16), pp. 8414–8426. DOI: [10.1039/c6nr00863a](https://doi.org/10.1039/c6nr00863a).
- Nguyen, Hieu T. et al. (2014). "Electric field stimulation through a biodegradable polypyrrole-co- polycaprolactone substrate enhances neural cell growth". In: *Journal of Biomedical Materials Research Part A* 102 (8), pp. 2554 –2564. DOI: [10.1002/jbm.a.34925](https://doi.org/10.1002/jbm.a.34925).
- Novikova, Liudmila N et al. (2008). "Biodegradable poly- b -hydroxybutyrate scaffold seeded with Schwann cells to promote spinal cord repair". In: *Biomaterials* 29, pp. 1198–1206. DOI: [10.1016/j.biomaterials.2007.11.033](https://doi.org/10.1016/j.biomaterials.2007.11.033).
- O'Brien, Fergal J (2011). "Biomaterials & scaffolds for tissue engineering". In: *Materials Today* 14 (3), pp. 88–95. DOI: [10.1016/S1369-7021\(11\)70058-X](https://doi.org/10.1016/S1369-7021(11)70058-X).
- Olvera, Dinorath et al. (2019). "Electrospinning of highly porous yet mechanically functional microfibrillar scaffolds at the human scale for ligament and tendon tissue engineering". In: *Biomedical Materials*. DOI: [10.1088/1748-605X/ab0de1](https://doi.org/10.1088/1748-605X/ab0de1).
- Ondarcuhu, Thierry and Christian Joachim (1998). "Drawing a single nanofibre over hundreds of microns". In: *Europhysics Letters* 42 (2), pp. 215–220. DOI: [10.1209/epl/i1998-00233-9](https://doi.org/10.1209/epl/i1998-00233-9).

- Paneva, Dilyana et al. (2011). "Antibacterial electrospun poly(ϵ -caprolactone)/ascorbyl palmitate nanofibrous materials". In: *International Journal of Pharmaceutics* 416 (1), pp. 346–355. DOI: [10.1016/j.ijpharm.2011.06.032](https://doi.org/10.1016/j.ijpharm.2011.06.032).
- Park, Jonghyuck et al. (2018). "Reducing inflammation through delivery of lentivirus encoding for anti-inflammatory cytokines attenuates neuropathic pain after spinal cord injury". In: *Journal of Controlled Release* 290 (July), pp. 88–101. DOI: [10.1016/j.jconrel.2018.10.003](https://doi.org/10.1016/j.jconrel.2018.10.003).
- Patel, N. and M. M. Poo (1982). "Orientation of neurite growth by extracellular electric fields". In: *Journal of Neuroscience* 2 (4), pp. 483–496. DOI: [10.1523/jneurosci.02-04-00483.1982](https://doi.org/10.1523/jneurosci.02-04-00483.1982).
- Paul, Derek Henry (1975). *The physiology of nerve cells*. Blackwell Scientific Publications, p. 114.
- Pawar, Kiran et al. (2015). "Biomaterial bridges enable regeneration and re-entry of corticospinal tract axons into the caudal spinal cord after SCI: Association with recovery of forelimb function". In: *Biomaterials* 65, pp. 1–12. DOI: [10.1016/j.biomaterials.2015.05.032](https://doi.org/10.1016/j.biomaterials.2015.05.032).
- Peng, Ge et al. (2019). "Surface Modification of Multiple Bioactive Peptides to Improve Endothelialization of Vascular Grafts". In: *Macromolecular Bioscience*, pp. 1–12. DOI: [10.1002/mabi.201800368](https://doi.org/10.1002/mabi.201800368).
- Pokorny, P et al. (2014). "Effective AC needleless and collectorless electrospinning for yarn production". In: *Physical Chemistry* 16, pp. 26816–26822. DOI: [10.1039/C4CP04346D](https://doi.org/10.1039/C4CP04346D).
- Porto, Mariana Dias Antunes et al. (2019). "Immobilization of α -amylase in ultrafine polyvinyl alcohol (PVA) fibers via electrospinning and their stability on different substrates". In: *International Journal of Biological Macromolecules* 126, pp. 834–841.
- Prabaharan, M. and R. Jayakumar (2009). "Chitosan-graft- β -cyclodextrin scaffolds with controlled drug release capability for tissue engineering applications". In: *International Journal of Biological Macromolecules* 44 (4), pp. 320–325. DOI: [10.1016/j.ijbiomac.2009.01.005](https://doi.org/10.1016/j.ijbiomac.2009.01.005).
- Prabhakaran, Molamma P et al. (2008). "Surface modified electrospun nanofibrous scaffolds for nerve tissue engineering". In: *Nanotechnology* 19, pp. 1–8. DOI: [10.1088/0957-4484/19/45/455102](https://doi.org/10.1088/0957-4484/19/45/455102).

- Prasad, Arbind, M Ravi Sankar, and Vimal Katiyar (2017). "State of Art on Solvent Casting Particulate Leaching Method for Orthopedic Scaffolds Fabrication". In: *Materials Today: Proceedings* 4 (2), pp. 898–907. DOI: [10.1016/j.matpr.2017.01.101](https://doi.org/10.1016/j.matpr.2017.01.101).
- Qian, Yuna et al. (2015). "The effect of hyaluronan on the motility of skin dermal fibroblasts in nanofibrous scaffolds". In: *International Journal of Biological Macromolecules* 79, pp. 133–143. DOI: [10.1016/j.ijbiomac.2015.04.059](https://doi.org/10.1016/j.ijbiomac.2015.04.059).
- Qu, Jing et al. (2013). "Electrospun silk fibroin nanofibers in different diameters support neurite outgrowth and promote astrocyte migration". In: *Society for Biomaterials* 101 (9), pp. 2667–2678. DOI: [10.1002/jbm.a.34551](https://doi.org/10.1002/jbm.a.34551).
- Quian, Lei and Haifei Zhang (2013). "One-step synthesis of protein-encapsulated microspheres in a porous scaffold by freeze-drying double emulsions and tuneable protein release". In: *Chemical Communications* 49, pp. 8833 –8835. DOI: [10.1039/C3CC45012K](https://doi.org/10.1039/C3CC45012K).
- Ramakrishnan, S (1997). "Conducting Polymers: From a Laboratory Curiosity to the Market Place". In: *Resonance* 2 (11), pp. 48–55.
- Ramos, Daisy M et al. (2019). "Insulin immobilized PCL - cellulose acetate micro - nanostructured fibrous scaffolds for tendon tissue engineering". In: *Polymers Advanced Technologies* 30 (5), pp. 1205 –1215. DOI: [10.1002/pat.4553](https://doi.org/10.1002/pat.4553).
- Rampichova, M et al. (2018). "Composite 3D printed scaffold with structured electrospun nano fi bers promotes chondrocyte adhesion and infiltration". In: *Cell Adhesion and Migration* 12 (3), pp. 271–285.
- Rampichová, Michala et al. (2014). "Cell penetration to nanofibrous scaffolds: Forcespinning®, an alternative approach for fabricating 3D nanofibers". In: *Cell Adhesion and Migration* 8 (1), pp. 36–41.
- Ratner, Buddy D et al. (2013). *Biomaterials science: An Introduction to Materials in Medicine*. 3rd editio. Amsterdam: Academic Press, p. 1519.
- Ravichandran, Rajeswari et al. (2010). "Applications of conducting polymers and their issues in biomedical engineering". In: *Journal of the Royal Society Interface* 7, S559 –S579. DOI: [10.1098/rsif.2010.0120.focus](https://doi.org/10.1098/rsif.2010.0120.focus).
- Reneker, Darrell H. and Alexander L. Yarin (2008). "Electrospinning jets and polymer nanofibers". In: *Polymer* 49 (10), pp. 2387–2425. DOI: [10.1016/j.polymer.2008.02.002](https://doi.org/10.1016/j.polymer.2008.02.002).

- Rentsch, Claudia et al. (2014). "Healing properties of surface-coated polycaprolactone-co-lactide scaffolds: A pilot study in sheep". In: *Journal of Biomaterials Applications* 28 (5), pp. 654–666. DOI: [10.1177/0885328212471409](https://doi.org/10.1177/0885328212471409).
- Romanova, Olga A et al. (2019). "Non-woven bilayered biodegradable chitosan-gelatin-poly(lactide) scaffold for bioengineering of tracheal epithelium". In: *Cell Proliferation*, pp. 1–11. DOI: [10.1111/cpr.12598](https://doi.org/10.1111/cpr.12598).
- Rose, Jonas C et al. (2018). "Biofunctionalized aligned microgels provide 3D cell guidance to mimic complex tissue matrices". In: *Biomaterials* 163, pp. 128–141. DOI: [10.1016/j.biomaterials.2018.02.001](https://doi.org/10.1016/j.biomaterials.2018.02.001).
- Rujitanaroj, Pim-on, Nuttaporn Pimpha, and Pitt Supaphol (2008). "Wound-dressing materials with antibacterial activity from electrospun gelatin fiber mats containing silver nanoparticles". In: *Polymer* 49, pp. 4723–4732. DOI: [10.1016/j.polymer.2008.08.021](https://doi.org/10.1016/j.polymer.2008.08.021).
- Schneider, Matthias, Christina Günter, and Andreas Taubert (2018). "Co-deposition of a hydrogel/calcium phosphate hybrid layer on 3D printed poly(lactic acid) scaffolds via dip coating: Towards automated biomaterials fabrication". In: *Polymers* 10 (3). DOI: [10.3390/polym10030275](https://doi.org/10.3390/polym10030275).
- Schnell, Eva et al. (2007). "Guidance of glial cell migration and axonal growth on electrospun nanofibers of poly- ϵ -caprolactone and a collagen-poly- ϵ -caprolactone blend". In: *Biomaterials* 28, pp. 3012–3025.
- Sinha-Ray, S et al. (2012). "Encapsulation of self-healing materials by coelectrospinning, emulsion electrospinning, solution blowing and intercalation". In: *Journal of Materials Chemistry* 22 (18), pp. 9138–9146. DOI: [10.1039/c2jm15696b](https://doi.org/10.1039/c2jm15696b).
- Sisken, B F et al. (1989). "Stimulation of rat sciatic nerve regeneration with pulsed electromagnetic fields". In: *Brain Research* 485 (2), pp. 309–316. DOI: [10.1016/0006-8993\(89\)90575-1](https://doi.org/10.1016/0006-8993(89)90575-1).
- Skothiem, Terje A. and John R. Reynolds (2007). *Handbook of Conducting Polymers*. Ed. by Terje A. Skothiem and John R. Reynolds. 3rd editio. CRC Press.
- Smith, Dominique R et al. (2019). "Combinatorial lentiviral gene delivery of pro-oligodendrogenic factors for improving myelination of regenerating axons after spinal cord injury". In: *Biotechnology and Bioengineering* 116 (1), pp. 155–167. DOI: [10.1002/bit.26838](https://doi.org/10.1002/bit.26838).

- Snyder, Sarah, Carlisle DeJulius, and Rebecca Kuntz Willits (2017). "Electrical Stimulation Increases Random Migration of Human Dermal Fibroblasts". In: *Annals of Biomedical Engineering* 45 (9), pp. 2049–2060. DOI: [10.1007/s10439-017-1849-x](https://doi.org/10.1007/s10439-017-1849-x).
- Spearman, Benjamin et al. (2015). "Conductive interpenetrating networks of polypyrrole and polycaprolactone encourage electrophysiological development of cardiac cells". In: *ACTA BIOMATERIALIA* 28, pp. 109–120. DOI: [10.1016/j.actbio.2015.09.025](https://doi.org/10.1016/j.actbio.2015.09.025).
- Stanislav, Lukáš and Jana Bajáková (2013). "Multicomponent nano-yarns production device". In: *5th NANOCON International Conference*, pp. 438–442.
- Stewart, Elise et al. (2015). "Electrical Stimulation Using Conductive Polymer Polypyrrole Promotes Differentiation of Human Neural Stem Cells: A Biocompatible Platform for Translational Neural Tissue Engineering". In: *Tissue Engineering: Part C* 21 (4), pp. 385–393. DOI: [10.1089/ten.tec.2014.0338](https://doi.org/10.1089/ten.tec.2014.0338).
- Strnadová, K. et al. (2016). "Functionalization and biocompatibility evaluation of drawn fibers for neural tissue implants". In: *Fiber Society 2016 Spring Conference: Textile Innovations - Opportunities and Challenges*.
- Strnadová, K. et al. (2020). "Drawn aligned polymer microfibrils for tissue engineering". In: *Journal of Industrial Textiles* 50 (3). DOI: [10.1177/1528083718825318](https://doi.org/10.1177/1528083718825318).
- Strnadová, Kateřina et al. (2019). "Drawn aligned polymer microfibrils for tissue engineering". In: *Journal of Industrial Textiles* 0 (0), pp. 1–15. DOI: [10.1177/1528083718825318](https://doi.org/10.1177/1528083718825318).
- Sun, Xiaoming et al. (2014). "Use of ginsenoside Rg3-loaded electrospun PLGA fibrous membranes as wound cover induces healing and inhibits hypertrophic scar formation of the skin". In: *Colloids and Surfaces B: Biointerfaces* 115, pp. 61–70. DOI: [10.1016/j.colsurfb.2013.11.030](https://doi.org/10.1016/j.colsurfb.2013.11.030).
- Szewczyk, Piotr K et al. (2018). "Roughness and fiber fraction dominated wetting of electrospun fiber-based porous meshes". In: *Polymers* 11 (1). DOI: [10.3390/polym11010034](https://doi.org/10.3390/polym11010034).
- Theocharis, Achilleas D et al. (2016). "Extracellular matrix structure". In: *Advanced Drug Delivery Reviews* 97, pp. 4–27. DOI: [10.1016/j.addr.2015.11.001](https://doi.org/10.1016/j.addr.2015.11.001).

- Thomas, Aline et al. (2013). "Channel density and porosity of degradable bridging scaffolds on axon growth after spinal injury". In: *Biomaterials* 34 (9), pp. 2213–2220. DOI: [10.1016/j.biomaterials.2012.12.002](https://doi.org/10.1016/j.biomaterials.2012.12.002).
- Thomas, Vinoy et al. (2006). "Mechano-morphological studies of aligned nanofibrous scaffolds of polycaprolactone fabricated by electrospinning". In: *Journal of Biomaterials Science, Polymer Edition* 17 (9), pp. 969–984. DOI: [10.1163/156856206778366022](https://doi.org/10.1163/156856206778366022).
- Tian, Huayu et al. (2012). "Biodegradable synthetic polymers: Preparation, functionalization and biomedical application". In: *Progress in Polymer Science (Oxford)* 37 (2), pp. 237–280. DOI: [10.1016/j.progpolymsci.2011.06.004](https://doi.org/10.1016/j.progpolymsci.2011.06.004).
- Tiwari, Arjun Prasad et al. (2018). "pH / NIR-Responsive Polypyrrole Functionalized Fibrous Localized Drug Delivery Platform for Synergistic Cancer Therapy pH / NIR-Responsive Polypyrrole Functionalized Fibrous Localized Drug Delivery Platform Department of Bionanosystem Engineering , Gradua". In: *Applied Materials Interfaces* 10 (24), pp. 20256 –20270. DOI: [10.1021/acsami.7b17664](https://doi.org/10.1021/acsami.7b17664).
- Tokarev, Alexander et al. (2015). "Touch- and Brush-Spinning of Nanofibers". In: *Advanced Materials* 27 (41), pp. 6526–6532. DOI: [10.1002/adma.201502768](https://doi.org/10.1002/adma.201502768).
- Tuinstra, Hannah M et al. (2013). "Bridges delivering neurotrophin encoding lentivirus enhance regeneration following spinal cord injury". In: *Biomaterials* 33 (5), pp. 1618–1626. DOI: [10.1016/j.biomaterials.2011.11.002](https://doi.org/10.1016/j.biomaterials.2011.11.002).Bridges.
- Uchida, Shusaku et al. (2010). "Early Life Stress Enhances Behavioral Vulnerability to Stress through the Activation of REST4-Mediated Gene Transcription in the Medial Prefrontal Cortex of Rodents". In: 30 (45), pp. 15007–15018. DOI: [10.1523/JNEUROSCI.1436-10.2010](https://doi.org/10.1523/JNEUROSCI.1436-10.2010).
- Vacanti, Charles A (2006). "The history of tissue engineering". In: *Journal of Cellular and Molecular Medicine* 10 (3), pp. 569–576. DOI: [10.1111/j.1582-4934.2006.tb00421.x](https://doi.org/10.1111/j.1582-4934.2006.tb00421.x).
- Vacanti, Joseph P et al. (1988). "Selective cell transplantation using bioabsorbable artificial polymers as matrices". In: *Journal of Pediatric Surgery* 23 (1), pp. 3–9. DOI: [10.1016/S0022-3468\(88\)80529-3](https://doi.org/10.1016/S0022-3468(88)80529-3).
- Valtera, Jan et al. (2019). "Fabrication of dual-functional composite yarns with a nanofibrous envelope using high throughput AC needleless and collectorless

- electrospinning". In: *Scientific Reports* 9 (1), pp. 1–10. DOI: [10.1038/s41598-019-38557-z](https://doi.org/10.1038/s41598-019-38557-z).
- Vawda, Reaz et al. (2019). "Early Intravenous Infusion of Mesenchymal Stromal Cells Exerts a Tissue Source Age- Dependent Beneficial Effect on Neurovascular Integrity and Neurobehavioral Recovery After Traumatic Cervical Spinal Cord Injury". In: *Stem Cells Translational Medicine*, pp. 1–12. DOI: [10.1002/sctm.18-0192](https://doi.org/10.1002/sctm.18-0192).
- Vázquez-Torres, Nadia Adriana et al. (2019). "Influence of the PLGA/gelatin ratio on the physical, chemical and biological properties of electrospun scaffolds for wound dressings". In: *Biomedical Materials*. DOI: [10.1088/1748-605X/ab1741](https://doi.org/10.1088/1748-605X/ab1741).
- Vernitskaya, T V and O N Efimov (1997). "Polypyrrole: a conducting polymer ; its synthesis , properties and applications". In: *Russian Chemical Reviews* 66 (5), pp. 443–457.
- Wan, Meixiang (2008). *Conducting polymers with micro or nanometer structure*. Springer Berlin Heidelberg New York, pp. 1–292. DOI: [10.1007/978-3-540-69323-9](https://doi.org/10.1007/978-3-540-69323-9). arXiv: [arXiv:1011.1669v3](https://arxiv.org/abs/1011.1669v3).
- Wang, Bing Han et al. (2010). "Varying the diameter of aligned electrospun fibers alters neurite outgrowth and Schwann cell migration". In: *Acta Biomaterialia* 6 (8), pp. 2970–2978. DOI: [10.1016/j.actbio.2010.02.020](https://doi.org/10.1016/j.actbio.2010.02.020).
- Wang, Jing and Maiké Windbergs (2019). "Controlled dual drug release by coaxial electrospun fibers – Impact of the core fluid on drug encapsulation and release". In: *International Journal of Pharmaceutics* 556, pp. 363–371. DOI: [10.1016/j.ijpharm.2018.12.026](https://doi.org/10.1016/j.ijpharm.2018.12.026).
- Wang, Nuoxin et al. (2017). "In Vitro Evaluation of Essential Mechanical Properties and Cell Behaviors of a Novel Poly(lactic-co-glycolic Acid) (PLGA)-Based Tubular Scaffold for Small-Diameter Vascular Tissue Engineering". In: *Polymers* 9 (318), pp. 1–17. DOI: [10.3390/polym9080318](https://doi.org/10.3390/polym9080318).
- Wang, Xiaodong et al. (2004). "Evaluation of biocompatibility of polypyrrole in vitro and in vivo". In: *Journal of Biomedical Materials Research Part A* 68, pp. 411–422. DOI: [10.1002/jbm.a.20065](https://doi.org/10.1002/jbm.a.20065).

- Wang, Yaming et al. (2005). "Thermal and Thermomechanical Behaviour of Polycaprolactone and Starch/Polycaprolactone Blends for Biomedical Applications". In: *Macromolecular Materials and Engineering* 290 (8), pp. 792–801. DOI: [10.1002/mame.200500003](https://doi.org/10.1002/mame.200500003).
- Web of Science [v.5.34] - Web of Science Core Collection Result Analysis (2020).
- Wenk, Esther, Hans P Merkle, and Lorenz Meinel (2011). "Silk fibroin as a vehicle for drug delivery applications". In: *Journal of Controlled Release* 150 (2), pp. 128–141. DOI: [10.1016/j.jconrel.2010.11.007](https://doi.org/10.1016/j.jconrel.2010.11.007).
- Wenk, Esther et al. (2009). "Microporous silk fibroin scaffolds embedding PLGA microparticles for controlled growth factor delivery in tissue engineering". In: *Biomaterials* 30 (13), pp. 2571–2581. DOI: [10.1016/j.biomaterials.2008.12.073](https://doi.org/10.1016/j.biomaterials.2008.12.073).
- Williams, R L and P J Doherty (1994). "A preliminary assessment of poly (pyrrole) in nerve guide studies". In: *Journal of Materials Science: Materials in Medicine* 5 (6 - 7), pp. 429–433. DOI: [10.1007/BF00058978](https://doi.org/10.1007/BF00058978).
- Williamson, Matthew R. and Allan G.A. Coombes (2004). "Gravity spinning of polycaprolactone fibres for applications in tissue engineering". In: *Biomaterials* 25 (3), pp. 459–465. DOI: [10.1016/S0142-9612\(03\)00536-2](https://doi.org/10.1016/S0142-9612(03)00536-2).
- Woo, Byung H et al. (2001). "Preparation , characterization and in vivo evaluation of 120-day poly (D ,L -lactide) leuprolide microspheres". In: *Journal of Controlled Release* 75, pp. 307–315.
- Woodruff, Maria Ann and Dietmar Werner Hutmacher (2010). "The return of a forgotten polymer - Polycaprolactone in the 21st century". In: *Progress in Polymer Science (Oxford)* 35 (10), pp. 1217–1256. DOI: [10.1016/j.progpolymsci.2010.04.002](https://doi.org/10.1016/j.progpolymsci.2010.04.002).
- World Health Organization (2013). *Spinal Cord Injury*.
- Xing, Xiaobo, Yuqing Wang, and Baojun Li (2008). "Nanofiber drawing and nanodevice assembly in poly (trimethylene terephthalate)". In: *Optics Express* 16 (14), pp. 10815–10822. DOI: [10.1364/OE.16.010815](https://doi.org/10.1364/OE.16.010815).
- Xu, Wenyuan et al. (2016). "Activation of Bcl-2-Caspase-9 Apoptosis Pathway in the Testis of Asthmatic Mice". In: *Plos One* 11 (3), pp. 1–14. DOI: [10.1371/journal.pone.0149353](https://doi.org/10.1371/journal.pone.0149353).

- Yan, Eryun et al. (2014). "Biocompatible core-shell electrospun nanofibers as potential application for chemotherapy against ovary cancer". In: *Materials Science and Engineering C* 41, pp. 217–223. DOI: [10.1016/j.msec.2014.04.053](https://doi.org/10.1016/j.msec.2014.04.053).
- Yang, Anneng et al. (2015). "Fabrication of aligned, porous and conductive fibers and their effects on cell adhesion and guidance". In: *Colloids and Surfaces B: Biointerfaces* 134 (24), pp. 469–474. DOI: [10.1016/j.colsurfb.2015.07.028](https://doi.org/10.1016/j.colsurfb.2015.07.028).
- Yang, F et al. (2004). "Fabrication of nano-structured porous PLLA scaffold intended for nerve tissue engineering". In: *Biomaterials* 25 (10), pp. 1891–1900. DOI: [10.1016/j.biomaterials.2003.08.062](https://doi.org/10.1016/j.biomaterials.2003.08.062).
- Yang, F et al. (2005a). "Electrospinning of nano / micro scale poly (L-lactic acid) aligned fibers and their potential in neural tissue engineering". In: *Biomaterials* 26, pp. 2603–2610. DOI: [10.1016/j.biomaterials.2004.06.051](https://doi.org/10.1016/j.biomaterials.2004.06.051).
- Yang, Junyan and David C. Martin (2004a). "Microporous conducting polymers on neural microelectrode arrays: I electrochemical deposition". In: *Sensors and Actuators, B: Chemical* 101 (1-2), pp. 133–142. DOI: [10.1016/j.snb.2004.02.056](https://doi.org/10.1016/j.snb.2004.02.056).
- Yang, Junyan and David C Martin (2004b). "Microporous conducting polymers on neural microelectrode arrays: II. Physical characterization". In: *Sensors and Actuators, A: Physical* 113 (2), pp. 204–211. DOI: [10.1016/j.sna.2004.02.029](https://doi.org/10.1016/j.sna.2004.02.029).
- Yang, Quing et al. (2008). "Polymer Micro or Nanofibers for Optical Device Applications". In: *Journal of Appl* 110, pp. 1080–1084. DOI: [10.1002/app.28716](https://doi.org/10.1002/app.28716).
- Yang, Yang et al. (2005b). "Neurotrophin releasing single and multiple lumen nerve conduits". In: *Journal of Controlled Release* 104, pp. 433–446. DOI: [10.1016/j.jconrel.2005.02.022](https://doi.org/10.1016/j.jconrel.2005.02.022).
- Yang, Yang et al. (2009). "Multiple Channel Bridges for Spinal Cord Injury : Cellular Characterization of Host Response". In: *Tissue Engineering: Part A* 15 (11), pp. 3283–3295.
- Yarin, Alexander L, Behnam Pourdeyhimi, and Seeram Ramakrishna (2014). *Fundamentals and Applications of Micro- and Nanofibers*. 1st. Cambridge: Cambridge University Press.
- Ye, Xiaofeng et al. (2013). "The Effect of Heparin-VEGF Multilayer on the Biocompatibility of Decellularized Aortic Valve with Platelet and Endothelial Progenitor Cells". In: *Plos One* 8 (1). DOI: [10.1371/journal.pone.0054622](https://doi.org/10.1371/journal.pone.0054622).

- Yeong, Wai Yee et al. (2006). "Indirect fabrication of collagen scaffold based on inkjet printing technique". In: *Rapid Prototyping Journal* 12 (4), pp. 229–237. DOI: [10.1108/13552540610682741](https://doi.org/10.1108/13552540610682741).
- Youngstrom, Daniel W et al. (2013). "Functional Characterization of Detergent-Decellularized Equine Tendon Extracellular Matrix for Tissue Engineering Applications". In: *Plos One* 8 (5). DOI: [10.1371/journal.pone.0064151](https://doi.org/10.1371/journal.pone.0064151).
- Yuan, Hanwen, Scott D Cambron, and Robert S Keynton (2015). "Prescribed 3-D Direct Writing of Suspended Micron / Sub-micron Scale Fiber Structures via a Robotic Dispensing System Prescribed 3-D Direct Writing of Suspended Micron / Sub-micron Scale Fiber Structures via a Robotic Dispensing System". In: *Journal of Visualized Experiments* 100, pp. 1–10. DOI: [10.3791/52834](https://doi.org/10.3791/52834).
- Zeng, Jingwen et al. (2013). "Fabrication of conductive NGF-conjugated polypyrrole-poly(l-lactic acid) fibers and their effect on neurite outgrowth". In: *Colloids and Surfaces B: Biointerfaces* 110, pp. 450–457. DOI: [10.1016/j.colsurfb.2013.05.012](https://doi.org/10.1016/j.colsurfb.2013.05.012).
- Zhang, Qiang et al. (2017). "Electrospun polymeric micro/nanofibrous scaffolds for long-term drug release and their biomedical applications". In: *Drug Discovery Today* 22 (9), pp. 1351–1366. DOI: [10.1016/j.drudis.2017.05.007](https://doi.org/10.1016/j.drudis.2017.05.007).
- Zhang, Shu Xin et al. (2013). "Role of endogenous Schwann cells in tissue repair after spinal cord injury". In: *Neural Regeneration Research* 8 (2), pp. 177–185. DOI: [10.3969/j.issn.1673-5374.2013.02.011](https://doi.org/10.3969/j.issn.1673-5374.2013.02.011).
- Zhang, Ze et al. (2007). "Electrically conductive biodegradable polymer composite for nerve regeneration: Electricity-stimulated neurite outgrowth and axon regeneration". In: *Artificial Organs* 31 (1), pp. 13–22. DOI: [10.1111/j.1525-1594.2007.00335.x](https://doi.org/10.1111/j.1525-1594.2007.00335.x).
- Zhao, Min, John V. Forrester, and Colin D. McCaig (1999). "A small, physiological electric field orients cell division". In: *Proceedings of the National Academy of Sciences of the United States of America* 96 (9), pp. 4942–4946. DOI: [10.1073/pnas.96.9.4942](https://doi.org/10.1073/pnas.96.9.4942).
- Zhou, Xiaqing et al. (2019). "Controlled released of drug from doubled-walled PVA hydrogel/PCL microspheres prepared by single needle electrospaying method". In: *Colloids and Surfaces B: Biointerfaces*, p. 110645. DOI: [10.1016/j.colsurfb.2019.110645](https://doi.org/10.1016/j.colsurfb.2019.110645).

- Ziabicki, Andrzej (1976). *Fundamentals of Fibre Formation*. 1st. Chichester, United Kingdom: John Wiley and Sons Ltd, p. 504.
- Ziadan, Kareema Majeed (2012). "Conducting Polymers Application". In: *New Polymers for Specials Applications*. In Tech. Chap. Chapter1, pp. 3–24. DOI: [10.5772/76437](https://doi.org/10.5772/76437).
- Zussman, E., D. Rittel, and A. L. Yarin (2003). "Failure modes of electrospun nanofibers". In: *Applied Physics Letters* 82 (22), pp. 3958–3960. DOI: [10.1063/1.1579125](https://doi.org/10.1063/1.1579125).